FLUID FLOW REGULATES ARTICULAR CHONDROCYTE MECHANOTRANSDUCTION PATHWAYS IN 3D CULTURE

A Dissertation

Presented to the Faculty of the Graduate School

of Cornell University

In Partial Fulfillment of the Requirements for the Degree of

Doctor of Philosophy

by

Satish Degala

May 2010

FLUID FLOW REGULATES ARTICULAR CHONDROCYTE MECHANOTRANSDUCTION PATHWAYS IN 3D CULTURE

Satish Degala, Ph. D.

Cornell University 2010

Mechanically compressing cartilage leads to fluid flow which regulates chondrocyte matrix metabolism. The mechanism through which this occurs is unclear, in part because of the coupled nature of physical stimuli associated with flow interactions with cartilage extracellular matrix as well as the lack of experimental techniques to directly quantify fluid flow through porous scaffolds used as tissue analogues.

The objective of this research was to investigate the effects of physiologically relevant fluid flow on the metabolic response of chondrocytes cultured in three-dimensional hydrogel scaffolds. The hypothesis of this research is that fluid flow regulates mechanotransduction of chondrocytes in 3-D alginate scaffolds through a calcium-mediated signaling pathway. In order to decouple the effects of the multiple stimuli associated with fluid flow the material properties of alginate hydrogels were characterized and used calculate the physical forces presented to cells via finite element models. The first aim developed a novel technique to visualize fluid flow in porous scaffolds in order to measure fluid velocity and generate flow profiles. The second aim examined the effects of fluid flow, particularly hydrostatic pressure and wall shear stress, on the calcium signaling response of chondrocytes seeded in alginate scaffolds. The third aim investigated the effects of cell-scaffold adhesion on chondrocyte calcium signaling response to fluid flow.

These studies demonstrate that by directly measuring fluid flow through porous media and characterizing scaffold material properties, the physical stimuli presented to chondrocytes during perfusion can be calculated and correlated to metabolic response. Chondrocyte metabolism in three-dimensional alginate culture was dependent on the velocity of fluid rather than hydrostatic pressure or wall shear stress as previous monolayer studies have suggested. Additionally, this metabolic response was further modulated by chondrocyte attachment via integrins to the alginate substrate in a ligand density-dependent manner. This may indicate the involvement of focal adhesion complexes in mechanosensation of fluid flow. These findings indicate that the mechanism by which chondrocytes respond to fluid flow in vivo or in three-dimensional suspension culture is dependent on some combination of cell shape and surface attachment.

BIOGRAPHICAL SKETCH

Satish was born in Walsall, a town in the West Midlands of England, but raised in various locales in the United States with his parents Prasad and Ajita and brother Sarath. He received a B.S. degree with honors in Zoology from the University of Florida before attending medical school at New York Medical College. After two years he realized that medicine was not his passion and returned to the University of Florida to complete a post-baccalaureate degree in biological engineering.

In 2004, Satish started his PhD at Cornell University with his academic advisor, Larry Bonassar, PhD. While completing his research, Satish married Yeulanda and they became the proud parents of Saira. In addition to his main research focus he participated in an exciting project in biomaterial modification with an amazing group of undergraduate and MEng students.

To my family.

ACKNOWLEDGMENTS

Though only my name appears on the cover of this dissertation, a number of people have contributed to its production. I would like to thank my advisor and mentor Prof. Lawrence Bonassar for his encouragement and support throughout my graduate career. I am indebted to Larry for believing in me and teaching me how to think like a scientist. Thanks to Larry I have also grown as a writer and take pride in crafting my scientific writing, a fact that I never would have imagined 6 years ago. It has been an honor to work with someone whose passion for science, good humor, and dedication to teaching has made my tenure at Cornell so memorable.

I would also like to thank the other members of my committee, namely Profs. Barbara Baird and Warren Zipfel. Barbara and Warren continually challenged my assumptions, forcing me to think outside my comfort zone. Their expertise in their respective fields solidified the work presented in this dissertation.

I was also fortunate to work with several other collaborators who made my graduate experience something I will cherish forever. Thank you Rebecca Williams, Itai Cohen, Brian Kirby, Jason Gleghorn and Mark Buckley. In addition to my collaborators, there have been several individuals who have helped me in countless ways over the years. Thank you Abhishek Ramkumar, Peter Doerschuk , and Kirk Gunsallus for your programming help and Judy Thoroughman for keeping everything running smoothly. I also thank the other members of the Bonassar group who were unstinting with their time as they shared their specialized skill sets with me as well as the Biomechanics group for providing sounding board for ideas.

I could not have done any of this without the love and endless support of my wife Yeulanda and daughter Saira. You both were wellsprings of serenity and strength from which I drew constantly while keeping me committed to our dreams.

This research was funded by the Cornell NBTC (NSF-STC, No. ECS-9876771), the Air Force Office of Scientific Research-DOD (AF-AFOSR) Project ID: FA9550-06-1-0536, NIBIB/NCRR-NIH grant-9 P41 EB001976-16 and the Cornell Center for Materials Research (CCMR)

TABLE OF CONTENTS

LIST OF FIGURES

CHAPTER 1:

CHAPTER 2:

CHAPTER 3:

CHAPTER 4:

APPENDICES:

LIST OF TABLES

CHAPTER 3:

LIST OF ABBREVIATIONS

3-D	three-dimensional
ANOVA	analysis of variance
Ca^{2+}	calcium
$CaCl_2$	calcium chloride
$CaSO_4$	calcium sulfate
CC	covalently crosslinked
EC_{50}	half maximal effective concentration
ECM	extracellular matrix
F-12	Ham's F-12 media
FBS	fetal bovine serum
FE	finite element
fps	frames per second
g	gram
GAG	glycosaminoglycans
Hz	hertz
IC_{50}	concentration with half of maximal inhibition
kPa	kilopascal
Mg^{2+}	magnesium
μg/ml	micrograms per milliliter
μm	micrometer
μg/ml	micrograms per milliliter
μm/s	micrometer per second
μM	micromolar
$\mu W/cm^2$	microwatts per centimeter squared
mm	millimeter
mM	millimolar
MPa	megapascal
ms	millisecond
MRI	magnetic resonance imaging
nm	nanometer
NMR	nuclear magnetic resonance
OA	osteoarthritis
Pa	pascal
PBS	phosphate buffered saline
PEG	poly(ethylene glycol)
PLGA	poly(lactic-co-glycolic acid)
RGD	Arginine-Glycine-Aspartate
mm/s	millimeter per second
M	molar
R^2	coefficient of determination
RMSE	root mean square error
ROI	region of interest
^{35}[S]	Sulfur 35

SD	standard deviation
SEE	standard error of estimate
UPLVG	ultrapure, low viscosity
U/ml	units per milliliter
UV	ultraviolet
V/m	volts per meter
Wt%	weight percent or weight per volume

LIST OF SYMBOLS

Symbol	Variable or parameter	Dimensions
°C	degrees Celsius	$L^2 M T^{-2}$
D	diffusion constant	$L^2 T^{-1}$
μ	dynamic viscosity	$M L^{-1} T^{-1}$
HA	aggregate modulus	$M L^{-1} T^{-2}$
Q	flow rate	L^3 T-1
p	pressure	$M L^{-1} T^{-2}$
σ	Darcy number	$L^2 L^{-2}$
τ	shear stress	$M L^{-1} T^{-2}$
v	velocity	$L T^{-1}$
V/m	streaming current potential	$M L T^{-2}$

CHAPTER 1

INTRODUCTION

1.1 ARTICULAR CARTILAGE: STRUCTURE, FUNCTION AND PATHOLOGY

Articular cartilage is an avascular and aneural load bearing material covering the ends of diarthrodial joints. It acts to evenly distribute loads to the underlying bony surface as well as provide a low friction interface to reduce wear during joint articulation [1]. During joint loading, cartilage is able to withstand compressive forces several time body weight, measured as high as 3000 pounds per square inch in the hip joint [2]. The mechanical properties of cartilage are due to the structure and composition of the cartilage extracellular matrix (ECM) and the chondrocytes which create and maintain it. Cartilage ECM makes up more than 90% of the dry weight of the tissue and is composed of a complex network of fibrillar collagen enmeshed with a high concentration of charged proteoglycan aggregates and other small molecules [3].

Cartilage proteoglycans are large molecules composed of chains of the negatively charged, sulfated, carbohydrate glycosaminoglycan (GAG), mainly chondroitin sulfate, covalently bound to a protein core [4]. The main proteoglycan by weight in cartilage ECM is aggrecan [5]. When cartilage ECM is hydrated, the negative charges of GAG chains become ionized, attracting positive counterions from the surrounding fluid and causing osmotic swelling of the tissue. Swelling is checked by the collagen network, mainly type II collagen covalently cross-linked with type IX collagen [6]. The collagen network is linked to aggrecan by molecules such as fibromodulin, decorin and biglycan [7, 8] and this relationship gives rise to the mechanical properties of articular cartilage.

The structure and composition of the ECM is maintained by chondrocytes which alter the synthesis and degradation of matrix components based on a number of signals. As chondrocytes only make up 5% of the volume of cartilage and have no direct connections with neighboring cells, maintenance of the ECM is dependent on cell-matrix interactions [9]. Cartilage ECM interacts with chondrocytes through a number of transmembrane receptors to regulate phenotype, metabolism and response to mechanical loading [10]. Chondrocytes bind to hyaluronic acid, containing 50 proteoglycans each, via the CD44 receptor [11] and to the collagen network through anchorin CII and integrins [12, 13]. Integrins have also been shown to mediate adhesion to fibronectin, matrix Gla protein, vitronectin, type VI collagen and osteopontin [10]. These receptors, particularly integrins , are believed to transmit mechanical cues to chondrocytes which then translate them into biochemical responses. For example, joint immobilization leads to an overall catabolic response of articular cartilage while joint motion, through physical exercise, leads to an overall anabolic response and improved tissue mechanical properties [14-17].

Knowledge of how chondrocytes sense, process, and respond to changes in their mechanical environment is an important component in understanding the progression of cartilage degeneration which occurs with aging and following traumatic injury or infection. These changes include increased swelling of the tissue, decreased proteoglycan content, shortened GAG chains, loss of tensile and compressive properties, and an overall increase in the activity of degradative enzymes [18-22]. The degradation of articular cartilage is the starting point for development of degenerative osteoarthritis and all subsequent changes in the joint are secondary to this initial damage [23].

Osteoarthritis (OA) is a leading cause of long-term disability in the United States and other developed countries [18, 24]. More than half of all people over the age of 55 develop some feature of OA in some joint and the prevalence further increases with age. Other factors that correlate to development of OA include acute injury, repetitive joint loading, obesity, nutrition, genetics ethnicity, bone density or osteoporosis and changes in sex hormones brought on by menopause [18]. OA is defined by a combination of joint symptoms and structural pathology. The major symptoms include joint pain and stiffness. The pathology is wide-ranging and includes focal damage with loss of articular cartilage, abnormal remodeling and attrition of subarticular bone, osteophytes (bone growth at joint margins), ligamentous laxity, weakening of periarticular muscles and synovial inflammation [18, 23-25].

In studies characterizing cartilage following joint destabilization or impact injury OA features were was seen to develop as well, illustrating the role of mechanical loading on OA pathogenesis [17, 18, 26, 27]. As such, discerning the underlying mechanical mechanisms of OA has involved studying the regulation of chondrocyte-ECM interactions in normal, healthy cartilage.

1.2 MECHANOTRANSDUCTION IN CARTILAGE

Studies in Tissue Explant Culture

The physical and biological processes responsible governing mechanotransduction in cartilage are difficult to identify in vivo. Confounding variables in this identification include the biomechanics of loading (angle, force, contact area) and the difficulty in decoupling the direct effects of loading versus indirect effects. These indirect effects are due to other factors such as increased

vascularity of subchondral bone [28]. Therefore in vitro models of cartilage physiology have been developed using intact tissue explants, which if maintained in the correct culture conditions, synthesize proteoglycans at steady state levels [29, 30]. As such, in vitro studies of mechanical loading have used cartilage explants to investigate the effects of static compression, similar to joint immobilization, and dynamic compression, similar to joint loading during exercise. Static compression of cartilage explants has been shown to inhibit GAG synthesis and amino acid uptake in a dose-dependent manner [31-33]. Dynamic compression of explants at strains of ~1-5% and frequencies of 0.01-1 Hz increased both collagen and GAG synthesis [34-36].

While cartilage deformation alters chondrocyte metabolism, the physical mechanism controlling this behavior is unclear. Due to the complex nature of cartilage structure and the number of components found in the ECM, compressing the tissue leads to a number of coupled physical phenomena, all of which can play a role in regulating chondrocyte response (Fig. 1.1). Compression of cartilage results in cell and ECM deformation [37], hydrostatic pressure gradients, fluid flow, streaming potentials [38-42], and changes in the chemical composition of interstitial fluid [32, 43]. Therefore, investigating the role of a single stimulus is difficult to clearly elucidate in explant culture, particularly in light of the multiple connections between cells and ECM, which add another layer of complexity. Due to the density and low permeability of cartilage ECM it is difficult to add specific blocking antibodies or other chemical treatments to isolate specific molecular pathways of interest.

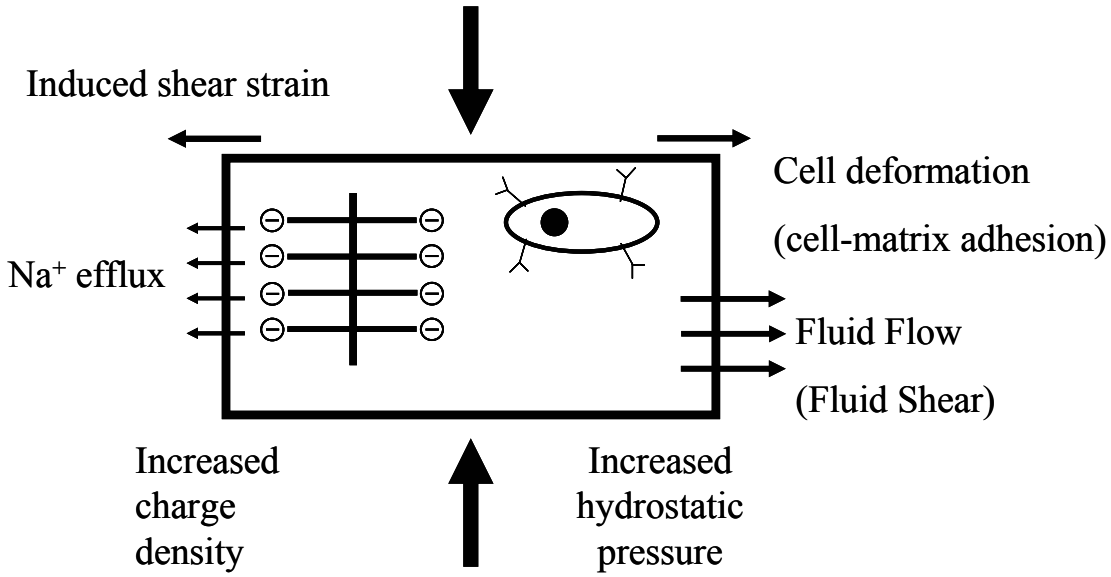

Figure 1.1: Compression of cartilage creates coupled physical phenomena which can act to regulate chondrocyte metabolism

Studies in Monolayer Culture

In order to better understand the molecular pathways governing metabolism these chondrocytes have been cultured successfully in monolayer. This culture method removes any influence of cartilage ECM and allows the addition of specific receptor antagonists and other cytokines in a highly controlled manner. Monolayer studies of chondrocytes have clearly shown the importance of integrins in binding to surfaces coated with collagen and fibronectin [44] and that integrin are adherent to Arg-Gly-Asp (RGD) sequences presented by these molecules [45]. Monolayer studies have also been used to investigate metabolic changes caused by single cell deformation [46, 47], fluid flow [48-52], and hydrostatic pressure [53, 54]; decoupling these stimuli and studying specific pathways for each.

Chondrocyte phenotype is commonly characterized by its production of aggrecan and type II collagen. When these cells are released from their matrix and grown in high density monolayer culture there is a reduction in gene expression and production of these cartilage-specific molecules [55-58]. In addition, there is a shift in cell morphology from a spherical shape to a more spread, fibroblastic appearance. Characteristic of this more “fibroblastic” phenotype, the levels of proteoglycan are greatly reduced, and collagens I, III, and V are produced. The integrin subunits which mediate mechanotransduction also change in monolayer culture compared to cartilage as well [59].

Studies in 3-D Hydrogel Culture

In order to maintain normal phenotype without the confounding influences of cartilage ECM, chondrocytes have been maintained in 3-D hydrogel culture [60].

When cultured in agarose gels, chondrocytes maintained a spherical morphology and demonstrated normal production of proteoglycan and collagen type II [60, 61]. In fact, the switching of chondrocyte phenotypes is reversible as seen when monolayer cultured cells were moved to agarose scaffolds [60, 61].

Hydrogels as scaffold materials offer have a number of qualities that make them ideal for chondrocyte culture. These materials are composed of well-hydrated polymer networks and are highly biocompatible. There are a number of studies which have used various hydrogels as model systems for cartilage culture. Cells can be seeded within these gels by mixing cells into a polymer solution. The cell-polymer mixture is then solidified by gelation through polymer specific means which include crosslinking with divalent cations (alginate) [62], temperature (agarose, poly(ethylene oxide)) [60, 63], or ultraviolet light (poly(ethylene glycol)) [64]. While there are advantages and disadvantages to each type of hydrogel, alginate has several features which make it an excellent choice for chondrocyte culture. The range of pore sizes in biodegradable alginate gels commonly used for cell culture or tissue engineering purposes are an order of magnitude larger (30-300 μm) [65-68] than seen in non-biodegradable agarose gels (25-300 nm) [69-71] allowing larger molecules easier access and allowing more complete tissue formation as alginate is degraded. Scaffold properties , such as modulus or permeability, of poly(ethylene glycol) (PEG) and alginate gels can be altered by varying crosslinking method; however the methods used in PEG gelation can alter chondrocyte metabolism and may have cytotoxic effects [72].

Alginate [62] is an anionic polysaccharide derived from seaweed composed of alternating segments of mannuronic acid (M blocks) and guluronic acid (G blocks). Alginate monomers are crosslinked by ionic bonding through the G blocks in the presence of divalent cations such as Ca^{2+} or Mg^{2+}. Initial studies using alginate as a cell culture material involved formation of cell-encapsulated beads crosslinked in $CaCl_2$ solution [62, 73]. However, by using $CaSO_4$ solution the gelation time was extended and allowed cell-seeded alginate gels to be injection molded into specific shapes and sizes [74, 75].

Long term hydrogel cultures of chondrocytes have produced matrix with similar composition as cartilage [62, 76]. As seen in cartilage explants, static compression of cell-seeded hydrogels showed an inhibition of matrix synthesis while dynamic compression led to an increase in cartilage specific matrix proteins [63, 77-79]. However, the full effects of mechanical loading were not apparent for several days until the chondrocytes had synthesized a pericellular matrix [77, 79], illustrating the role of cell-matrix interactions in transmitting physical stimuli to cells.

One drawback of hydrogels such as alginate and agarose is that they do not allow direct cell anchorage and therefore cells are unable to interact directly with their polymer matrix. Cell attachment is a requirement for man cell types and plays a role in migration, proliferation, differentiation and apoptosis [10]. While there are polymer scaffolds that facilitate cell adhesion, the hydrophilic nature of alginate and its negative charge balance do not allow the adsorption of proteins which can bind cells to the hydrogel [80, 81].

In order to study specific cell adhesion in a model system that allows the use of various receptor antagonists, RGD ligands have been incorporated into several hydrogel systems including alginate [81], agarose [82] and PEG [83]. This provided model systems with cell-matrix interactions and allowed the response to ligand density, species, and receptor specificity to be assessed. Chondrocytes cultured in RGD-alginate demonstrated an immediate sensitivity to static compression at strains too low to cause any inhibition of matrix synthesis in unmodified alginate gels [84]. In RGD-PEG gels, chondrocyte response to dynamic loading was regulated by RGD ligand concentration. RGD modified hydrogels are therefore an excellent model system to fully investigate the effects of mechanical stimuli seen to produce changes in chondrocyte metabolism without the confounding effects of cartilage ECM while still maintaining important cell-matrix interactions.

1.3 FLUID FLOW REGULATES CHONDROCYTE METABOLISM

Physical Mechanisms

One of the major mechanical stimuli presented to chondrocytes during dynamic loading is fluid flow which is itself made up of several separate stimuli. The mechanical stimuli associated with fluid flow include hydrostatic pressure, shear stress, and streaming potentials. Fluid flow was shown to have an effect on chondrocyte biosynthesis of matrix proteins during dynamic compression of cartilage explants and agarose gels [34, 35, 77, 85]. In these studies, newly synthesized matrix proteins were preferentially located in the periphery of the scaffolds in areas of

increased fluid flow compared to central regions where hydrostatic pressure was greater. In order to decouple the multiple stimuli associated with fluid flow a number of approaches were taken in both monolayer and 3-D experimental models. The outcome variables measured in most of these studies were matrix protein synthesis or gene expression although changes in intracellular calcium concentration are also used to as indicators of mechanical signaling response.

Hydrostatic Pressure

Mechanical loading of cartilage increases the hydrostatic pressure of the tissue leading to movement of fluid through the porous ECM. However, hydrostatic pressure has been shown to regulate chondrocyte metabolism independently of any convective fluid transport. Chondrocytes in monolayer subjected to static hydrostatic pressure of 0.5 MPa showed an increased Ca^{2+} response [53]. However, while cells in statically pressurized explants (0.5-2 MPa) showed a decrease in protein biosynthesis [86], cells in collagen and agarose gels (2.8, 5 MPa) showed increases in matrix synthesis [87, 88]. Dynamic pressurization of cartilage explants (5 MPa, 0.5 Hz) [54] and collagen sponges (2.8 MPa, 0.015 Hz) [87] increased matrix synthesis while in 4% agarose gels (5 MPa, 1 Hz) [88] there was an insignificant decrease in matrix synthesis. It is interesting to note that dynamic pressurization only had an effect in matrices that enabled direct cell adhesion.

Fluid Shear

Fluid flow has been shown to induce morphological and metabolic changes in chondrocytes including elongation, reorientation, and proteoglycan synthesis [51].

Ca^{2+} signaling in response to fluid flow occurs in a dose-dependent manner at supraphysiologic velocities of 1.7-54 mm/s in monolayer [48, 52]. These velocities are 1000 times higher than estimated to stimulate protein synthesis in dynamically compressed explants [34] or in perfusion bioreactors [89-91], suggesting that signaling pathways governed by chondrocyte phenotype may regulate this response. In addition, fluid flow in monolayer has been shown to activate mitogen-activated protein (MAP) kinases [92] which are features of integrin mediated signaling in several cell types [93-95].While this pathway may not function to regulate chondrocyte response to flow in 3-D hydrogel culture, it suggests that cell-matrix interactions may also play a role in chondrocyte response to fluid flow.

Biological Mechanisms

Primary Cilia

Recently a number of researchers have suggested that chondrocyte response to fluid flow may be regulated by the oft overlooked primary cilia. Primary cilia are single, non-motile organelles that grow from the centrosome of most fully differentiated mammalian cells [96]. Chondrocyte cilia extend from the cell surface ~1-5 μm [97] and are composed of a 9+0 microtubule arrangement and contain kinesin and dynein motors for tubulin, integrin receptors, and stretch-activated ion channels [98]. In kidney epithelial cells primary cilia bend in response to fluid flow after which elevated Ca^{2+} levels spread as a wave to neighboring cells [99]. This Ca^{2+} signaling response is abolished if the cilia are absent or present in a diseased state [100, 101]. The cilium's role as a flow sensor has also been demonstrated in MC3T3-E1 osteoblasts where they were deflected in response to dynamic fluid flow [102]. These

organelles were essential for bone-specific responses to flow such as osteopontin mRNA, prostaglandin E_2 release and cyclooxygenase 2 mRNA levels; however these responses occurred via a Ca^{2+} and stretch-activated ion channel independent mechanisms. In cartilage an in depth investigation found that α2, α3, β1 integrins as well as NG2 are present on cilia [103]. These receptors indicate that primary cilia are able to bind type II collagen, fibronectnin and type VI collagen, normally found in the pericellular matrix, such that a direct link exists between the ECM and the primary cilium mediated by integrins. Therefore primary cilia may act as a flow sensor for cells through bending, interaction with the ECM via integrins, or some combination of the two.

Quantifying Mechanotransduction

Calcium Signaling Response

Changes in intracellular Ca^{2+} concentration have been shown to regulate a wide variety of processes including cell growth, secretion, and sensory perception through inositol triphosphate mediated pathways [104]. The Ca^{2+} signaling response is an early indicator of mechanical signaling transduction in chondrocytes and may be regulated by the stretch-activated ion channels in the plasma membrane; the evidence of this hypothesis being that the response can be attenuated by the stretch-activated ion channel blockers amiloride and gadolinium [105, 106].

Although the mechanism through which chondrocytes sense physical stimuli is not clear, single cell deformation [105-107], matrix deformation [108], hydrostatic pressure [53, 106], osmotic pressure [109], small signaling molecules [110] and fluid shear stress [48, 51, 111] all cause changes in Ca^{2+} signaling response. Using

fluorescent dyes and confocal microscopy it is possible to observe transient changes in Ca^{2+} concentration which acts as a real-time indicator of cell metabolism [112]. Other methods used, such as quantification of proteoglycan synthesis [113], ^{35}[S] incorporation [35] or hydroxyproline synthesis [114] all require that cells be cultured for days and provide information about the tissue level response to any stimulus. In contrast, monitoring Ca^{2+} response captures signaling events in real-time and as a series of single cell measurements as stimuli are applied [105, 110].

1.6 MODELING FLOW THROUGH POROUS MEDIA

While a number of studies have shown the effects of fluid flow on cell-seeded porous scaffolds, quantifying the full-thickness flow profile has proved much more difficult. Investigations of fluid flow in monolayer are commonly implemented by culturing cells on coverslips and applying fluid flow through some modification of a parallel plate flow chamber [49, 52, 115-118]. In these systems, flow can be easily modeled as Poiseuille flow and fluid velocities and wall shear stresses calculated very accurately. This is not the case in 3-D scaffolds where pore structure, pore geometry, and permeability can greatly alter the profile of flow through the depth [119]. However, while a number of predictive models of flow in porous media exist, there have been very few studies experimentally verifying them.

Several studies have developed and applied techniques to measure flow profiles in porous media. . These fluid visualization techniques include shadowgraph

[120], dye tracers [121], laser-doppler anemometry [122], nuclear magnetic resonance (NMR) [123, 124], and magnetic resonance imaging (MRI) [125]. While these techniques have proven effective in describing velocity profiles in the porous materials tested, they may not be applicable to measurements in biological tissue or porous scaffolds used for 3-D cell culture. The maximum spatial resolution reported from these studies was obtained using NMR (0.4 x 0.4 x 5 mm^3), although the authors stated that it could be increased at the cost of temporal resolution [124]. This resolution is insufficient for measuring fluid velocity profiles at the cellular scale required in cartilage or hydrogel culture.

Cartilage behaves as a hydrated, charged, porous, permeable composite made up of an organic solid matrix. Fluid and ion flows that dictate both physical behavior and biological activity occur when these tissues are deformed [34, 35, 85] or a pressure gradient is applied across them [89-91, 126]. In these studies, flow rates were estimated through the bulk of the scaffolds or were defined by the volumetric flow during perfusion. However, no studies have quantified the local flow profile at the cellular scale.

Accurately describing the flow profiles presented to cells with high spatial resolution is particularly important for tissues or scaffolds with anisotropy. In cartilage ECM the distribution and orientation of collagen and proteoglycan varies with depth from the surface leading to changes in local material properties which can occur at length scales of 50-125 μm [127-130]. On an ever smaller scale, the material properties of the pericellular matrix, a specialized matrix immediately surrounding individual chondrocytes, varies from the surrounding ECM and alter the transmission of mechanical stimuli at the cellular length scale [105, 131-134]. When chondrocytes

are seeded into relatively homogenous hydrogel scaffolds and mechanically loaded the result is an inhomogenous distribution of ECM which would alter the flow profile presented to cells by region [61, 63, 77].

Fluid flow through porous media is classically described by Darcy's Law, Brinkman's equation, or several variations of these two models. Using these models, a number of analytic tools have been developed to simulate flow in various porous scaffolds. However, their application is limited by scaffold geometry, material properties of the media, or length scale of interest [135].

Darcy's law describes the isotropic flow of a Newtonian fluid through an isotropic, homogenous, porous structure at a macroscopic scale (a scale large in comparison to scaffold pore size) and assumes that pores are interconnected. However, Darcy's law is not compatible with boundary layer flow and therefore describes an instantaneous assumption of a bulk flow rate from the surface of a scaffold.

Brinkman [119] describes flow through low densities of fixed particles or through low-density fiber beds with specific boundary conditions [135]. Unlike Darcy, it describes the development of fluid velocity from the scaffold boundary to a fully developed flow in the bulk and has been commonly applied to several porous structures for predictive purposes. Attempts to verify the model numerically and experimentally have shown that it incorrectly predicts flow behavior, particularly near permeable boundaries, in certain scaffolds [122, 135, 136]. Studies have shown that Brinkman model parameters are very sensitive to small changes in pore geometry and porosity [137-139]. This may limit the ability of this model to predict local flow behavior in inhomogenous materials. While this model has been applied to simulate boundary layer flow in cartilage the accuracy of the predictions have not been

experimentally verified [140].

Darcy's law can be extended through the boundary layer region using the Brinkman-extended Darcy model of flow [141, 142]. This model maintains the continuity of shear stress and fluid velocity previously lacking near the edge of the permeable surface in Darcy's law [143] and accurately describes nonlinear flow in boundary regions transitioning to Darcy flow in the bulk of the material both numerically numerically [135, 141, 142, 144] and experimentally [122]. This model of flow is not as sensitive to changes in pore structure, but rather depends on the permeability of the scaffold. Regardless, no studies have directly measured fluid flow in cartilage or porous scaffolds used as 3-D culture materials.

The mechanical stimuli associated with non-physiologic fluid flow have been shown to modulate chondrocyte metabolism through Ca^{2+} dependent pathways in monolayer culture [48, 49, 52, 111]. While the stimuli and mechanotransduction pathways regulating this response in 3-D scaffolds are unclear, there is evidence that Ca^{2+} response to mechanical loading is mediated by integrin adhesion to the ECM [145]. The experiments described in this thesis use a novel method of measuring fluid flow in porous scaffolds and established scaffold characterization techniques to calculate the forces caused by flow in alginate hydrogels. Characterizing the mechanical environment confers the ability to relate chondrocyte response to fluid flow to specific mechanical signals. Furthermore, by functionalizing alginate scaffolds with cell adhesion ligands the role cell-matrix interactions play in flow sensing can be explored as well.

1.7 RESEARCH HYPOTHESES AND SPECIFIC AIMS

The hypotheses of this dissertation are that fluid flow regulates mechanotransduction of chondrocytes in 3-D alginate scaffolds and that the response to fluid flow is mediated by cell-adhesion to the surrounding scaffold.

Specific Aims

Specific Aim 1 (Chapter 2):

Develop a new visualization technique capable of high spatial and temporal resolution of fluid velocity profiles in porous scaffolds used as tissue analogues.

Fluid flow through a porous medium regulates cell metabolism in a number of biological tissues and materials used as tissue analogues. Many studies have modeled flow through these materials; however these models have not been experimentally validated. In this paper we introduce a novel method of visualizing fluid velocity profiles in porous scaffolds at the micron scale. By tracking the movement of a photobleached area during perfusion we measured fluid velocity in the boundary layer of porous alginate hydrogels. Using our fluid visualization technique we were able to accurately measure fluid velocities in alginate hydrogels across distances of less than 2 μm with a temporal resolution of less than 0.06 s. Fluid velocity gradients were measured in the boundary layers of scaffolds which were not described by existing models of flow. The depth of the boundary layers increased with scaffold permeability and may result in the unexplained inhomogeneous tissue formation seen during perfusion culture. Therefore it is essential that the flow profiles be directly

measured to accurately define physical stimuli imposed on cells in perfused 3-D scaffolds.

Specific Aim 2 (Chapter 3):

Investigate the hypothesis that fluid flow modulates chondrocyte Ca^{2+} signaling response in 3-D alginate culture

Quantifying the effects of mechanically loading cartilage on the corresponding metabolic response of chondrocytes is difficult due to complicated structure of cartilage ECM and the coupled nature of the mechanical stimuli presented to the cells. In this study we describe the effects of fluid flow, particularly hydrostatic pressure and wall shear stress, on the Ca^{2+} signaling response of bovine articular chondrocytes. We utilized a well-established alginate hydrogel scaffold to maintain spherical chondrocyte morphology and altered the solid volume fraction to change scaffold mechanics. Fluid velocities in the bulk of the scaffolds were measured and the scaffolds were characterized to determine permeability and aggregate modulus in order to quantify the mechanical stimuli presented to cells. Ca^{2+} signaling response to direct perfusion of chondrocyte-seeded scaffolds increased monotonically with flow rate and was found to be more directly dependent on the fluid velocity rather than shear stress or hydrostatic pressure. Chondrocytes in alginate scaffolds responded to fluid flow at velocities and shear stresses 2-3 orders of magnitude lower than seen in monolayer culture. As such, the flow-induced Ca^{2+} signaling response of chondrocytes in alginate culture may be due to mechanical signaling pathways is influenced by the 3-dimensional nature of cell shape or surface attachments.

Specific Aim 3 (Chapter 4):

Investigate the hypothesis that matrix adhesion regulates the Ca^{2+} signaling response of chondrocytes to fluid flow

The interaction between chondrocytes and their surrounding extracellular matrix plays an important role in regulating cartilage metabolism in response to environmental cues. This study characterized the role of cell adhesion on the Ca^{2+} signaling response of chondrocytes to fluid flow. Bovine chondrocytes were suspended in RGD functionalized alginate hydrogels with ligand concentrations of 0-400 μM. The hydrogels were perfused and the calcium signaling response of the cells was measured over a range of flow rates. Attachment to RGD-alginate significantly doubled the sensitivity of cells to low levels of fluid flow relative to unmodified alginate in a concentration-dependent manner. At higher flow rates the contribution of cell adhesion to the observed calcium signaling response was no longer apparent. The RGD-enhanced sensitivity to flow was completely inhibited by the addition of soluble RGD which acted as a competitive inhibitor. The results of this study expand the role of matrix adhesion to include regulating chondrocyte response to fluid flow through a calcium dependent mechanism.

CHAPTER 2

HIGH-RESOLUTION MEASUREMENTS OF FLOW PROFILES IN POROUS MATERIALS USED IN 3-D CELL CULTURE AND TISSUE ENGINEERING

2.1 ABSTRACT

Fluid flow through a porous medium regulates cell metabolism in a number of biological tissues and materials used as tissue analogues. Many studies have modeled flow through these materials; however these models have not been experimentally validated. In this paper we introduce a novel method of visualizing fluid velocity profiles in porous scaffolds at the micron scale. By tracking the movement of a photobleached area during perfusion we measured fluid velocity in the boundary layer of porous alginate hydrogels. Using our fluid visualization technique we were able to accurately measure fluid velocities in alginate hydrogels across distances of less than 2 μm with a temporal resolution of less than 0.06 s. Fluid velocity gradients were measured in the boundary layers of scaffolds which were not described by existing models of flow. The depth of these boundary layers increased with scaffold permeability and may be the cause of unexplained inhomogeneous tissue formation seen in studies using perfusion culture. Therefore it is essential that the flow profiles of porous media be directly measured to accurately define physical stimuli imposed on cells in perfused 3-D scaffolds.

2.2 INTRODUCTION

Fluid flow is generally believed to be an important mediator of metabolic function for a number of cell and tissue types. The effect of fluid flow on cellular response is directly related to the properties of the tissue in question. Most tissues behave as hydrated, charged, porous permeable composites made up of an organic solid matrix. Fluid and ion flows that dictate both physical behavior and biological activity occur when these tissues are deformed or a pressure gradient is applied across them. As such, perfusive or deformation-induced flows have been shown to stimulate or maintain a variety of engineered tissues and 3D cell cultures including cartilage [34, 85, 89-91], bone [146-148], liver [149-151], and mesenchymal stem cells [152-154].

In such studies, flow rates have been estimated through the bulk of scaffolds [34, 35, 85], bulk flow rates were defined by controlled perfusion [89-91, 155]. However, no studies have quantified the local flow rates at or below the cellular length scale (10-50 μm). Accurately describing the flow profiles presented to cells with high spatial resolution is particularly important for tissues or scaffolds with anisotropy. For example, cartilage extracellular matrix (ECM) is composed mainly of collagen fibers and charged proteoglycans whose distribution and orientation varies with depth from the surface leading to changes in local material properties that can occur at length scales of 50-125 μm [127-130]. Material properties in the pericellular matrix immediately surrounding chondrocytes also vary from the surrounding ECM and can alter the transmission of mechanical stimuli at the cellular length scale [105, 131-134]. An inhomogenous distribution of ECM also occurs when chondrocytes are seeded into relatively homogenous hydrogel scaffolds, cultured statically or exposed to mechanical loading, altering the flow profile presented to cells by region [61, 63, 77].

In addition, several recent studies have specifically attempted to impart such heterogeneity in engineered cartilage, which would lead to heterogenous flow patterns when loaded [156-158].

Fluid flow through porous media is classically described by Darcy's Law or by Brinkman's equation, a modification of Navier-Stokes equation, to describe flow through hyperporous media. A number of analytic tools have been developed to simulate flow through porous media using these models; however they are limited by length scales, material properties, and material geometry in which they are valid [135]. Darcy's (Eq.1) is valid for isotropic and macroscopically homogenous porous media in the form

$$\langle v \rangle_i = -\frac{K}{\mu}\frac{\partial p}{\partial X_i} \tag{1}$$

where ‹v› is the average velocity, K is the permeability tensor, μ is the dynamic viscosity, p is the pressure and X is the space variable. Due to the creation of unrealistic velocities, and therefore shear stress discontinuities, in boundary layer regions it cannot be used to describe the full flow profile [141]. Brinkman's equation (Eq. 2) describes flow through low densities of fixed particles or fibers under restrictive conditions [135] and has been used to describe flow through cartilage as well [140]. It states

$$\frac{\partial p}{\partial X_i} = \frac{\mu}{K}\langle v \rangle_i + \mu_e \Delta_X \langle v \rangle_i \tag{2}$$

where μ_e is an effective viscosity which may be different than μ, though is often assumed equal. The large permeability required for Brinkman's equation to be valid increases the inertial effects present. However, adding an inertial term (Forchheimer's

law, Eq. 3) requires independently describing the permeability, porosity, and Forchheimer coefficient in order to calculate a fluid velocity profile [124]. This takes the form

$$0 = -\nabla p + \mu_e \nabla^2 v - \left(\frac{\mu v}{K} + \frac{c\rho |v| v}{K^{\frac{1}{2}}} \right) \tag{3}$$

where ρ is the fluid density and c is a constant coefficient.

Darcy's law can be extended through the boundary layer region using the Brinkman-extended Darcy model of flow [141, 142]. This model maintains the continuity of shear stress and fluid velocity previously lacking near the edge of the permeable surface [143] and accurately described nonlinear flow in the boundary region transitioning to Darcy flow in the bulk of the material [142]. This solution of Brinkman-extended Darcy (Eq. 4) is

$$v(d,\sigma) = \frac{Q \cosh \frac{1}{2\sigma}}{\cosh \frac{1}{2\sigma} - 2\sigma \sinh \frac{1}{2\sigma}} \left\{ 1 - \frac{\cosh \left[\left(d - \frac{1}{2} \right) / \sigma \right]}{\cosh \frac{1}{2\sigma}} \right\} \tag{4}$$

where v = velocity, d = depth, Q=flow, σ = Darcy number (k/h^2), h = chamber height (m), and k = permeability (m^2). However, the extent to which this Brinkman-Darcy formulation describes flow in porous materials typically used for cell culture is not known.

A number of techniques have been developed to measure velocity of fluid in porous media under forced convection. These fluid visualization techniques include shadowgraph [120], dye tracers [121], laser-doppler anemometry [122], nuclear magnetic resonance (NMR) [123, 124], and magnetic resonance imaging (MRI)

[125]. While these techniques have proven effective in describing velocity profiles in the porous materials tested, they may not be applicable to measurements in biological tissue or porous scaffolds used for 3-D cell culture. The maximum spatial resolution reported from these studies was obtained using NMR (0.4 x 0.4 x 5 mm^3), although the authors stated that it could be increased at the cost of temporal resolution [124]. This resolution is insufficient for measuring velocity profiles at the cellular scale.

A potential alternative solution to resolving flows on this scale involves the use of fast confocal microscopy. This approach has been used to track the movement of colloidal crystals undergoing oscillatory shear with a spatial and temporal resolutions of 150 nm and 120 Hz respectively [159, 160]. It has been successfully applied to track depth-dependent shear properties in articular cartilage using chondrocytes as fiducial markers of strain [161]. The resolution was significantly enhanced by fluorescently staining the tissue, photobleaching multiple lines onto the surface, and tracking their displacement during oscillatory shear [162]. A reasonable application of this technique is the measurement of flow-induced displacement of soluble fluorescein molecules in a porous scaffold.

The objective of this study was to develop a fluid visualization technique, based on fast confocal microscopy, capable of high spatial and temporal resolution of fluid velocity profiles in porous scaffolds used as tissue analogues. Specifically, A) we describe the use of fast confocal microscopy to track the movement of fluorescent media on the scale of ~2 μm; B) describe the flow profiles with Brinkman and Brinkman-Darcy models to calculate local permeability C) describe conditions wherein these models can be accurately implemented to simulate flow through porous media.

2.3 MATERIALS AND METHODS

Scaffold Creation

Flow visualization was performed in porous alginate hydrogels which were perfused with a fluorescein solution. Fluid flow was directed through the scaffolds in a custom-made device containing a chamber of rectangular cross-section with rounded ends with openings for fluid movement (Fig. 2.1a). These chambers were filled with a well mixed alginate suspension crosslinked with a $CaSO_4$ solution (20mg/mL) in a 2:1 ratio using an injection molding technique and flattened with a plate [74]. These gels were injected into custom-made devices and flattened with a plate. The alginate was allowed to crosslink for 30 min before the plate was removed and the chamber sealed by glass coverslips secured by metal plates and opening for imaging (Fig 2.1b). The gels were deliberately oversized and compressed upon coverslip mounting, compressing the gel approximately 10% and preventing fluid leakage around the periphery. Flow measurements were performed on 3 alginate mixtures containing solid-volume fractions of 1, 2, and 3 wt% in order to obtain scaffolds of varying permeability.

Devices were perfused via syringe pump at flow rates of 5-25 μL/min with 1.75 mg/mL fluorescein in phosphate-buffered saline (PBS). The devices were mounted on an inverted fast confocal microscope (LSM 5 Live; Carl Zeiss Inc.; Jena, Germany) capable of imaging up to 120 frames per second (fps).

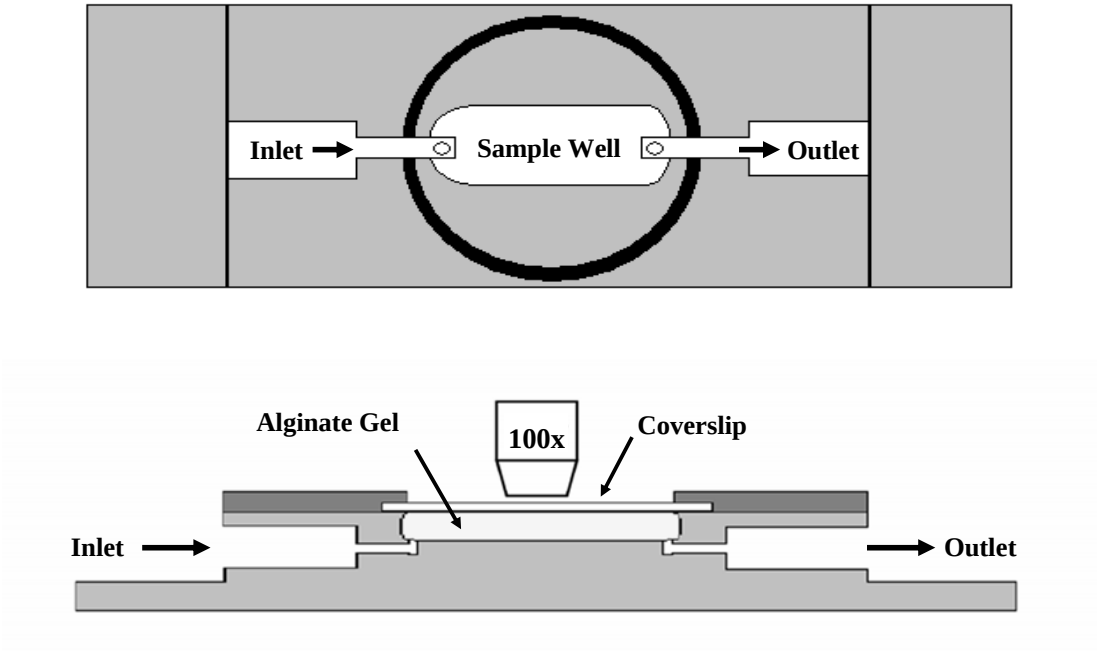

Figure 2.1: a) Empty flow device illustrating the connection between flow path and sample location; b) Cross-section of flow device loaded with alginate scaffold and sealed with a coverslip

Fluid Visualization

Flow was visualized by photobleaching a 1-pixel wide (0.11 μm) line perpendicular to the flow direction for ~ 1 s in the center of the field of view. Line scans were taken at 100 frames per second to capture the movement of the photobleached area with time. Images were averaged perpendicular to the bleach direction, converting the image to a 1-D intensity profile. The method used to calculate flow velocity was based on the case of a 1-D model of diffusion with flow given a Gaussian bleach profile where the concentration of fluorophore (C) is described by C(x,t):

$$C(x,0) = C_{\max}\left(1 - e^{-\left(\frac{x^2}{\sigma^2}\right)}\right) \tag{5}$$

where x = location, t = time, and σ = width of bleach profile. Solving for this initial condition (Eq. 5) leads to:

$$C(x,t) = C_{\max}\left(1 - \frac{\exp\left(\frac{-x^2 + 2xvt - v^2t^2}{4Dt + \sigma^2}\right)}{\sqrt{\frac{4Dt + \sigma^2}{\sigma^2}}}\right) \tag{6}$$

where v = fluid velocity and D = diffusion constant. From the solution (Eq. 6) it is clear that the minimum will always be at x = vt such that the location of the minimum (x) will change as vt. Therefore the location of the intensity minimum was tracked over successive images in Matlab by fitting a parabola about the global minimum of the intensity profile for each image (Fig. 2.2a). The location of each parabola's minimum calculated and plotted against its corresponding timestamp; fluid velocity was calculated as the slope (Fig. 2.2b). The parabolic fit used was chosen to minimize

fit error and more accurately describe the intensity profile (Appendix F).

The technique was first validated with scaffold-free devices perfused with 0.125 mg/mL fluorescein solution. Fluid flow was visualized by photobleaching a one pixel-wide line for 300 ms and imaging at 60 fps with a 10x, 0.30 NA objective. Measurements were taken at flow rates of 10-50 μL/min at depths of 0-200 μm (3 flow rates at 5 depths measured 8 times for repeatability). Velocity measurements through the devices were compared to a Poiseuille model of flow in a rectangular channel with width > > height (Eq. 6)

$$v(z,Q) = z(h-z)\frac{6Q}{wh^3} \tag{6}$$

where v = local fluid velocity, z = depth from surface, Q = flow rate, h = chamber height, and w = chamber width.

After validating the technique without scaffolds, 1, 2, and 3 wt% alginate hydrogels were perfused and flow was visualized at 100 fps with a 100x, 1.4 NA objective. In order to determine the flow profile with depth velocity measurements were taken in 5 μm increments from the surface at 25 μL/min for all alginate mixtures (3 scaffolds/wt% at 10-11 depths each measured 3-6 times for repeatability). The data was fit to both the Brinkman-extended Darcy model (Eq. 4) and Brinkman's equation (Eq. 2) in order to quantify the flow profile and calculate permeability. To compare the applicability of the unmodified Brinkman formulation to describe these flows, Brinkman's equation (Eq. 2) was solved numerically using COMSOL Multiphysics (COMSOL, Burlington, MA) and fit to the data assuming apparent viscosity (μ_e) equal to fluid viscosity (μ) such that

$$\rho\frac{\partial v}{\partial t}+\left(\frac{\mu}{k}\right)v=\nabla\cdot\left[-P+\mu\left(\nabla v+(\nabla v)^{T}\right)\right]+F \text{ with } \nabla\cdot v=0 \quad (7)$$

where ρ = density, v = velocity, μ = dynamic viscosity, k = permeability, P = pressure and F = volume force.

Finite Element Modeling

Finite element (FE) models were used to simulate the experimental perfusion system and calculate local fluid velocities and hydrostatic pressures. 2-D isotropic FE models of our devices filled with alginate gels were created in COMSOL Multiphysics (COMSOL, Burlington, MA). The governing equation for the model was Brinkman's equation (Eq. 7) and was used to calculate flow through porous media. The no-slip boundary conditions were imposed at all walls, fluid velocity set at the inlet, and the outlet was set as a pressure condition (p = 0 Pa). Rectangular mesh elements exponentially biased to the imaging surface were implemented to capture the nonlinear fluid behavior in the boundary layer (Fig. 2.5a). The values input into the model included solid-volume fraction, thickness, viscosity and permeability (derived experimentally). Perfusion was added to one opening via a hemi-sine loading function over 2 s and maintained as constant. Outcomes were observed at 100 s, well after steady state had been reached. Model variables calculated were pressure and local fluid velocities (Fig. 2.5b).

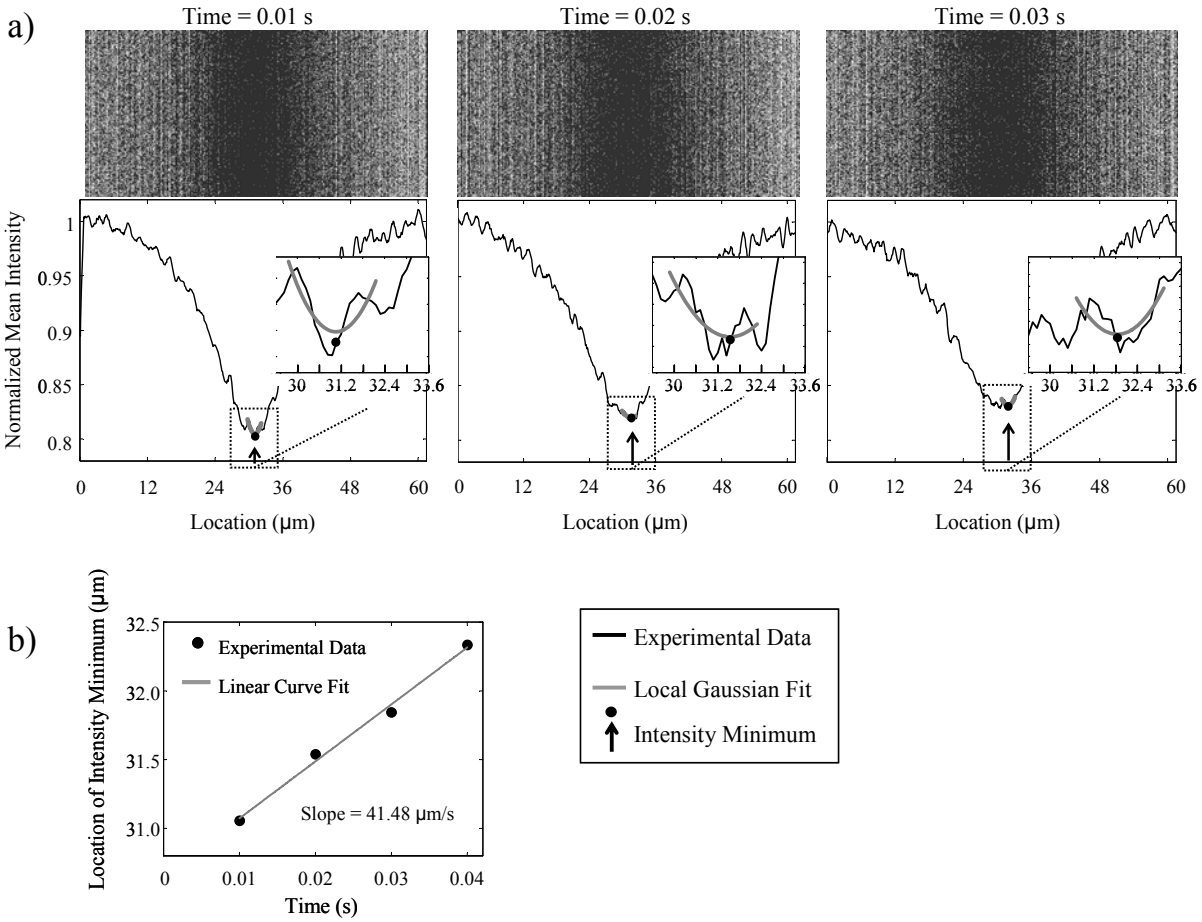

Figure 2.2: Methods for fluid visualization; a) The location of the intensity minimum of the photobleached line is tracked over successive images by fitting a parabola around it b) The location of the intensity minimum is plotted against time to obtain the fluid velocity

Hydraulic Permeability Measurements

Hydraulic permeability was calculated based on stress relaxation of alginate gels undergoing confined compression using an established method [163]. In brief, alginate cylinders (6 mm diameter, 1mm thick) were loaded in 5 steps of 0.1 mm in confined compression (EnduraTech; Electroforce (ELF) 3200 System, Minnetonka, MN). Stress relaxation was recorded and data fit to a poroelastic model to calculate hydraulic permeability.

2.4 RESULTS

In order to track the movement of fluorescent media we tracked the location of a photobleached line in alginate scaffolds under direct perfusion. Images were captured every 0.01 s after photobleaching and the fluorescent intensities were found to resemble a moving Gaussian distribution (Fig. 2.2a). The locations of the intensity minima from photobleaching were plotted with time and fit to a linear model to calculate fluid velocity (Fig. 2.2b). We found that fluid velocities could be accurately resolved at the 5 μm length scale with a temporal resolution of 60 ms.

To confirm the validity of our flow visualization technique, measurements of flows in empty devices were compared to profiles of Poiseuille flow (Fig. 2.3). Experimental velocity measurements in scaffold free devices were consistent with Poiseuille flow through rectangular channels (Fig. 2.4; $R^2 \geq 0.96$, RMSE $\leq 4.0\%$).

In order to assess the effect of permeability on the flow profile 1, 2, and 3 wt% alginate gels were perfused with fluorescein at 25 μL/min and fluid velocities were measured at depths of 0-50 μm (Fig. 2.4a-c). The measurements were fit to both Brinkman-Darcy and Brinkman models of flow. The flow profiles were well described

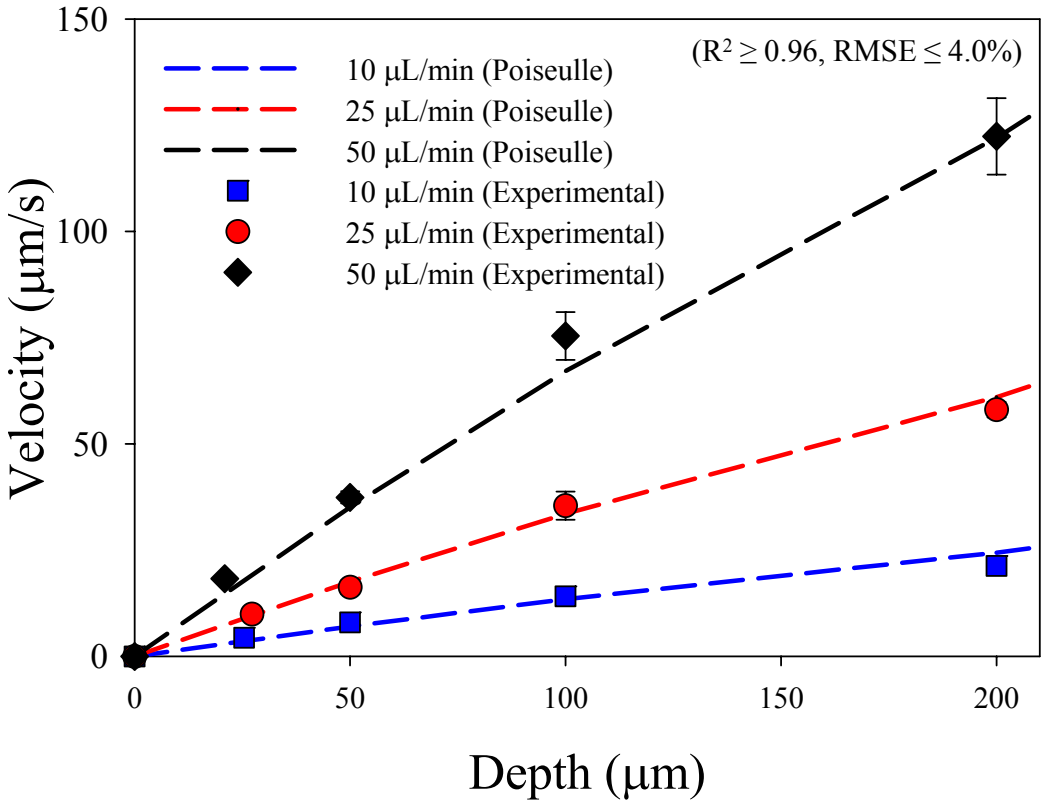

Figure 2.3: Velocity measurements in scaffold-free channels were consistent with Poiseuille flow through rectangular channels (width >> height) ($R^2 \geq 0.96$, RMSE ≤ 4.0).

by both models for all 3 alginate mixtures ($R^2 > 0.94$, RMSE < 2.5 %). The boundary layer, or the depth at over which Darcy velocities (Eq. 1) were reached, increased with permeability. The Darcy velocities from both model fits varied < 10% from the average with the exception of the 1 wt% Brinkman-Darcy model fit where the Darcy velocity varied by 19%. Permeability for each alginate mixture was calculated from both model fits and compared to the hydraulic permeability derived from stress relaxations tests (Fig. 2.4d).

Hydraulic permeability for the 3 alginate mixtures measured via confined compression was 2.7×10^{-14} m^2 for 1 wt% gels, 6.0×10^{-15} m^2 for the 2 wt% gels, and 2.5×10^{-16} m^2 for the 3 wt% gels. Permeabilities calculated from Brinkman's equation were 3.0×10^{-10} m^2, 1.6×10^{-10} m^2, and 6.0×10^{-11} m^2 for 1, 2 and 3 wt% gels respectively. Permeabilities calculated from Brinkman-Darcy were 2.8×10^{-08} m^2, 1.25×10^{-08} m^2, and 8.0×10^{-09} m^2 for 1, 2 and 3 wt% gels respectively. Boundary layer thickness was calculated by fitting flow profile data (Fig. 2.4a-c) to an exponential rise to max. The edge of this region was defined as the depth at which fluid velocity attained 95% of its steady-state value. Boundary layer thickness was 71 μm, 32 μm, and 20 μm for 1, 2, and 3 wt% alginate scaffolds respectively and scaled linearly with hydraulic permeability (data not shown; $R^2 = 0.999$).

After establishing the boundary layer we compared COMSOL simulations for 2 wt% alginate and velocity measurements at the edge of the boundary region. The local fluid velocities and pressures calculated by COMSOL were based on hydraulic permeability calculations (Fig. 2.5b). These models predicted Darcy flow for the

a)

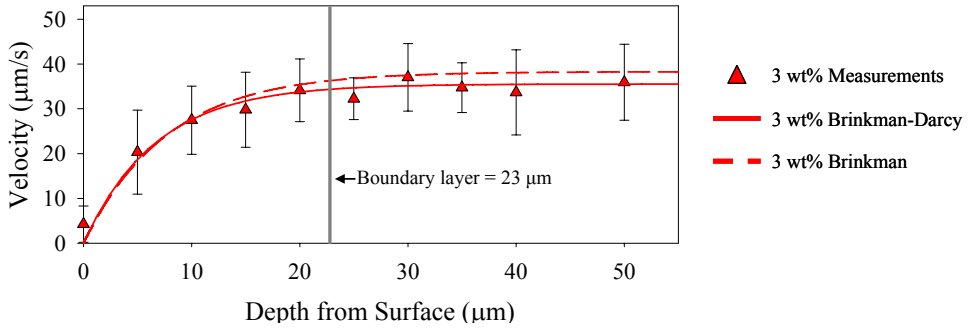

b)

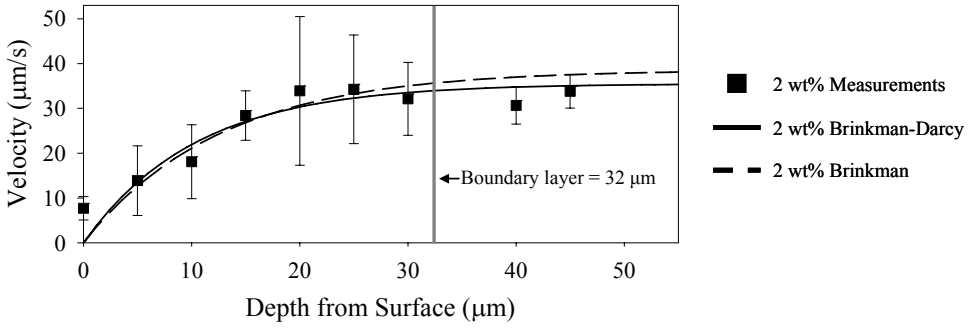

c)

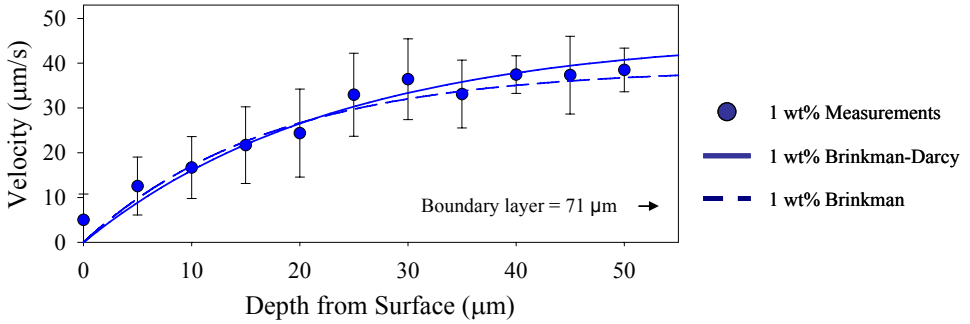

d)

Permeability (m^2)

	1 wt%	2 wt%	3 wt%
Confined Compression	2.80E-14	6.00E-15	2.50E-16
Brinkman's	3.00E-10	1.60E-10	6.00E-11
Brinkman-extended Darcy	2.80E-08	1.25E-08	8.00E-09

Figure 2.4: Velocity measurements were taken every 5 μm from the imaging surface for 3 (a), 2 (b), and 1 wt% (c) alginate gels and fit to both Brinkman's equation and Brinkman-extended Darcy model of flow through porous media ($R^2 > 0.94$; RMSE < 2.5). Boundary layer thickness was noted for each alginate mixture. d) Permeability was calculated from the model fits and compared to hydraulic permeability measurements.

majority of the sample excepting inlet/outlet regions and thin areas on the top and bottom surface. COMSOL predictions of Darcy flow for flow rates of 0, 5, 10, and 25 μL/min were consistent with velocity measurements near the edge of the boundary layer region (Fig. 2.6; $R^2 = 0.94$, RMSE ≤ 2.3). However, the model was unable to predict the flow profile within the boundary layer.

2.5 DISCUSSION

This study describes the application of fast confocal microscopy to visualize and measure local fluid velocities in porous alginate scaffolds. This technique successfully measured local fluid velocities with cell scale resolution and described the flow profile through the entire boundary layer region, demonstrating that boundary layer thickness is regulated by scaffold permeability. Local permeability was calculated by fitting velocity measurements to Brinkman and Brinkman-Darcy models of flow. Velocity measurements allowed the comparison of these models and their effectiveness in describing fluid flow though alginate scaffolds.

Fluid flow tracking one the cellular scale was enabled using fast confocal microscopy. By photobleaching fluorescent dye and tracking the location of the intensity minimum we measured convective flow over 2-5 μm and 40-60 ms (Figs. 2.2a, b). This spatial resolution is much greater than reported by NMR (400 μm) [124]. The resolution of our flow tracking technique was verified by comparison of Poiseuille flow to measured fluid velocities in scaffold-free devices (Fig. 2.3). Velocity measurements varied by less than 5% from Poiseuille predictions with the maximum variation occurring at high flow rates and large depths.

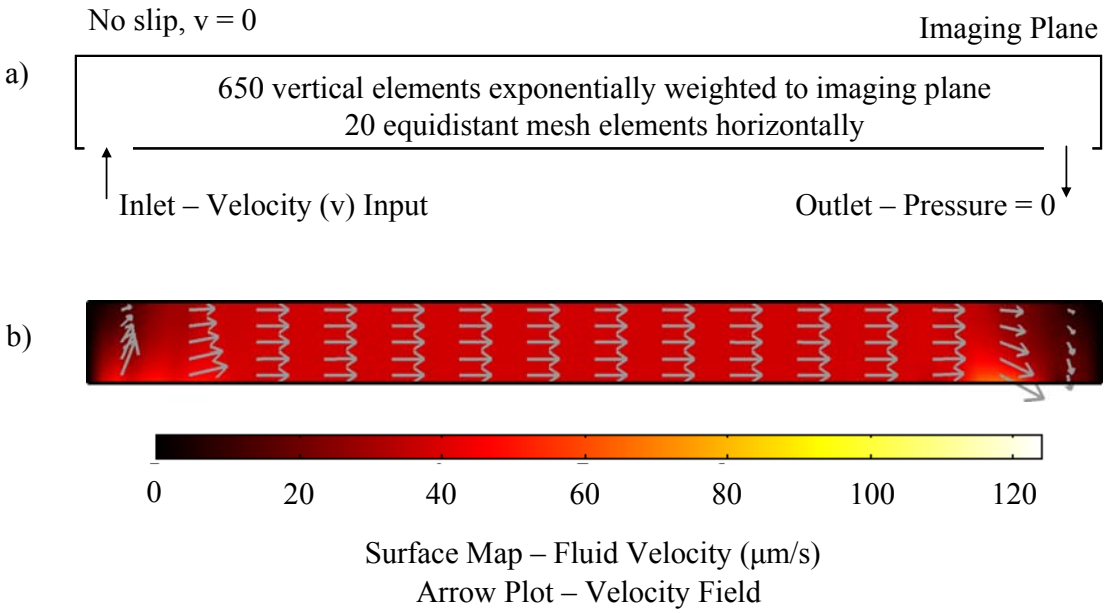

Figure 2.5: a) COMSOL model with boundary conditions (no-slip) to simulate fluid flow through an alginate gel using Navier-Stoke's equation with the Brinkman correction b) COMSOL predictions of pressure and velocity field in 2 wt% alginate at 25 μL/min.

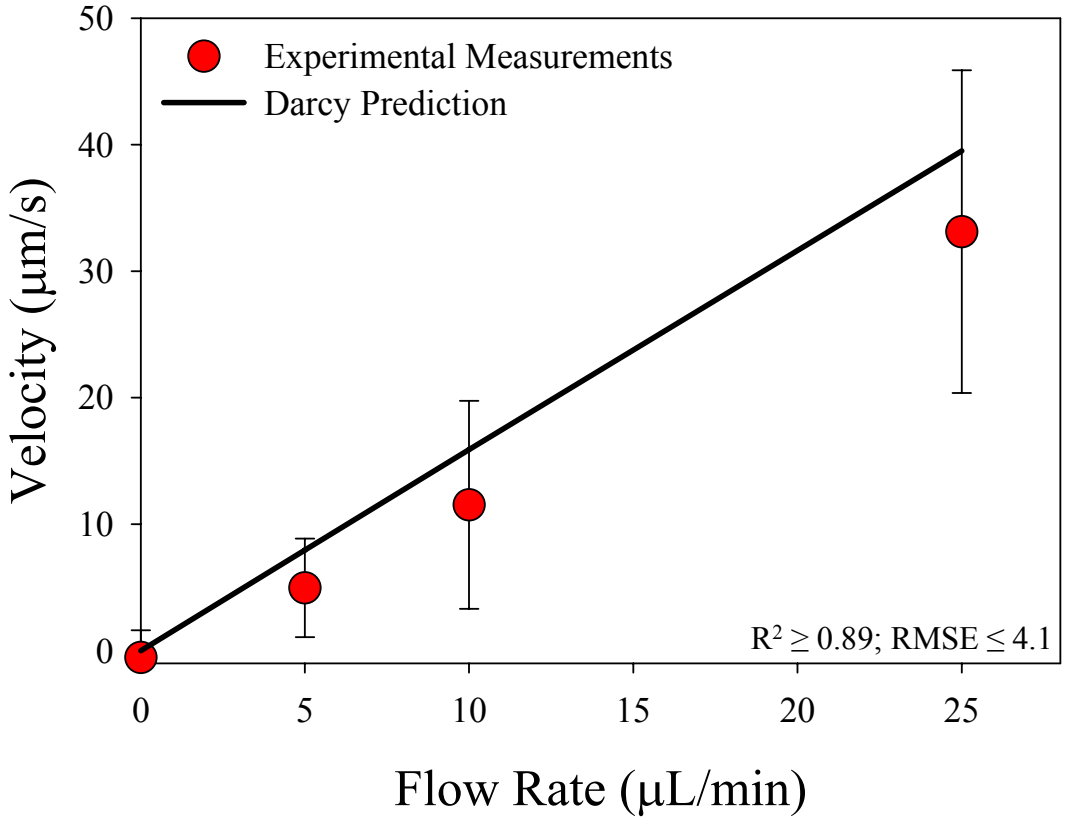

Figure 2.6: Velocity measurements in 2 wt% alginate scaffolds at 25 μm depth were consistent with Darcy predictions of flow ($R^2 \geq 0.89$, RMSE ≤ 4.1).

Mathematical models of flow, such as Brinkman and Brinkman-Darcy, are commonly used to predict fluid velocities in porous scaffolds when scaffold properties are known. With the assumption that these models accurately describe flow behavior, fluid velocity measurements should enable the prediction of scaffold properties. Boundary layer flow profiles were quantified in 5 μm increments from the surface of 1, 2, and 3 wt% alginate scaffolds and identified a velocity gradient which increased from the surface to a maximum value (Fig. 2.4a, b, c). The length of this boundary layer decreased as alginate solid volume fraction increased, suggesting a dependence on scaffold permeability. The flow profiles for all 3 alginate mixtures were well-described by both Brinkman and Brinkman-Darcy models and permeability was calculated for each. These calculated values varied by 2 orders of magnitude from each other and 4-6 orders of magnitude from hydraulic permeability calculations, indicating the differences in the underlying assumptions of both models (Fig. 2.4d).

Brinkman's equation was originally introduced to describe flow through swarms of fixed, solid particles [119] and has since been commonly applied to several types of porous structures for predictive purposes. Attempts to verify the model numerically and experimentally have shown that that it incorrectly predicts flow behavior, particularly near permeable boundaries [122, 135, 136]. In order for Brinkman's equation to accurately describe flow behavior in media with inhomogeneous pore geometry, a boundary layer thickness was calculated separately using independent measurements of permeability and pore structure [122, 137]. This limits the effectiveness of the Brinkman model in predicting flow behavior in alginate scaffolds which demonstrate random pore orientation and highly variable pore sizes [65, 66, 68]. As such, a model of flow less dependent on pore geometry will provide a

better prediction of flow. Brinkman's solution predicts that boundary layer thickness (b) = √k [119] while we observed b = 1.9√k to b = 4.1 √k (Fig. 2.4a-c). Specifically, the boundary layer thickness for the 1, 2, and 3 wt% alginate gels were predicted to be 17, 13, and 8 μm based on Brinkman's solution, but were found to measure 71, 32 and 20 μm experimentally.

Brinkman's extension of Darcy's law was shown effective in describing flow profiles in situations where boundary layer flow is evident as previously shown numerically [135, 141, 142, 144] and experimentally [122]. The solution of Brinkman-extended Darcy formulated by Huang and Liu [142], similar to the solution derived by Kaviani [164], is dependent on the Darcy number to describe the flow profile. The solution is independent of the viscosity of the fluid medium and depends on the relationship between microstructure and the overall thickness of the porous medium. However, there is no direct relationship between the calculated permeability and scaffold properties. Therefore, caution must be exercised in assuming that the model fit provides a correct solution.

Hydraulic permeability calculated from fits of stress relaxation experiments in confined compression was 6-8 orders of magnitude lower than calculations from Brinkman and Brinkman-Darcy models fit to flow profiles. While it is not completely clear why this variation was so large, possible mechanisms for the difference may lie in the underlying assumptions inherent in the permeability calculations. Specifically, calculating permeability from poroelastic theory assumes that all time-dependent mechanics result from pressurization and flow through the scaffolds [163, 165]. While this may hold true in some hydrated, porous media, data suggests that in alginate gels the ionic cross-links may dissipate the energy from applied strain [166]. As such,

calculating permeability in this manner may underestimate the contribution of the solid matrix to observed viscoelastic behavior and therefore underestimate hydraulic permeability.

Fluid velocity measurements demonstrate that relying on the Brinkman model to describe fluid flow is problematic in boundary layer regions. However, outside of this region, Darcy flow predicted by COMSOL simulations described local fluid velocities very well (Fig. 2.5b). Velocity measurements were consistent with Darcy flow near the edge of the measured boundary layer (Fig. 2.6); however estimates of the boundary layer depth differed from measurements by a factor of 30 (Fig. 2.4b).

Verifying the actual depth of the boundary region for a porous scaffold becomes particularly important as permeability increases. This study describes boundary layers 23-71 μm thick in scaffolds with an overall thickness of 1.2 mm. As such Darcy's law adequately describes flow in 88-97% of the scaffold. However, assuming the linear relationship between permeability and boundary layer thickness seen in alginate can be extended to other porous materials under flow, the depth of this boundary region may be quite significant. Permeabilities measured for scaffolds such as polyacrylamide [167], collagen [168], or poly(D,L)-lactide coglycolide [169, 170] range from 9e-15 to 2e-12 m^2. Based on a linear scaling with permeability, the boundary layer thicknesses could vary from 40 μm to 4mm. In a more permeable materials, such as poly(ε-caprolactone) [171] a fluid velocity gradient may extend throughout entirety of the scaffold. Therefore, caution must be taken when applying Darcy's law to describe an experimental system. There are several examples of inhomogeneous tissue formation produced by perfusion at the periphery of cultured

samples which may be a result of unidentified fluid velocity gradients [172, 173]. Therefore it is essential that the flow profiles be directly measured to accurately define physical stimuli imposed on cells in perfused 3-D scaffolds.

CHAPTER 3

CALCIUM SIGNALING IN RESPONSE TO FLUID FLOW BY CHONDROCYTES IN 3-D ALGINATE CULTURE

3.1 ABSTRACT

Quantifying the effects of mechanically loading cartilage on the corresponding metabolic response of chondrocytes is difficult due to complicated structure of cartilage ECM and the coupled nature of the mechanical stimuli presented to the cells. In this study we describe the effects of fluid flow, particularly hydrostatic pressure and wall shear stress, on the Ca^{2+} signaling response of bovine articular chondrocytes. We utilized a well-established alginate hydrogel scaffold to maintain spherical chondrocyte morphology and altered the solid volume fraction to change scaffold mechanics. Fluid velocities in the bulk of the scaffolds were measured and the scaffolds were characterized to determine permeability and aggregate modulus in order to quantify the mechanical stimuli presented to cells. Ca^{2+} signaling response to direct perfusion of chondrocyte-seeded scaffolds increased monotonically with flow rate and was found to be more directly dependent on the fluid velocity rather than shear stress or hydrostatic pressure. Chondrocytes in alginate scaffolds responded to fluid flow at velocities and shear stresses 2-3 orders of magnitude lower than seen in monolayer culture. As such, the flow-induced Ca^{2+} signaling response of chondrocytes in alginate culture may be due to mechanical signaling pathways is influenced by the 3-dimensional nature of cell shape or surface attachments.

3.2 INTRODUCTION

The ability of chondrocytes to sense their mechanical environment is important in the structural adaptation of cartilage to the demands of differential loading. As a result, numerous studies have attempted to characterize the metabolic response of articular cartilage to many loading conditions. For example, static compressive strain applied to cartilage explants has an anti-anabolic effect on the production of major matrix constituents while dynamic compression increases matrix biosynthesis in a frequency and strain-dependent manner [32, 36]. Due to the complex nature of cartilage, compressing the tissue creates a number of coupled phenomena that are believed to play a role in modulating chondrocyte metabolism; compression of cartilage results cell deformation [174], streaming currents [38], hydrostatic pressure [86], and fluid flow [40]. Because a single loading event elicits many physical responses, how tissue loading is perceived at the cellular level and the specific contribution of each of these stimuli on the cellular response is currently unclear. Understanding the role of these stimuli in regulating healthy cartilage could provide insight into the pathological processes that lead to cartilage degeneration as well as inform tissue regeneration strategies.

Observations of local matrix synthesis during dynamic compression studies strongly suggest that fluid flow may play an important role in regulating chondrocyte metabolism [34, 35, 77, 85]. Fluid flow in monolayer has been shown to modulate chondrocyte synthesis of matrix proteins, cytokines and catabolic enzymes by way of changing cell alignment and shape [51]. In 3-D cultures, fluid flow stimulated the

synthesis of collagen and glycosaminoglycan by chondrocytes cultured in perfusion bioreactors [89-91] and was found to be dependent on both the amplitude and duration of flow [89].

The effects of fluid flow on chondrocytes may be regulated by an intracellular calcium signaling pathway which also regulates glycosaminoglycan metabolism [49]. Studies have shown that the chondrocyte Ca^{2+} signaling demonstrates a dose dependent response to fluid flow in monolayer cultures [48, 52]. However, the fluid velocities that triggered an increase in Ca^{2+} signaling in monolayer culture were 1000 times higher than estimated to stimulate aggrecan synthesis in cyclically compressed cartilage explants [34] and matrix synthesis in perfusion bioreactor cultures [89-91]. An explanation of the large variability in fluid velocities may be the phenotypic differences between chondrocytes cultured within 3-D scaffolds and those cultured in monolayer [60].

One strategy to address these considerations is to observe the calcium response of chondrocytes to fluid flow in a 3-D environment. Alginate has been widely used as a substrate for 3-D chondrocyte culture in part because of its ease of use and its ability to maintain normal chondrocyte phenotype [76]. The open pore architecture and high permeability of alginate gels have been exploited in perfusion bioreactors wherein fluid flow was directed through cell-seeded alginate scaffolds at low pressures and fluid velocities [126]. The present study uses a well-established chondrocyte-alginate culture system [74, 175, 176] to investigate the hypothesis that fluid flow modulates chondrocyte Ca^{2+} signaling response in 3-D culture.

3.3 METHODS

Cell Isolation and Gel Preparation

Articular cartilage was sterilely harvested from the femoral condyles and patellofemoral groove of 1-3 day old calves (Gold Medal Packing; Oriskany, NY) and digested for 12-16 hours in 0.2 mg/mL collagenase type II (CITE) dissolved in F-12 media, 100 U/mL penicillin and 100μg/mL streptomycin at 37°C. The cells were subsequently washed and counted with methods previously established [74]. In order to investigate the roles of fluid velocity, pressure and shear stress the scaffold solid volume fraction was altered to produce samples with a range of permeabilities and pore sizes. UPLVG alginate (Pronova; Lysaker, Norway) was suspended in PBS at 10, 20, or 30 mg/mL (1, 2, or 3 wt%) and sterilized with 0.45 μm filters. Chondrocytes were then suspended in an alginate solution with $10x10^6$ cells/mL.

Flow Devices

Custom-made devices for studying the effects of flow on the calcium signaling response of chondrocytes suspended within alginate scaffolds were fabricated with chambers of rectangular cross-sections with rounded ends containing openings for fluid movement (Fig. 3.1). The chambers were covered by glass coverslips seated on o-rings and sealed with metal plates attached with openings exposing the coverslips below. Flow was controlled via syringe pump which perfused gels from below at flow rates of 5-50 μL/min.

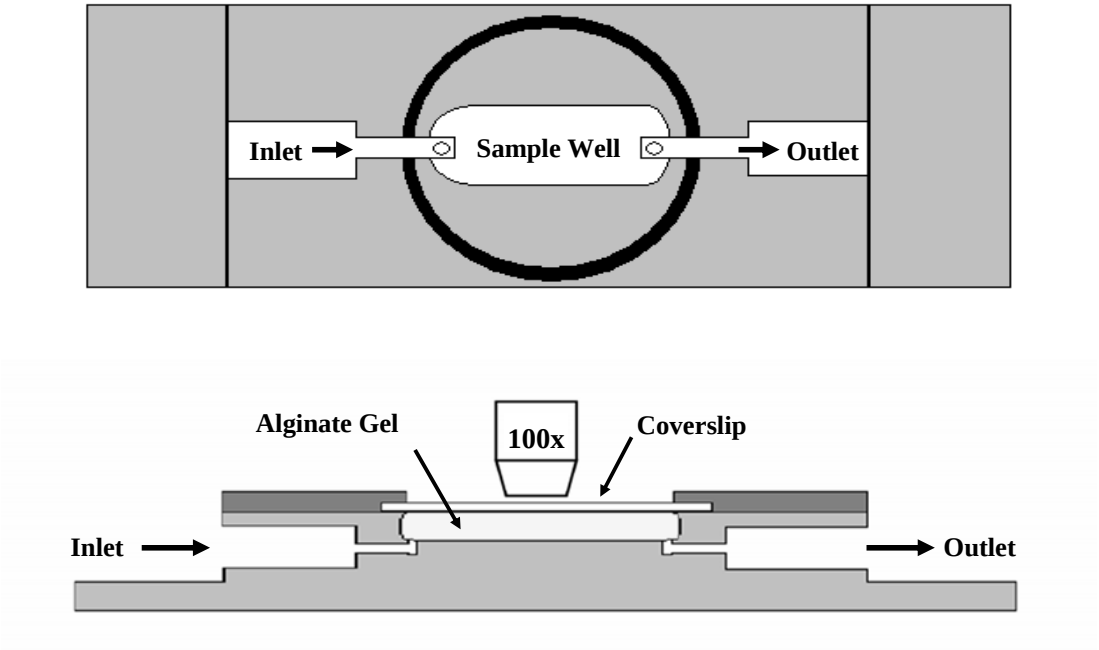

Figure 3.1: a) Empty flow device illustrating the connection between flow path and sample location; b) Cross-section of flow device loaded with alginate scaffold and sealed with a coverslip

Scaffold Creation

The well mixed alginate-cell suspension was combined with $CaSO_4$ solution (20mg/mL) via a 3-way stopcock as previously described [74]. The gel was injected between the open chamber of the device and a sterile plate separated with 0.4 mm spacers allowing the resulting gel to extend above the lip of the chamber. The alginate was allowed to crosslink for 30 min before the plate and spacers were removed. The gels were allowed to cross-link further in a 60 mM $CaCl_2$ solution for 30 min, washed thoroughly, and incubated in F-12 media with 100 U/mL penicillin and 100 µg/mL streptomycin for 12-20 hours. 1, 2, and 3 wt% alginate disks (6 mm diameter, 1mm thick) and cylinders (15 mm diameter, 8 mm height) were made for mechanical testing.

Chondrocytes were labeled with Fluo-4 AM dye (Molecular Probes; Eugene, Oregon) in order to visualize intracellular calcium. Gels were rinsed in situ with Tyrodes buffer plus 200 µM sulfinpyrazone, 5 mM glucose and 2 µM Fluo-4 AM and incubated for 25 min before a coverslip was secured to the device.

Because the gel was larger than the chamber in the device, the addition of the coverslip compressed the gel approximately 7% and ensured that the construct filled the well completely, thereby preventing fluid from leaking around the gel. The devices were then connected to a syringe pump to apply a range of flow rates (5-50 µL/min) of Tyrodes buffer with 200 µM sulfinpyrazone, and 5 mM glucose.

Scaffold Characterization

Alginate disks (6 mm diameter, 1mm thick) were tested in confined compression to measure the equilibrium modulus and permeability (EnduraTech;

Electroforce (ELF) 3200 System, Minnetonka, MN). Stress relaxation tests were performed on the gels with 5 steps of 0.1 mm and the resultant loads fit to a poroelastic model to calculate equilibrium modulus [74].

Pore size of alginate scaffolds for all solid volume fractions was characterized using capillary flow porometry (Porous Materials Inc.; Ithaca, NY). The alginate cylinders (15 mm diameter, ~8 mm thick) frozen at -20 °C in order to maintain spherical, interconnected pores [68] before lyophilizing. The samples were then soaked with a wetting solution (Galwick, Porous Materials Inc.; Ithaca, NY) and placed in the porometer. The porometer was then pressurized in a step-wise manner forcing fluid out of the scaffold. The volume of fluid collected at each pressure was used to calculate the mean size and size distribution of pores within the alginate scaffolds.

Finite Element Modeling

Finite element (FE) models were used to simulate the experimental perfusion system and calculate local fluid velocities, hydrostatic pressures, and shear stresses. 2-D isotropic FE models of our devices filled with alginate gels were created in COMSOL Multiphysics (COMSOL, Burlington, MA). As described previously, the governing equations for the model combined Darcy flow and plane strain to simulate fluid and mechanical forces with an interaction term linking the two[177]. The values input into the model included solid-volume fraction (1, 2, or 3 wt%), thickness (1.2 mm), viscosity (0. 98 mPa·s), and modulus and permeability as measured from confined compression tests[74]. No-slip conditions were imposed on all solid boundaries and 96 quadrilateral mesh elements were constructed without optimization

with 1323 degrees of freedom (Fig. 3.2a). Perfusion was input through the inlet with a hemi-sine loading function over 2 s and maintained as constant while the outlet was set as a pressure condition (0 Pa). Outcomes were observed at 60 s, well after steady state had been reached. Model variables calculated included local fluid velocities, shear stresses (using measured pore sizes), and overall pressure drop across the gels (Fig 3.2b).

Fluid Velocity Measurements

Fluid velocity through the alginate scaffolds was measured using a fluid visualization technique based on tracking the movement of a photobleached area within the scaffold during perfusion [Chapter 2]. Briefly, devices with alginate gels, prepared as described above, were connected to a syringe pump and perfused at flow rates of 0-25 μL/min with PBS labeled with fluorescein at a concentration of 1.75 mg/mL. Devices were mounted on an inverted fast confocal microscope (LSM 5 Live; Carl Zeiss Inc.; Jena, Germany) and imaged at a rate of 100 frames per second using a 100x objective. A 1-pixel wide line was photobleached perpendicular to the direction of flow and images were recorded to track the movement of the photobleached fluid at a depth of 25 μm to establish Darcy flow (Fig. 2c). Measurements were repeated 7 times for each flow rate.

Assuming a 1-dimensional model of diffusion with convection is given by a typical Gaussian bleach pattern:

$$C(x,0) = C_{\max}\left(1 - e^{-\left(\frac{x^2}{\sigma^2}\right)}\right) \quad (1)$$

where C(x,t) = fluorophore concentration, x = location, and σ = width of bleach profile. Solving the diffusion-convection equation for the initial condition (Eq. 1) leads to:

$$C(x,t) = C_{\max}\left(1 - \frac{\exp\left(\frac{-x^2 + 2xvt - v^2t^2}{4Dt + \sigma^2}\right)}{\sqrt{\frac{4Dt + \sigma^2}{\sigma^2}}}\right) \quad (2)$$

where v = convective velocity and D = diffusion constant. From the solution (Eq. 2) it is clear that the minimum will always be at x = vt such that the location of the minimum (x) will change as vt and remain independent of diffusion [178]. Therefore, in order to calculate flow velocity a parabola was fit about the intensity minimum of the 1-D intensity profile and tracked with time. The minima location and corresponding timestamp were then plotted wherein the velocity was calculated as the slope. Fluid velocity measurements were used to verify Darcy flow in the region of interest (Fig. 3.2c).

Pressure and Shear Stress Calculations

The measured scaffold and flow parameters were used to calculate forces acting upon chondrocytes during perfusion. Permeability and fluid velocity values were used to calculate the peak pressure across the scaffold at each flow rate. Shear stress at the pore wall was estimated by assuming a unidirectional, laminar flow through pores modeled as unconnected, cylindrical tubes of uniform pore diameter using the wall shear stress equation:

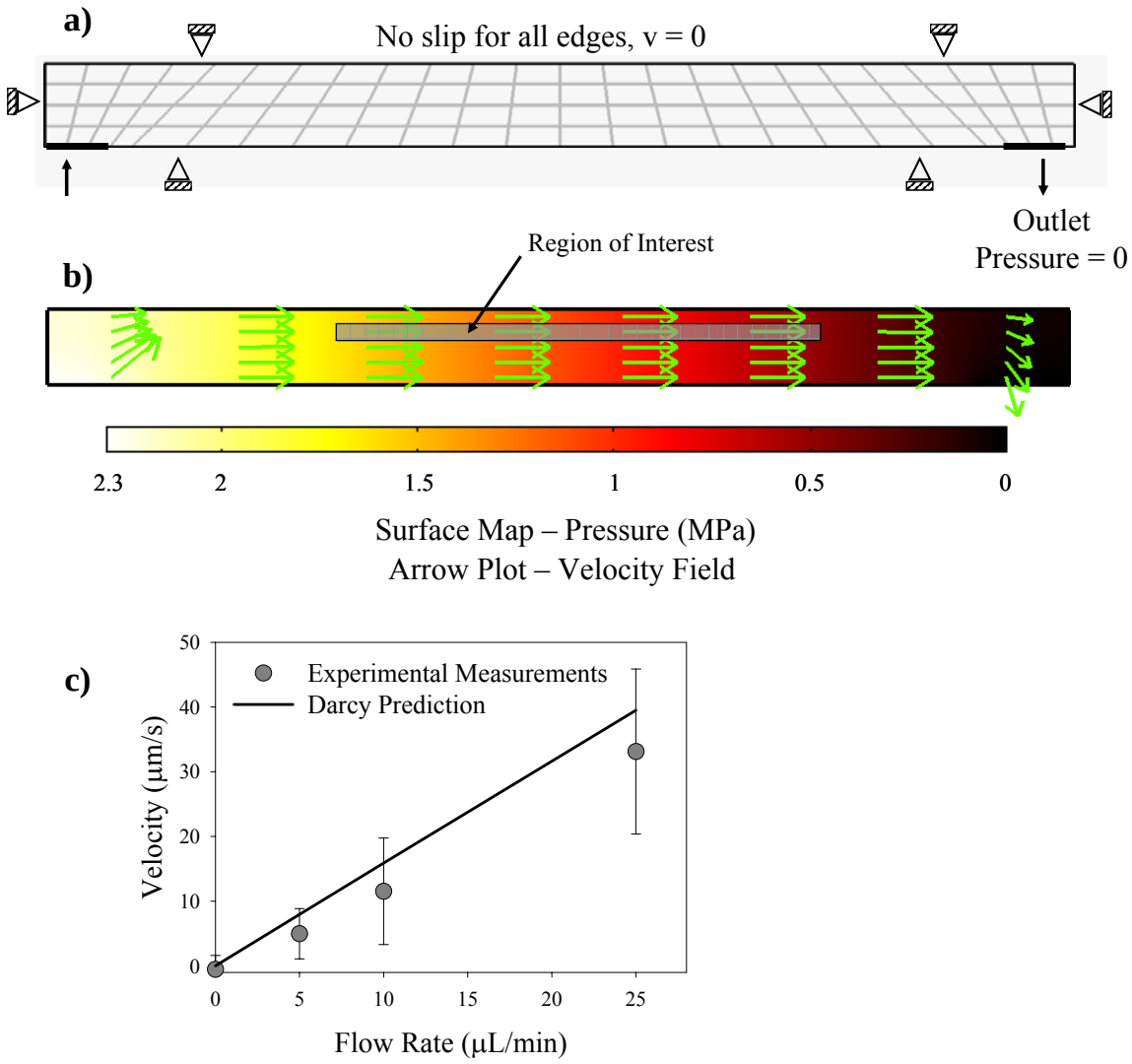

Figure 3.2: a) COMSOL model with mesh and boundary conditions used to simulate experimental conditions b) COMSOL predictions of pressure (surface map) and velocity field (arrows) in a 3 wt% alginate scaffold with flow rate = 25 μL/min; Region of interest for imaging (grey inset) is located at depth > 200 μm; c) Velocity measurements in 2 wt% alginate scaffolds at 25 μm depth at flow rates of 0-25 μL/min were consistent with COMSOL predictions in the region of interest ($R^2 \geq 0.89$, RMSE ≤ 4.1)

$$\tau = \frac{4\mu Q}{\pi r^3} \quad (2)$$

where τ is shear stress, μ is viscosity, Q is the local flow rate, and r is mean pore radius. Flow rate (Q) was calculated using local fluid velocities measured as described above multiplied by the cross-sectional area of the pores in COMSOL Multiphysics.

Cell Imaging

Cells were imaged using a confocal microscope (LSM 510; Carl Zeiss Inc.; Jena, Germany) with an excitation wavelength of 488 nm and emission wavelength ranging from 500-550 nm. 3-11 gels at each solid volume fraction and fluid velocity were imaged with 1 field of view per gel. Images containing more than 30 well-spaced cells in the field of view were captured with a 10x, 0.45 NA, water immersion objective lens at a depth of greater than 100 μm from the surface of the gel. Immediately after the coverslip was secured, cells were imaged every 6 s for 50 min in order to determine the effect of gel deformation on the Ca^{2+} signaling response. This was done to establish a suitable equilibration time to remove the effect of strain and determine if the response to strain varied due to changes in solid volume fraction.

After connecting the devices to the syringe pump, but before applying flow, images were taken every 5 s for 4-5 min in order to establish a baseline signaling response and account for variation between cell source and environmental variables. Flow was then applied and images taken every 5 s for 7-9 min for each flow rate.

Ca^{2+} Signaling

Images were analyzed with a custom Matlab code wherein quadrilateral regions of interest were created for each cell in every frame through the entire imaging period. For each cell, the mean intensity, I(t), and rate of change of the intensity (dI/dt) were calculated (Fig 3.3). A Ca^{2+} signaling event was defined for each cell individually by fitting all positive dI/dt to a Gaussian distribution and defining a Ca^{2+} signaling response as a dI/dt greater than 3 standard deviations above the mean, a modification of published methods [48, 52, 179]. Data was normalized by subtracting the number of cells exhibiting a Ca^{2+} response without flow from the number of cells responding with flow and dividing by the total number of cells imaged for each device.

Statistics

The Ca^{2+} response induced by the ~7% strain for 1, 2, and 3 wt% gels was compared with a 2-way ANOVA with Student-Newman-Keuls post-hoc analysis (SigmaStat) ($\alpha = 0.05$), and fit to a 3-parameter decaying exponential function (SigmaPlot). The variation in Ca^{2+} signaling response due to fluid velocity was compared using a 2-way ANOVA with Student-Newman-Keuls post-hoc analysis (SigmaStat) ($\alpha = 0.05$). The threshold of statistical significance used was $p < 0.05$ for all tests. Data are expressed as mean ± standard deviation unless otherwise indicated.

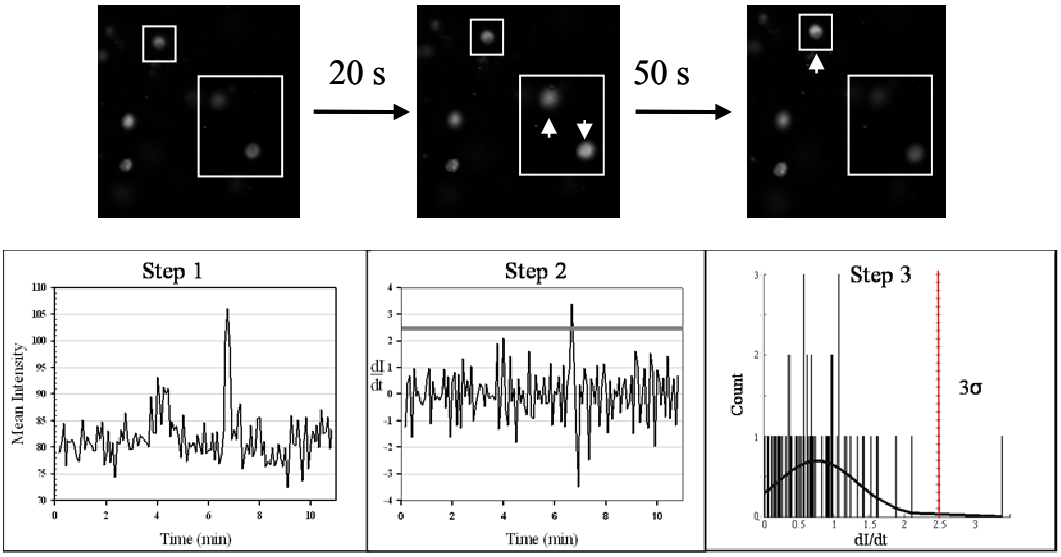

Step 1: Mean intensity measured for individual cells at each time point

Step 2: dI/dt plotted with time for each cell (analyzed individually)

Step 3: Positive dI/dt fit to a Gaussian distribution

Step 4: Ca^{2+} response defined as $dI/dt > 3\sigma$

Figure 3.3: Protocol for calculating Ca^{2+} response from fluorescent intensity of chondrocytes

3.4 RESULTS

Scaffold characterization

In order to calculate the physical stimuli presented to the chondrocytes we conducted extensive mechanical and structural characterization of our alginate scaffolds. The mean pore diameter, equilibrium modulus, and permeability were found to be 150±80 μm, 2.9±2 kPa and 2.7 x 10^{-11} m^2/Pa·s for 1 wt% gels, 223 ±141 μm, 4.1±0.9 kPa, and 6.0 x 10^{-12} m^2/Pa·s for the 2 wt% gels, and 127 ±71 μm, 17.5±6.3 kPa and 2.5 x 10^{-13} m^2/Pa·s for the 3 wt% gels (Table 3.1). These structural properties were incorporated into COMSOL models and pressure, wall shear stress, and fluid velocities were calculated (Fig. 3.2b). Experimental fluid velocity measurements taken in the bulk of the alginate scaffolds for verification purposes were consistent with COMSOL predictions of Darcy flow (Fig. 3.2c; $R^2 \geq 0.89$, RMSE ≤ 4.1) for flow rates of 0-25 μL/min. Therefore, velocities within the alginate scaffolds were defined by COMSOL predictions while examining chondrocyte response.

Material properties and fluid velocity findings were used to calculate the mechanical stimuli present in the alginate scaffold using COMSOL simulations (Table 3.1). Pressure drop across the three alginate scaffolds was calculated and found to be 4-41 kPa for 1 wt% gels, 17-174 kPa for 2 wt% gels, and 420-4200 kPa for 3 wt% gels. For fluid velocities ranging from 7-68 μm/s, shear stresses were calculated to be 3.3e-4 to 4e-3 Pa for all alginate mixtures.

In response to the ~7% strain induced in the alginate gels in mounting the device chondrocytes in all alginate concentrations experienced an initial elevation of Ca^{2+} signaling that decayed exponentially with time (Fig. 3.4). There was no significant difference between the 3 alginate mixtures. The fraction of cells responding

Table 3.1: The range of pressures, fluid velocities and shear stresses presented to chondrocytes in 3-D alginate scaffolds for flow rates of 5-50 μL/min.

Solid Volume Fraction	Pressure Drop (kPa)	Fluid Velocities (μm/s)	Shear Stress (mPa)
1 wt%	4-41	7-68	0.33-3.3
2 wt%	17-174	7-68	0.22-2.2
3 wt%	420-4200	7-68	0.4-4

initially to the applied strain (f_i) and the equilibrium fraction of cells responding (f_e) was $f_i = 0.48$ and $f_e = 0.2$ for the 1 wt% gels ($R^2 = 0.87$, RMS = 0.035), $f_i = 0.31$ and $f_e = 0.05$ for the 2 wt% gels ($R^2 = 0.81$, RMS = 0.032), and $f_i = 0.37$ and $f_e = 0.16$ for the 3 wt% gels ($R^2 = 0.73$, RMS = 0.044).

The Ca^{2+} signaling response of chondrocytes in alginate gels increased monotonically with fluid flow for fluid velocities of 13-68 μm/s ($p < 0.001$) (Fig. 5). However there was no significant difference in the Ca^{2+} response due to changes in the solid volume fraction.

3.5 DISCUSSION

This study demonstrated a model system to measure the real-time metabolic response of chondrocytes to fluid flow in 3-D culture. Seeding cells within alginate scaffolds maintained a normal spherical morphology in the absence of any direct cell-matrix interaction. Scaffolds with a range of pore sizes and permeabilities were created by altering polymer concentration, producing different pressures and shear stresses for a given fluid velocity or compressive strain.

COMSOL finite element simulations were used to calculate the pressure, shear stress and fluid velocity within alginate hydrogels in order to correlate these physical stimuli to the observed Ca^{2+} signaling response. The accuracy of the finite element model was verified with experimental measurements of fluid velocity (Fig. 3.2c). Fluid velocity measurements in the centerline of the alginate scaffolds was found to be slightly lower than expected assuming a uniform distribution of flow across the entire cross-section of the gel. This may be due, in part, to fluid moving around the periphery of the gel despite all precautions taken to minimize this effect. However, the fluid

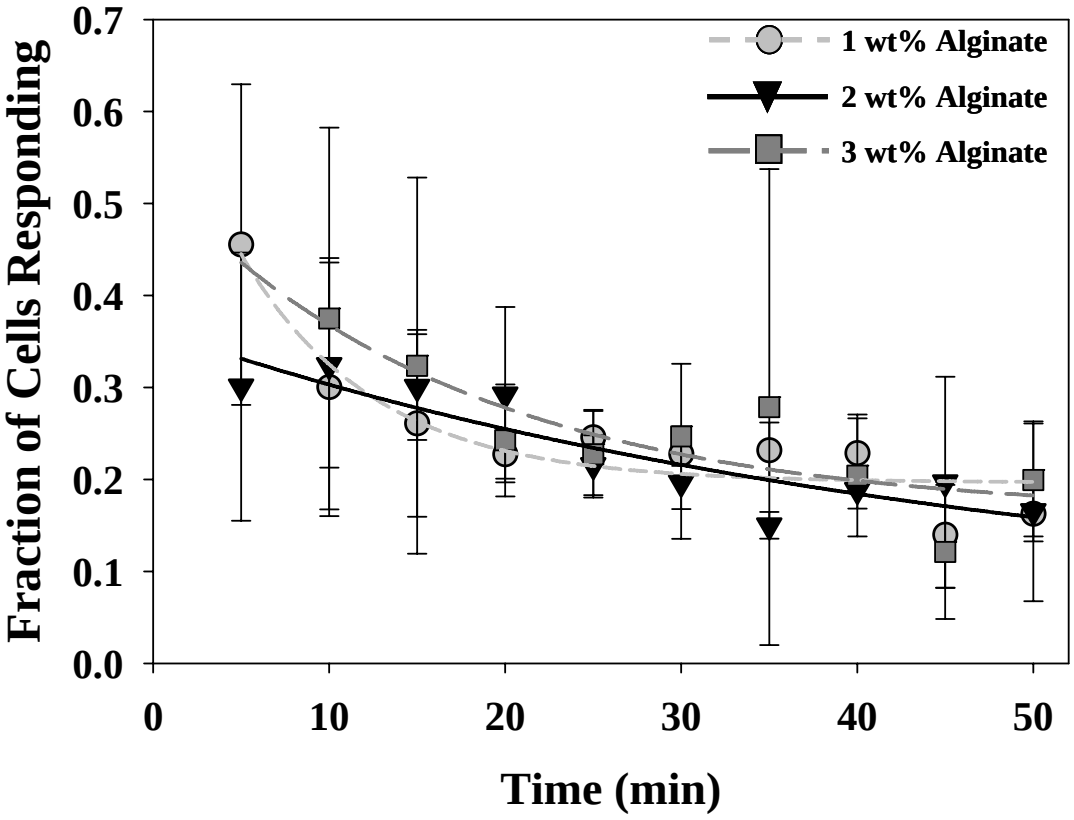

Figure 3.4: Time course of the Ca^{2+} signaling response of chondrocytes in 1, 2, and 3 wt% alginate scaffolds to the applied (7%) strain. Data corresponding to cells in each scaffold were fit to a 3-parameter exponential decay model with no significant difference between experimental groups ($n = 4$; $R^2 \geq 0.73$; RMSE $\leq 4.4\%$).

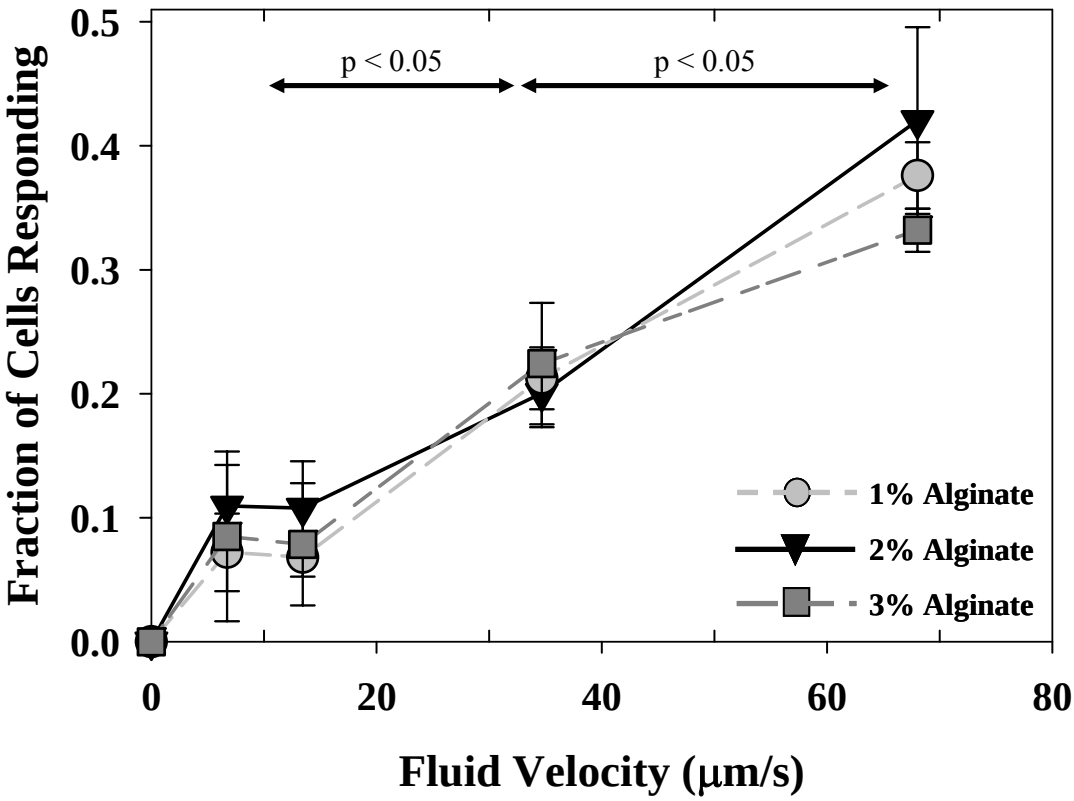

Figure 3.5: The fraction of cells exhibiting Ca^{2+} signaling response increased monotonically for fluid velocities of 13-68 μm/s ($p<0.05$) in 1, 2, and 3 wt% alginate scaffolds; Ca^{2+} signaling response similar for all alginate mixtures (N = 3-11)

velocities measured at each flow rate and depth were consistent across all samples tested. The shear stress values calculated from the model, based on the simplified assumptions of alginate pore structure, are upper bounds of the actual values. However, they are adequate for comparison to other studies.

Previous studies have suggested that chondrocytes seeded in hydrogels are relatively insensitive to mechanical loading compared to native tissue and that a developed matrix is a prerequisite for transduction of these loads to occur [77, 79]. Alginate hydrogels provide non-adherent scaffolds for chondrocyte culture, thereby removing the effects of cell adhesion on Ca^{2+} response [180]. We observed that chondrocytes responded to static compression with an immediate increase in Ca^{2+} signaling for approximately 50% of cells followed by an exponential decay in the percentage of cells responding for all three scaffolds, suggesting that chondrocytes are capable of detecting small mechanical loads in the absence of an extracellular matrix (Fig. 3.4). However, the effects of these small mechanical loads on cellular response are not maintained. The similarity in Ca^{2+} response seen in all alginate mixtures suggests that the cells responded to matrix deformation rather than pressure or fluid flow after compression due to the difference in stress relaxation times between scaffolds.

Ca^{2+} signaling response increased monotonically with fluid velocity and did not change with solid volume fraction (Fig. 5). The three alginate mixtures encompassed 2 orders of magnitude in permeability which led to a large variation in hydrostatic pressures. The maximum pressure generated by direct perfusion of our alginate scaffolds was 4.2 MPa for 3wt% gels and 41 kPa for 1 wt% gels at the fluid inlet (Table 3.1), and approximately half of that in the imaging region. Hydrostatic

pressures of 2.8 MPa or higher have been shown to cause a significant Ca^{2+} signaling response in chondrocytes seeded in hydrogel scaffolds [87, 88], however there was no significant difference between the 3 alginate mixtures. Therefore hydrostatic pressure is unlikely to be a factor in the Ca^{2+} response we observed.

In contrast, the fluid velocities found to be stimulatory in our system were similar to those estimated to increase matrix protein synthesis in cyclically compressed cartilage explants and perfused PLLA/PGA sponges [34, 85, 91]. In cartilage explants and PLLA/PGA sponges, fluid velocities of ~1 μm/s were found stimulatory compared to fluid velocities of 7-13 μm/s in this study. The sensitivity of cells in these other studies to lower fluid velocities may be due to the presence of cartilage matrix which was absent our scaffold. In addition to changes in the response due to cell-matrix interactions, flow through cartilage ECM, creates increased charge densities and streaming potentials [38] which are largely absent from this study.

A comparison of the flow induced Ca^{2+} signaling response in monolayer and 3-D cultures shows that chondrocytes in 3-D culture are sensitive to fluid velocities 2-3 orders of magnitude lower than in monolayer culture (Fig. 3.6a). Unlike our study, which closely matched stimulatory fluid velocities seen within cartilage explants [34, 85], these monolayer Ca^{2+} signaling studies [48, 52] were designed to expose cells to specific shear stresses which were shown to be stimulatory in monolayer culture [51]. We observed that the Ca^{2+} response in alginate scaffolds occurred at wall shear stresses 3 orders of magnitude lower than seen in monolayer culture (Fig. 3.6b). The variation in pore size among the alginate mixtures created a range of shear stresses for a given fluid velocity. Our data indicated that the Ca^{2+} response in 3-D culture varied more directly with fluid velocity than wall shear stress or hydrostatic pressure.

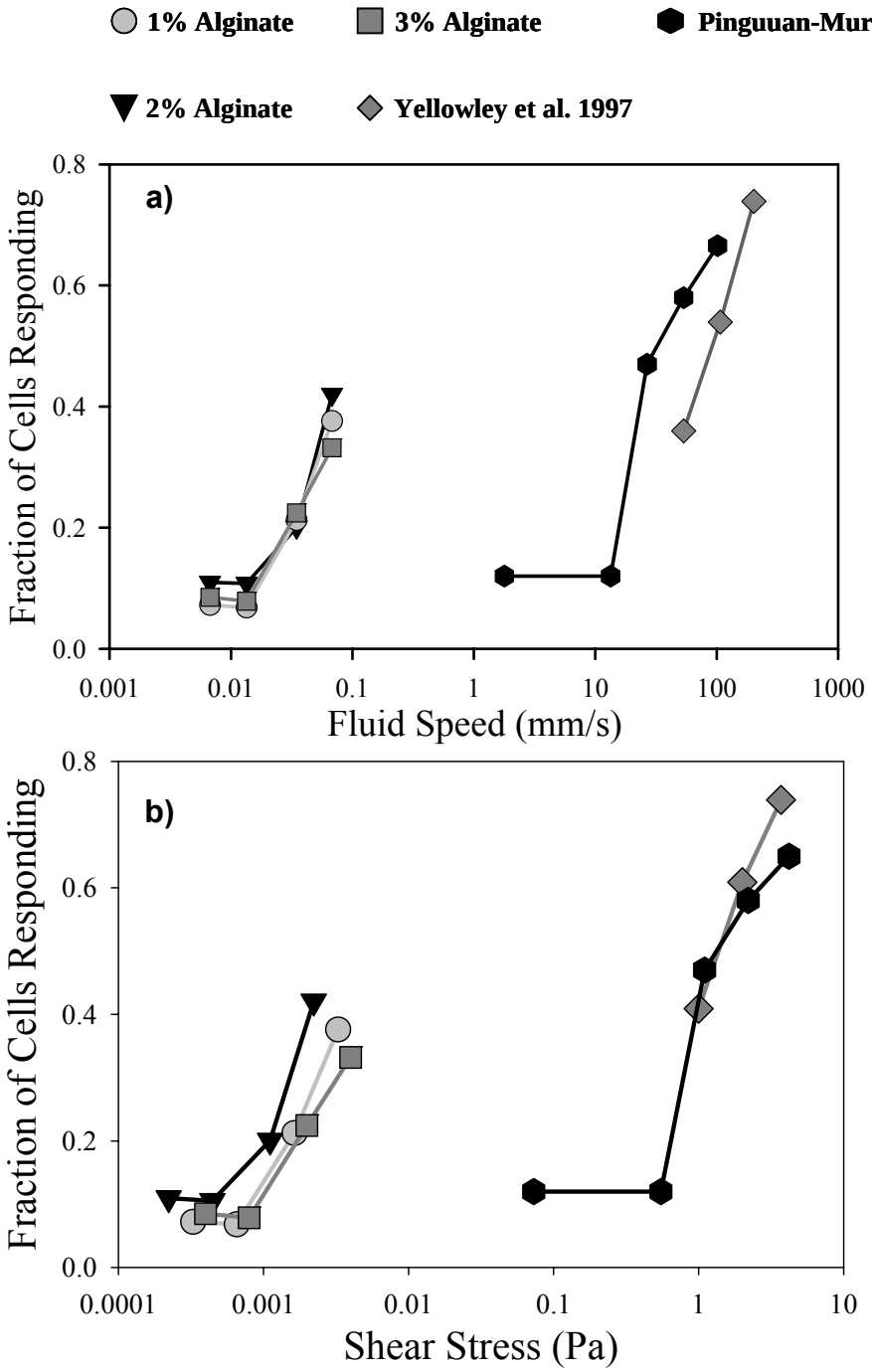

Figure 3.6: Fraction of cells exhibiting a Ca^{2+} response to fluid flow in monolayer and 3-D culture systems compared by fluid velocity (a) or wall shear stress (b)

The way in which a chondrocyte senses changes in fluid velocity, rather than shear stress or pressure, may be through the bending of its primary cilium in response to fluid flow. Primary cilia are single cytoplasmic organelles present in most fully differentiated mammalian cells [96]. It has clearly been shown that primary cilia in renal epithelial cells respond to bending from fluid flow through a Ca^{2+} signaling pathway [99] and that this response is abolished if the cilia are removed or present in an abnormal (diseased) state [100, 101]. The degree of the Ca^{2+} signaling response was proportional to the degree in which the cilium was bent. Primary cilia have also been shown to regulate response to flow in osteocytes, although this occurs independently of a Ca^{2+} signaling pathway [102]. However there is evidence that the mechanism through which primary cilia act in chondrocytes is mediated by a Ca^{2+} dependent pathway [181]. Any changes in the structure or function of these cilia in monolayer could alter their ability to sense fluid flow.

The increased sensitivity of chondrocytes to flow in 3-D alginate scaffolds may indicate that this culture method better mimics the natural environment of cartilage than monolayer culture. The change in cell shape from spherical in 3-D culture to a spread, more fibroblastic appearance in monolayer culture is accompanied by changes in phenotypic expression in chondrocytes [60, 61]. These changes in gene expression may be accompanied by changes in signaling pathways that alter the perception of the effects of fluid flow. Ca^{2+} signaling has been shown to occur in response to deformation of the cell membrane at least partially through the action of mechanosensitive ion channels [46, 47] which have also been shown to play a role in the Ca^{2+} signaling response to fluid flow [52]. In 3-D culture the entirety of the membrane surface is in contact with the perfusion medium, while in monolayer fluid

flow passes only along the exposed face of the cell, which may alter the number of ion-channels exposed to the stimulus. The increased surface area could also increase the likelihood of exposing a primary cilium to fluid flow. In addition to membrane deformation, monolayer cultured cells also receive mechanical signals through adhesion to the substrate completely separately from any external input which may attenuate their response to other stimuli [182]. A third mechanism shared by both culture systems is convective transport which increases Ca^{2+} signaling response with net fluid transport [48, 116].

In conclusion, in this study we have shown that bovine articular chondrocytes cultured in 3-D alginate scaffolds respond to perfusion with a Ca^{2+} signaling response in a flow velocity dependent manner. We have shown that this response is not altered through large changes in pressure or variations in wall shear stress. Furthermore, we have shown that the Ca^{2+} response to fluid flow occurs at fluid velocities orders of magnitude lower in 3-D culture than in monolayer. The increased sensitivity of chondrocytes in 3-D culture may be due to phenotypic mechanotransduction behavior regulated by cell shape or surface attachment.

CHAPTER 4

CHONDROCYTE CALCIUM SIGNALING RESPONSE TO FLUID FLOW IS REGULATED BY MATRIX ADHESION IN 3-D ALGINATE SCAFFOLDS

4.1 ABSTRACT

The interaction between chondrocytes and their surrounding extracellular matrix plays an important role in regulating cartilage metabolism in response to environmental cues. This study characterized the role of cell adhesion on the Ca^{2+} signaling response of chondrocytes to fluid flow. Bovine chondrocytes were suspended in RGD functionalized alginate hydrogels with ligand concentrations of 0-400 μM. The hydrogels were perfused and the calcium signaling response of the cells was measured over a range of flow rates. Attachment to RGD-alginate doubled the sensitivity of cells to low levels of fluid flow relative to unmodified alginate. At higher flow rates the contribution of cell adhesion to the observed calcium signaling response was no longer apparent. The enhanced sensitivity to flow was dependent on the density of RGD-ligand present in the scaffolds. The RGD-enhanced sensitivity to flow was completely inhibited by the addition of soluble RGD which acted as a competitive inhibitor. The results of this study expand the role of matrix adhesion to include regulating chondrocyte response to fluid flow through a calcium dependent mechanism.

4.2 INTRODUCTION

The interaction between chondrocytes and their surrounding extracellular matrix (ECM) plays an important role in regulating cartilage metabolism in response to environmental cues. Cartilage ECM interacts with chondrocytes through a number of transmembrane receptors to regulate phenotype, metabolism and response to mechanical loading [10]. For example, dynamic loading upregulates the production of ECM components by chondrocytes in cartilage explants [32, 36]. However, in non-adherent polymer scaffolds, the full effect of mechanical loading was not apparent until chondrocytes produced a pericellular matrix [79]. Understanding the mechanism through which cell-matrix adhesion alters chondrocyte response to loading is difficult due to the mechanical and biochemical complexity of cartilage ECM.

Mechanically loading cartilage creates a number of coupled stimuli that may play a role in regulating chondrocyte metabolism; these stimuli include cell deformation [174], streaming currents [38], and fluid flow [40]. For example, increased ECM synthesis was localized in regions of higher fluid flow during dynamic loading of cartilage explants and cell-seeded polymer scaffolds [34, 35, 77, 85]. However, isolating the contribution of fluid flow in cartilage is difficult due to coupling of mechanical stimuli.

Chondrocyte response to fluid flow has been studied without the confounding effects of cartilage ECM in both monolayer and 3D culture systems. Fluid flow in monolayer has been shown to regulate synthesis of matrix proteins, cytokines and catabolic enzymes [51] through a Ca^{2+} dependent pathway [48, 49, 52]. Chondrocytes cultured in 3-D hydrogel scaffolds demonstrated an elevated Ca^{2+} response [Chapter 3] and ECM synthesis [90, 91, 126] to fluid flow orders of magnitude lower than

found stimulatory in monolayer studies [48, 51, 52]. However, unlike cartilage ECM or surfaces used in monolayer culture, hydrogel scaffolds lack sites for direct cell adhesion.

Alginate, a hydrogel that does not support cell adhesion, is used extensively as a synthetic ECM for chondrocyte culture [62, 76]. In order to enable cell adhesion, alginate has been modified to present the adhesion ligand Arg-Gly-Asp (RGD) [81], an adhesion protein found on several ECM components including fibronectin and collagen type VI [183, 184]. Chondrocytes cultured on RGD-modified surfaces demonstrate significantly increased attachment in monolayer [180, 185] and increased sensitivity to mechanical loading in 3-D culture [84, 186]. These effects are reversed through competitive inhibition by soluble RGD which acts to block integrin-matrix adhesion and reverse the effects of cell attachment [13, 84, 180]. While adhesion to RGD modified scaffolds alters chondrocyte response to both static [180] and dynamic [83] matrix deformation, it's unknown if it also modulates chondrocyte response to fluid flow.

We previously demonstrated that direct perfusion increases the Ca^{2+} signaling response of chondrocytes seeded in non-adherent alginate scaffolds [Chapter 3]. Introducing RGD-alginate to this system we hypothesized that matrix adhesion regulates the Ca^{2+} response of chondrocytes to fluid flow. Specifically, the objectives of this study were to determine if adhesion altered the sensitivity of chondrocytes to fluid flow and if the adhesion-dependent response was regulated by RGD ligand density.

4.3 MATERIALS AND METHODS

Alginate Modification

Alginate hydrogels were modified with controlled densities of RGD adhesion ligands to promote cell adhesion. The peptide sequence GGGRGDY was covalently grafted to UPLVG alginate (Pronova, Sweden) using carbodiimide chemistry as described previously [81]. This surface modification procedure for attaching 10 mg RGD per 1 g of alginate was shown to produce a ligand spacing of 23 nm. The RGD-alginate was suspended in PBS at 2 wt% with final ligand densities of 400, 100, 40, and 4 μM based on previous work measuring the amount of RGD peptide incorporated into the polymer [81]. Control UPLVG alginate (0 μM RGD) was also suspended in PBS at 2 wt%.

Cell Isolation

Bovine articular chondrocytes were obtained from the femoral condyles and patellofemoral grooves of 1-3 day old calves (Gold Medal Packing; Oriskany, NY). The articular cartilage was digested overnight in 0.2 mg/mL collagenase type II (CITE) dissolved in F-12 media, 100 U/mL penicillin and 100μg/mL streptomycin at 37°C. The cells were subsequently washed and counted with methods previously established [74]. Chondrocytes were evenly suspended in alginate solutions at $10x10^6$ cells/mL.

Scaffold Preparation

Custom devices were fabricated to image chondrocyte-seeded alginate gels during perfusion and measure intracellular Ca^{2+} flux. These devices enclose

rectangular wells to maintain alginate gels with rounded ends with openings at each end for fluid movement (Fig. 4.1a). Alginate-cell suspensions were combined with $CaSO_4$ solution (20 mg/mL) in a 2:1 ratio as previously described [74]. The mixture was injected between the open chamber of the device and a sterile plate separated with 0.4 mm spacers such that the gel extended above the lip of the chamber. The plate and spacers were removed after 30 min of cross-linking and the gels were further cross-linked in 60 mM $CaCl_2$ for 30 min, washed thoroughly, and incubated in F-12 media with 100 U/mL penicillin and 100μg/mL streptomycin for 16-24 hours.

Chondrocytes were labeled with Fluo-4 AM dye (Molecular Probes; Eugene, Oregon) in order to visualize intracellular calcium. Gels were rinsed in situ with Tyrodes buffer plus 200 μM sulfinpyrazone, 5 mM glucose and 2 μM Fluo-4 AM and incubated for 25 min. The wells were then covered by glass coverslips seated on o-rings and sealed with metal plates with openings exposing the coverslips below (Fig. 4.1b). Because the gel was larger than the well in the device, the addition of the coverslip compressed the gel approximately 7% and ensured that the construct filled the chamber completely, thereby ensuring flow through the gels and not around. The devices were then connected to a syringe pump and perfused with Tyrodes buffer with 200 μM sulfinpyrazone, and 5 mM glucose.

Cell Imaging

Chondrocyte response to flow was assayed by monitoring Ca^{2+} response with confocal microscopy (LSM 510; Carl Zeiss Inc.; Jena, Germany) as previously described [Chapter 3]. Gels were imaged at depths greater than 100 μm from the surface in regions with 30 or more well-spaced cells using a 10x, 0.45 NA objective.

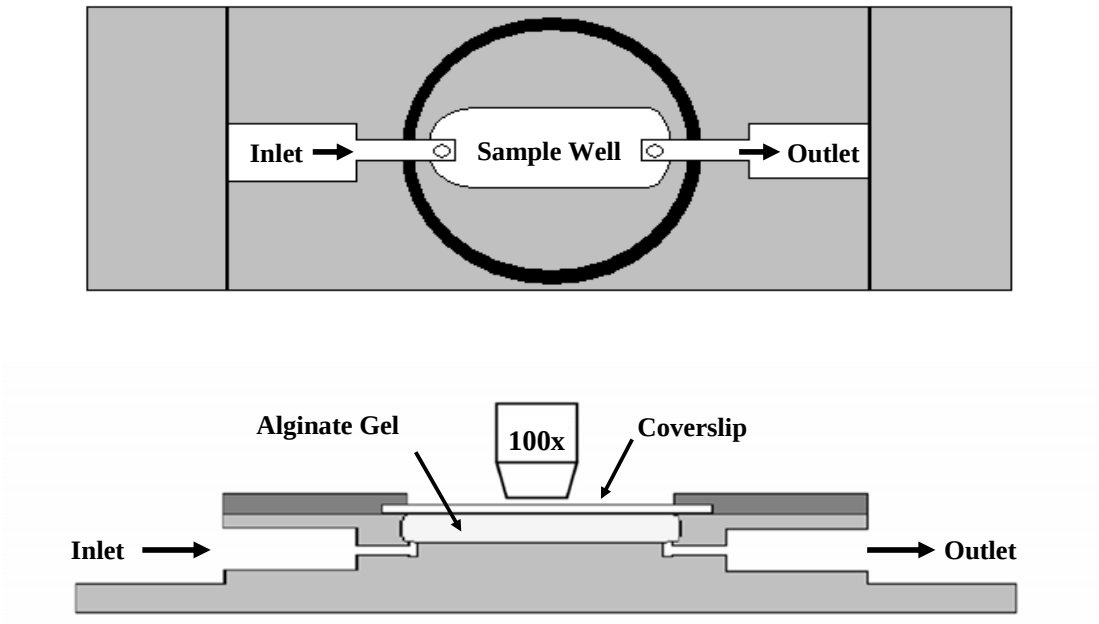

Figure 4.1: a) Empty flow device illustrating the connection between flow path and sample location; b) Cross-section of flow device loaded with alginate scaffold and sealed with a coverslip

In order to assess the effect gel compression on Ca^{2+} response during device preparation cells were imaged every 6s for 65 min immediately after sealing the devices in 0 and 400μM RGD alginate (n = 4). This process established equilibration times required to minimize the effects of strain on any responses due to transient fluid flow as well as the effect of RGD ligand on Ca^{2+} response to strain. Gels were incubated for 60 min (0 μM RGD) or 75 min (400 μM RGD) before flow experiments based on the equilibration times.

Ca^{2+} response to fluid flow was evaluated in 0, 40, and 400 μM RGD alginate for flow rates of 5-50 μL/min (n = 4-8). Before perfusing the gels, images were taken every 5 s for 4-5 min to establish a baseline signaling response and account for variation between cell sources and environmental variables. Flow was then applied and images taken every 5 s for 7-9 min for each flow rate. Fluid velocities were calculated assuming Darcy flow from the flow rate and scaffold geometry and ranged from 7–68 um/s [187]. This assumption was shown to be valid in 2 wt% alginate scaffolds at depths greater than 25 um [Chapter 2]. The effects of RGD ligand density on Ca^{2+} response to flow was more investigated in 0, 4, 100, and 400 uM RGD alginate gels with a flow velocity of 13 μm/s (n = 3-5).

In parallel studies, adhesion-dependent response to flow was evaluated in the presence of inhibition factors. Soluble RGD (0–1000 μM) was added to 100 μM RGD alginate-cell suspensions before cross-linking with the same amount added to media for the 16-24 hour incubation as previously described [180]. The Ca^{2+} response of chondrocytes with soluble RGD ligand were measured with flow of 13 μm/s (n = 3-5).

Ca^{2+} Signaling

Images were analyzed in Matlab as previously described (Fig. 4.2) [Chapter 3]. Briefly, each cell was individually tracked through the entire imaging period and its mean intensity, I(t), recorded. Ca^{2+} responses were counted by fitting the rate of change of the intensity (dI/dt) to a Gaussian distribution and defining a Ca^{2+} signaling response as dI/dt greater than 3 standard deviations above the mean. Ca^{2+} was normalized by subtracting the number of cells exhibiting a Ca^{2+} response without flow from the number of cells responding with flow and dividing by the total number of cells imaged for each device.

Statistics

The Ca^{2+} response induced by the 7% strain for 0 and 400 μM RGD alginate gels was compared by 2-way ANOVA with Student-Newman-Keuls (SNK) post-hoc analysis (SigmaStat) ($\alpha = 0.05$), and fit to a 3-parameter decaying exponential function (SigmaPlot). The effects of fluid flow for velocities of 7-68 μm/s and 0, 40 and 400 μM RGD concentrations were determined using a two-way ANOVA with SNK post-hoc analysis ($\alpha = 0.05$). Four-parameter logistic curves were fit to data from RGD ligand density studies and adhesion inhibition studies. Data are expressed as mean ± standard deviation unless otherwise indicated.

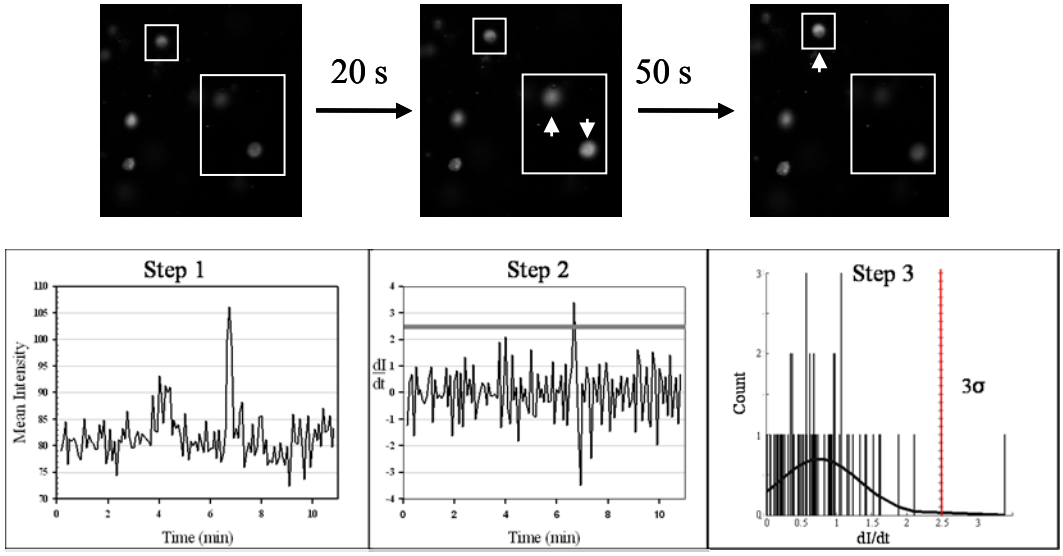

Step 1: Mean intensity measured for individual cells at each time point

Step 2: dI/dt plotted with time for each cell (analyzed individually)

Step 3: Positive dI/dt fit to a Gaussian distribution

Step 4: Ca^{2+} response defined as $dI/dt > 3\sigma$

Figure 4.2: Protocol for calculating Ca^{2+} response from fluorescent intensity of chondrocytes

4.4 RESULTS

In response to the 7% strain induced during sealing of the device, both control and RGD-alginate gel experienced elevated Ca^{2+} response that decayed exponentially with time (Fig. 4.3a), although the manner and rate of the measured response between the two were different ($p<0.001$). The response of both gels was fit to a 3-parameter exponential decay to calculate fraction of cells responding initially (max), at equilibrium (eq) and the time constant of decay (τ) (Fig. 4.3b). While the cell response was similar between the 2 experimental groups, an elevated Ca^{2+} response was maintained almost twice as long in the RGD-alginate gel.

The Ca^{2+} signaling response of the cells in the gels increased monotonically with fluid flow for fluid velocities of 13-68 μm/s ($p\leq0.001$) for all alginate gels (Fig. 4.4). Chondrocytes in 400 μM RGD gels responded to a greater degree than cells in control gels at fluid velocities of 7-35 μm/s ($p\leq0.013$). Trends were similar, but less pronounced in 40 μM gels ($p\leq0.03$) suggesting an increase in sensitivity to flow with RGD ligand density.

To investigate the effect of RGD ligand density more fully, these studies were repeated with a fluid velocity of 13 μm/s and ligand densities of 0, 4, 40, 100, and 400 μM. The increased sensitivity of chondrocytes to flow was clearly dependent on RGD concentration at and well described by a 4-parameter logistic model for 0-400 μm alginate mixtures ($R^2 > 0.99$, RMSE = 0.34) with model parameters: baseline response = 0.11, maximum response = 0.21, Hillslope = -3.1, and EC_{50} = 42 μM (Fig. 4.5).

a)

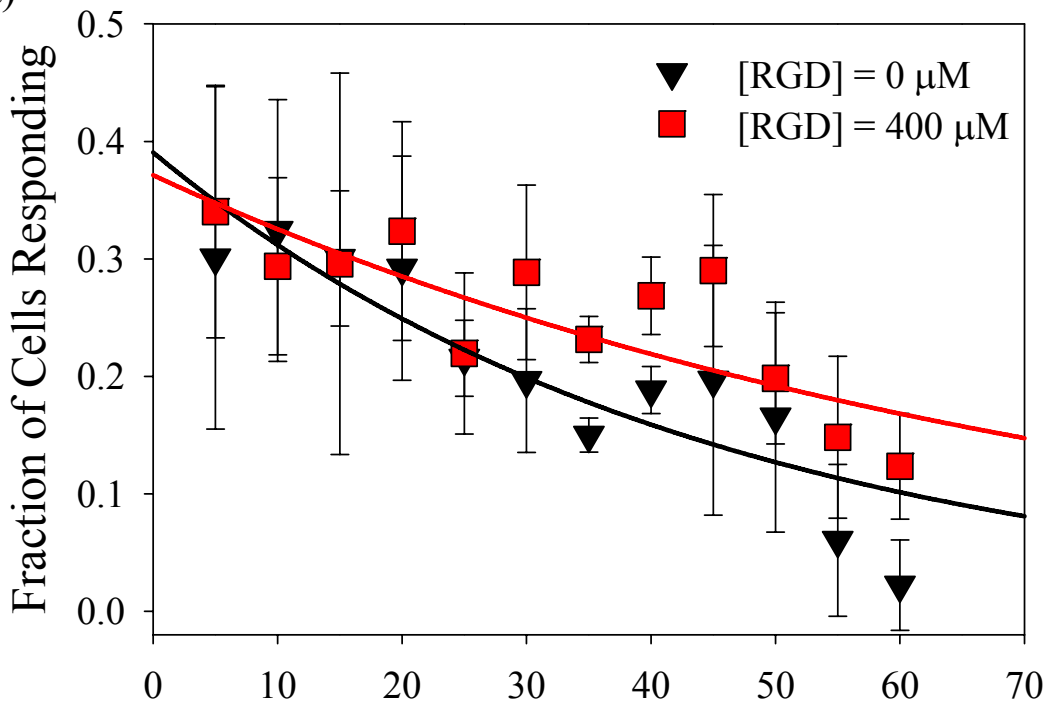

b)

[RGD]	τ (min)	max	min
0	44	0.39	0.027
400	76	0.37	0.044

Figure 4.3: a) Ca^{2+} signaling response induced by the 7% applied strain during device preparation was fit to a 3-parameter exponential decay for both 0 (R^2 = 0.8, RMSE = 4.7; n = 4) and 400 μM RGD-alginate (R^2 = 0.7; RMSE = 4.7; n = 4). The Ca^{2+} signaling response varied with RGD concentration ($p < 0.001$). b) The parameters calculated from the model fits were maximum response (max), equilibrium response (min) and time constant of decay (τ).

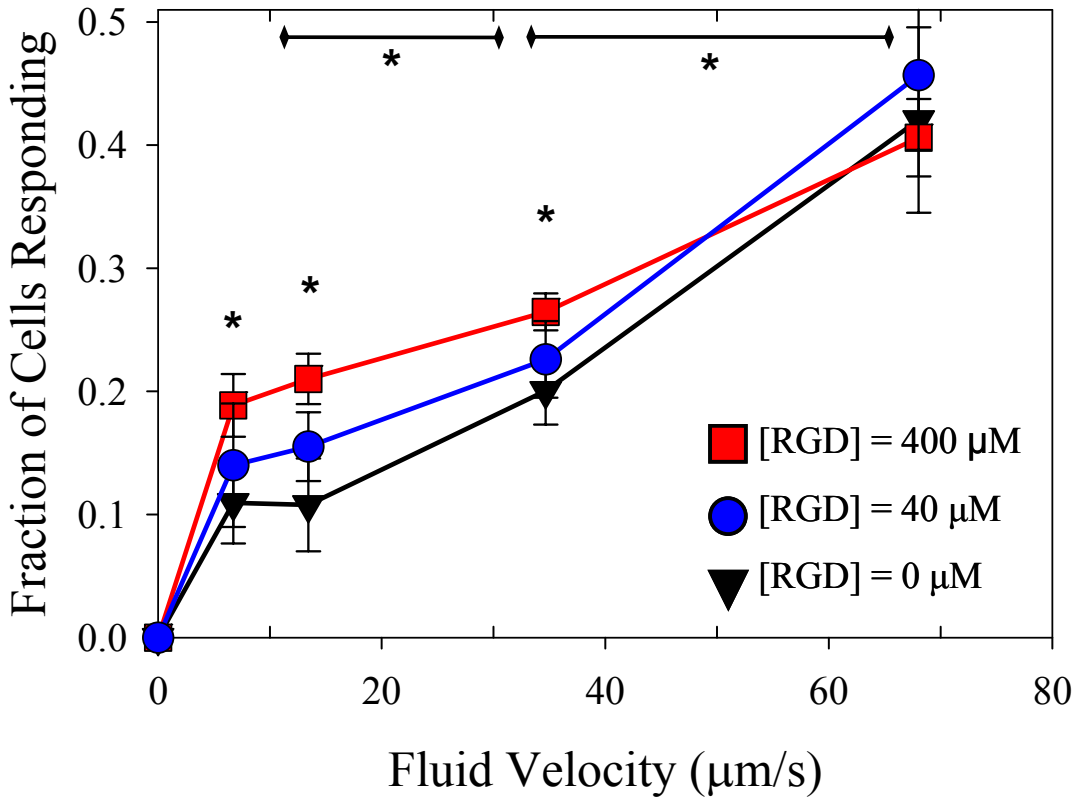

Figure 4.4: The fraction of cells showing a Ca^{2+} signaling response increased monotonically with fluid velocity from 13-68 μm/s for all RGD concentrations ($p < 0.001$; n = 4-8). Chondrocytes in 400 μM RGD-alginate were more responsive than control gels at fluid velocities of 7-35 μm/s and 40 μM RGD gels at 7 and 13 μm/s ($p < 0.02$). Increased response in 40 μM over controls was seen at 13 μm/s only ($p = 0.04$).

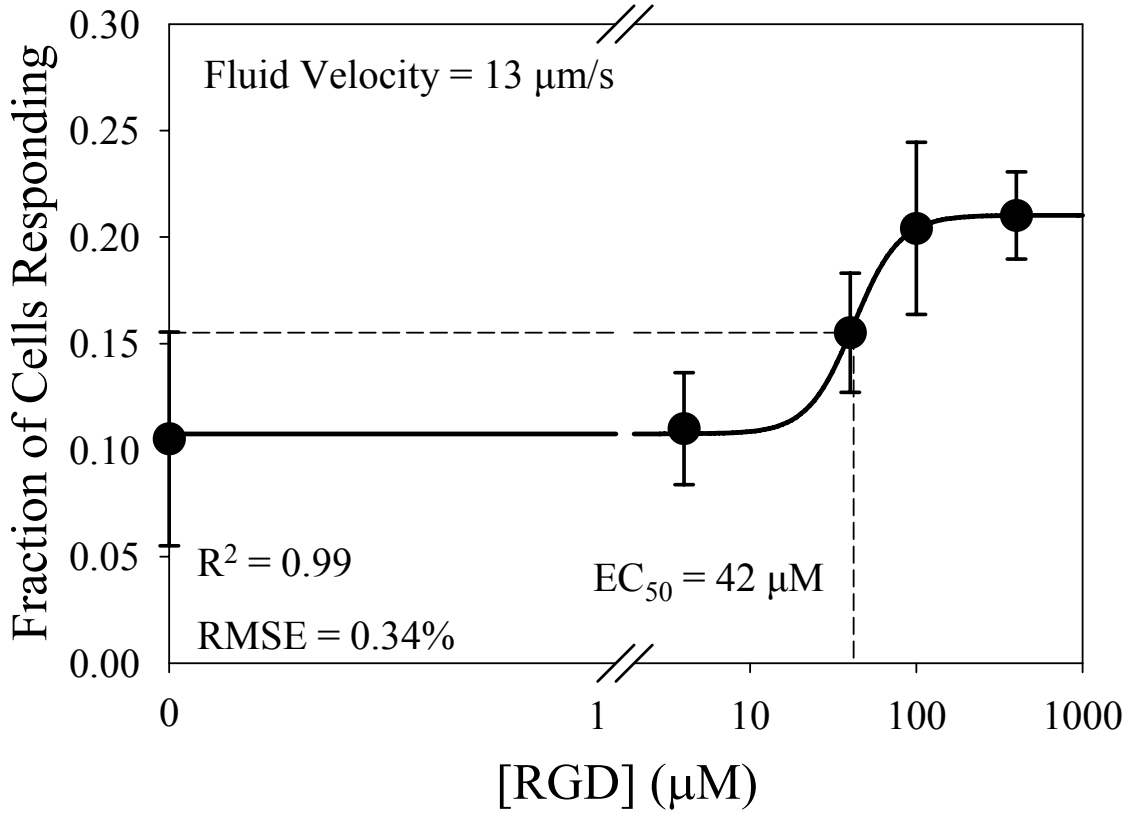

Figure 4.5: Ca^{2+} response of chondrocytes to scaffold-bound RGD ligand at 13 μm/s was concentration dependent and well described by a 4-parameter logistic model (R^2 = 0.99; n = 3-5). The model parameters calculated were maximum response = 0.21, minimum response = 0.11, Hillslope = -3.1, and EC_{50} = 42 μM.

The enhanced sensitivity of chondrocytes to fluid flow in 100 μM RGD-alginate was eliminated upon saturation with soluble RGD (Fig. 6) to levels seen in unmodified alginate under perfusion (Fig. 4.4). This response was also well described by a 4-parameter logistic model for soluble RGD concentrations of 0-1000 μM (R^2 = 0.98, RMSE = 1.14) with model parameters: baseline response = 0.11, maximum response = 0.22, Hillslope = 59, and IC_{50} = 99.4 μM.

4.5 DISCUSSION

In a previous study we demonstrated that direct perfusion altered the Ca^{2+} signaling response of chondrocytes to fluid flow in alginate scaffolds in a fluid velocity dependent manner [Chapter 3]. Other studies demonstrating that cell adhesion and response to mechanical loading was regulated by RGD ligand density [83, 188-191] led to the hypothesis that cell-matrix adhesion regulates the chondrocyte response to fluid flow. By altering both the flow rate and RGD density we found that chondrocytes respond to fluid flow through a mechanism partially regulated by cell adhesion.

Studies have shown that chondrocyte adhesion to its matrix allows cells to sense their mechanical environment and respond to changes in substrate stiffness or deformation [83, 84, 145, 180, 190-192]. Chondrocytes in RGD-alginate were more sensitive to small strains which had no significant effect on cells in control alginate [84]. This enhanced sensitivity to small strains was seen in the increased equilibrium Ca^{2+} signaling response after gels were compressed during device preparation (Fig 4.3). While effects of static deformation were recorded for a relatively short period of

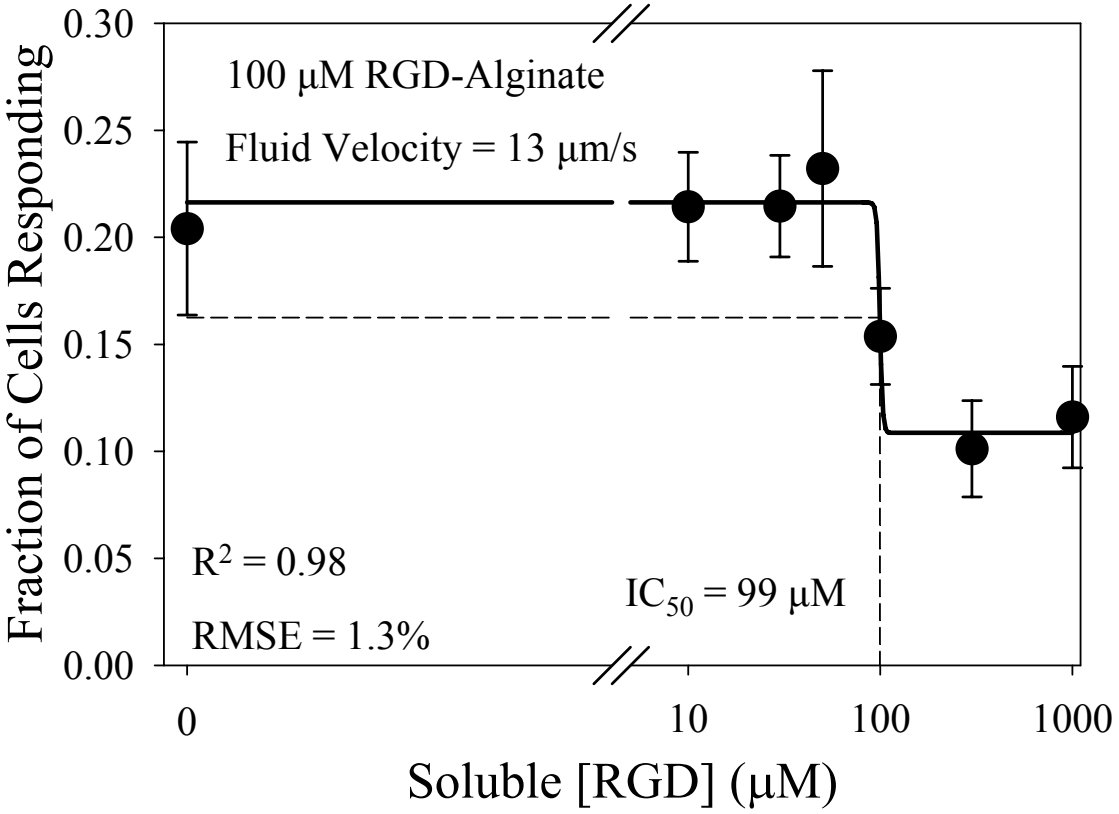

Figure 4.6: The enhanced sensitivity of chondrocytes to fluid flow at 13 μm/s in 100 μM RGD-alginate was eliminated upon saturation with soluble RGD and well described by a 4-parameter logistic binding model (R^2 = 0.98; n = 3-5). The model parameters calculated were maximum response = 0.22, minimum response = 0.11, Hillslope = 59, and IC_{50} = 99 μM.

time in this study compared to others (12 hours – 41 days) [32, 36, 77, 84] the anti-anabolic effects of static compression may be mediated through a Ca^{2+} dependent mechanism and maintained through cell-matrix interactions.

Cell adhesion altered the Ca^{2+} signaling response of chondrocytes to fluid flow and was regulated by both fluid velocity and RGD concentration (Fig. 4.4). Ca^{2+} signaling increased monotonically with fluid velocity. However the enhanced sensitivity to flow was only seen at low and intermediate fluid velocities and disappeared at the highest fluid velocity and appeared dependent on RGD density.

As such, we investigated the concentration dependence of the Ca^{2+} response at a fluid velocity where the enhanced sensitivity was most pronounced (Fig. 4.5). The signaling response demonstrated clear concentration dependence with an EC_{50} = 42 μM RGD. To further characterize the cell adhesion-dependent response flow studies in 100 μM RGD-alginate were carried out in the presence of soluble RGD ligands (Fig. 4.6). Soluble RGD inhibited Ca^{2+} signaling in a dose-dependent manner such that at saturation the Ca^{2+} response was similar to that in control alginate. The IC_{50} of inhibition (99 μM) was similar to the concentration of scaffold-bound RGD (100 μM) which could indicate that the binding affinities of bound and unbound RGD are similar, though only if integrin binding to both ligands is of the same order.

RGD ligand density has been shown to regulate the formation of signaling complexes in cells by altering the degree of cell attachment and spreading [191, 193, 194]. Adhesion via RGD ligand occurs through integrins, cell adhesion proteins which, upon binding to RGD ligands, cluster and form focal adhesion complexes [195, 196]. These focal adhesion complexes are associated with numerous signaling pathways and believed to mediate mechanotransduction of environmental cues to cells

[197-199]. RGD density directly altered cell response to environmental cues in a dose dependent manner in both monolayer [191] and 3-D hydrogel culture [190]. An average minimum RGD spacing of 440 nm was required for integrin mediated adhesion and an average spacing of 140 nm for focal adhesion formation for fibroblasts in monolayer culture [191]. Assuming that 1-D ligand spacing shown for the RGD formulations in monolayer [81] directly translates to 3-D alginate culture and that RGD ligands were all equally available for binding, the enhanced sensitivity of chondrocytes to fluid flow occurred with a minimum average RGD spacing of 230 nm (40 μM); the maximal enhancement occurred with an average RGD spacing of 92 nm (100 μM) or less. While focal adhesion complexes are not seen in cells cultured in 3-D scaffolds, the relationship between cell response and RGD density is suggests a related signaling mechanism.

The results of this study are novel in that they expand the mechanical signaling pathways regulated by substrate adhesion to include fluid flow, a stimulus not commonly associated with cell adhesion. The enhanced sensitivity of chondrocytes to non-saturating levels of fluid flow in RGD-alginate was mediated by Ca^{2+} dependent pathways and dependent on scaffold-bound ligand density. This system represents a novel vehicle for exploring the signaling pathways activated downstream of the adhesion-mediated Ca^{2+} response and their association with mechanisms governing chondrocyte response to other types of mechanical stimuli.

CHAPTER 5

CONCLUSIONS

Fluid flow is an important mediator of metabolic function for a number of cell and tissue types, although the mechanisms driving this response are not yet clear [34, 85, 89-91, 146-154]. This dissertation presents investigations to characterize the mechanical forces generated by flow in 3-D alginate scaffolds and their effects on metabolic signaling pathways in articular chondrocytes. Chapter 2 details a novel technique to measure fluid velocity in porous alginate hydrogels and uses the flow profiles generated to compare existing mathematical descriptions of fluid flow. Chapter 3 investigates the effects of fluid flow through porous alginate scaffolds on chondrocyte metabolic response and relates the observed response to specific mechanical stimuli. Chapter 4 examines the role of cell-matrix interactions on the metabolic response of chondrocytes to fluid flow through RGD-modified alginate scaffolds. This chapter discusses some of the major findings and presents future studies.

The study presented in Chapter 2 documents the development and validation of a novel technique to visualize fluid velocity profiles in porous scaffolds. Previous approaches have been presented which can track fluid in porous scaffolds, but are limited by spatial and temporal resolution [120-125]. This technique demonstrated a spatial resolution an order of magnitude greater than any shown previously. Fluid visualization of perfused alginate scaffolds demonstrated boundary layer regions of flow containing velocity gradients that approached a steady-state value in the bulk of

the gels. The thickness of these boundary layers increased with permeability, approaching 10% of the total scaffold thickness in the most permeable scaffolds. The significance of this study in the area of flow through porous media in general and tissue engineering in particular is that these boundary layer thicknesses are not adequately predicted by existing models of flow [119, 140, 142, 163, 165].

There have been no previous studies to measure the flow profile present in cartilage or materials used scaffolds for 3-D culture of chondrocytes. Much of the current work modeling boundary layer flow in cartilage or tissue engineered scaffolds is based on a several models of flow through these materials rather than empirical evidence [119, 140, 142, 163, 165]. Verifying the actual depth of the boundary region for a porous scaffold becomes particularly important as permeability increases. Several scaffolds used as tissue analogues have permeabilities of 9e-15 to 2e-12 m^2 [167-171]. Based on flow behavior in alginate gels, these scaffolds could have boundary layer thicknesses from 40 μm through the entirety of the scaffold. Therefore it is essential that the flow profiles be directly measured to accurately define physical stimuli imposed on cells in perfused 3-D scaffolds.

The work presented in Chapter 3 demonstrated that fluid flow modulates a Ca^{2+} dependent metabolic signaling pathway in chondrocytes seeded in alginate scaffolds. These findings are significant as an extension of previous monolayer culture studies [48, 51, 52] into a more physiologically relevant model of cartilage.

The effects of mechanical forces generated by fluid flow on metabolic response were decoupled through careful characterization of alginate gels. Specifically, hydrostatic pressure, wall shear stress, and fluid velocity were decoupled from flow rate. The metabolic response generated by direct perfusion of alginate scaffolds was

found more dependent on the magnitude of the fluid velocity and not on the hydrostatic pressure or shear stress induced by flow. Further, the fluid velocities shown to stimulate Ca^{2+} signaling pathways were 2 orders of magnitude lower in alginate gels than in monolayer culture [48, 52] and similar to estimated velocities found stimulatory in tissue explants and 3-D scaffolds [34, 85, 91]. This variation in sensitivity may be related to the differences seen in gene expression and ECM synthesis as chondrocytes are cultured in monolayer or non-adhesive hydrogel culture [60, 61]. Taken together, these findings strongly suggest that chondrocyte metabolic response to physical stimuli is a phenotype specific behavior which may be regulated by cell shape or surface attachment.

This hypothesis was examined in Chapter 4 by seeding chondrocytes in RGD-modified alginate gels which facilitate cell adhesion. The major finding of this study was that chondrocytes response to fluid flow through calcium-dependent signaling pathways was partially regulated by cell-matrix interactions. Many studies have examined the role of cell-matrix interactions in mechanical signaling pathways to substrate mechanics and dynamic strain [83, 84, 180, 185, 186]. The data strongly indicated that chondrocytes were responsive to stretch-induced deformation from spreading in response to mechanical loading or altered substrate stiffness. The major contribution of this study to the field of chondrocyte mechanotransduction is that it extends the role that substrate adhesion plays in mechanosensing to include fluid flow which is not normally associated with cell adhesion.

Chondrocytes demonstrated a heightened sensitivity to non-saturating levels of fluid flow in RGD-alginate compared to controls with an increased Ca^{2+} signaling response. This metabolic response was found dependent on RGD ligand density and

may be related to the formation of focal adhesion complexes believed to mediate mechanotransduction of several environmental and mechanical cues [197-199]. Cell adhesion and the formation of focal signaling complexes is dependent on adhesion ligand density [191, 193, 194]. The spacing required to maximally enhance sensitivity to fluid flow in this study was 92 nm, similar to the spacing required to form complete focal adhesion complexes in fibroblasts [191]. While focal adhesion complexes are not seen in cells cultured in 3-D scaffolds, the relationship between cell response and RGD density suggests a signaling mechanism which may be related.

While a few studies have utilized fluid flow in perfusion bioreactors to culture 3-D engineered constructs [89-91], none have investigated the specific mechanisms by which chondrocytes sense and respond to this stimulus within one system. In previous studies, these stimulatory fluid flows were not directly measured, but rather estimated based on bulk properties or computational models of flow in porous media. Using the technique introduced in this dissertation (Chapter 2) fluid flow can be experimentally measured and the physical stimuli generated by perfusion of cell-seeded scaffolds can accurately defined (Chapter 3). The studies documented within this dissertation confirm that the velocity of the fluid (Chapter 3), rather than wall shear stress, altered the metabolic response of chondrocytes seeded in 3-D porous scaffolds. In addition, the modulation of this response through cell-matrix adhesion via integrins, in combination with the dependence on ligand density, strongly suggests that focal adhesion complexes play a significant role in mechanotransduction due to fluid flow (Chapter 4). Understanding the mechanisms through which chondrocytes sense and respond to mechanical loading is an important consideration in designing scaffolds

tissue engineered cartilage as and targeting potential therapeutics to counteract the effects of injury or disease.

5.1 FUTURE DIRECTIONS

In exploring the response of chondrocytes to fluid flow in 3-D culture the findings described in this dissertation present several avenues for future research. This section presents other areas of investigation which could be pursued to better understand the role of fluid flow in regulating chondrocyte metabolism.

Experimental measurement of cartilage material properties

The use of finite element models to predict fluid flow in articular cartilage during has been implemented to better understand the mechanical forces generated within the tissue for a number of loading conditions [177, 200-204]. Incorporating the anisotropy of material properties present in cartilage, specifically permeability variation, is difficult with current methods. These measurements are typically made to describe the permeability in the bulk of the tissue and may not accurately depict local properties [163, 165] which can vary across the full thickness [127-130]. Measurements of fluid velocity and the development of the flow profile for the various regions of articular cartilage would provide an experimental measurement for implementation of new or updated computational models of cartilage. In particular, using the flow profiles to generate maps of the boundary layer of the tissue would provide a noninvasive analysis of relative local permeability throughout. Applying this technique to flow through or around the pericellular matrix would also be of value. The permeability of this specialized ECM has been measured and compared to the

surrounding matrix [105]. However, measuring the fluid flux in this region in conjunction with material property data facilitates calculation of the forces acting upon chondrocytes.

Investigate the role of streaming current on the calcium response to fluid flow

Cartilage ECM is contains a large amount of fixed negative charge which is normally ionized by positive counter ions from the surrounding fluid [3]. As this fluid is forced through the tissue, as occurs during mechanical loading, a streaming current is created may regulate chondrocyte metabolism [38-40]. By controlling the electrokinetic properties of alginate scaffolds, another stimulus can be used to study mechanical signaling pathways induced by fluid flow. An unpublished study recently introduced covalently crosslinked alginate gel doped with silica microparticles as a cell scaffold which is capable of introducing streaming current upon loading [205]. Incorporating this scaffold into the flow experiments introduced in this dissertation would allow the effects of various charge densities, fluid velocities, and streaming currents to be investigated independently (Appendix E).

Understanding the signaling pathways governing response to fluid flow

Another avenue of inquiry focuses on the adhesion mediated mechanosensation and the possible mechanisms governing this response. Further work on this topic should focus on characterizing on the mechanism by which cell adhesion in a 3-D substrate might mediate a metabolic response. Studies of integrin binding and formation of focal adhesion complexes in 3-D culture indicate that the mechanisms of adhesion may differ from that seen in monolayer [59]. Specifically, the fibroblast 3-D

"matrix adhesions" demonstrated a different structure, localization, and function from focal adhesions studied in monolayer. Therefore, labeling focal adhesion complex proteins and markers in both 3-D and monolayer culture of chondrocytes may demonstrate a mechanism for the enhanced sensitivity to flow in 3-D culture. Furthermore, identifying the signaling molecules downstream of the integrin-mediated Ca^{2+} response observed here and the specific metabolic changes they initiate should also be a research goal.

APPENDIX A

ANALYZING IMAGE DATA FROM FAST CONFOCAL MICROSCOPY: TRACKING FLUID FLOW IN POROUS ALGINATE SCAFFOLDS

INTRODUCTION

Flow visualization in scaffold-free and alginate filled devices (Chapter 1) was possible due to the ability of the fast, line-scanning, confocal microscope (LSM 5 Live; Carl Zeiss Inc.; Jena, Germany) capable of imaging up to 120 frames per second (fps). The devices were perfused with a fluorescein solution at various flow rates and fluid flow was visualized by photobleaching a one pixel-wide line for 300 ms and imaging at 60 fps (scaffold-free) or 100 fps (alginate scaffolds) perpendicular to the flow direction in the center of the field of view. In order to track the location of the photobleached line with time the images were analyzed in Matlab by tracking the location of the intensity minimum and the analysis was based on a model of diffusion with photobleaching and a constant drift term to account for convective flow (Eq. 3)

$$I(y,t) = \frac{A}{\sqrt{Dt}} \exp\left(\frac{-(y-ut)^2}{4Dt}\right) \quad (1)$$

where I = local image intensity, u = drift velocity, D = diffusion constant, t = time and A = constant dependent on photobleaching intensity. Using this model we modeled fluid velocity as a linear relationship between the tracked location of the intensity minima and the timestamps of the images.

Methods

In order to analyze the images tracking the movement of fluid a prexisting Matlab code [162] was modified. This preexisting code was used to track the displacement of multiple photobleached lines and was altered to track and analyze only one. Before the images were analyzed they were converted to an *.avi format. Twenty images were taken before photobleaching began to provide a baseline of

intensity values. The intensity of all pixels for the images taken after photobleaching was divided by the average intensity of these first 20 images in order to normalize the data. Outputs from this analysis include figures of intensity distribution for each image in the direction of flow and a plot of location versus time with a linear best-fit line plotted. In addition, a value for the calculated velocity and prediction bands for the calculation are provided as well.

Analysis Script

```
%This program tracks a horizontal photobleached line to determine flow as a function of x-position (FMOUNT, Flow Measurement of Optically Unresolvable Nanoscale Tracers)
%Written by Mark Buckley in December, 2008
 directory='F:\mrbuckle\LSM Databases\FLOW_090312.mdb\gel2.mdb\';
% SET DIRECTORY FOR LOCATION OF *.MDB FILE
avifile=([directory,'50upm_zeq100um']) %Don't add the .avi to this file name!
%CHANGEABLE
% convert to avi in ImageJ or LSM viewer
firstimage=501; %First image during period before photobleaching
%CHANGEABLE
nPBimages=20;  %Number of images taken before photobleaching
%CHANGEABLE
nimages=50;    %Number of images to analyze after photobleaching
%CHANGEABLE
ntiles=1; %Number of image tiles to analyze (put together into one giant image)
imagedelta=220; %Spacing between first image to analyze for each tile
 um_per_pix=1.24;  %CHANGEABLE
fps=100; %check this in the LSM software  %CHANGEABLE
frequency=0.1; %Oscillation frequency in Hz.
 horizontalthickness=512; %horizontal thickness of analyzed region in pix.  Should be a factor of the horizontal image size (usually 512)
overlap=0;
 minimathickness=15;
 maxmindisp= 20;
%%%%%%%%%%%%%%%%%%%%
 lastimage=firstimage+nPBimages-1 + nimages*ntiles + imagedelta*(ntiles-1);
period= 1/(frequency);
sec_per_frame=1/fps;
close all;
 clear fullimage0; clear fullimage; clear key; clear key2;
lastkey='i'; lastkey2='m';
 % OPEN IMAGES
 fullmovie=aviread(avifile,firstimage:lastimage);
```

```
 % APPLY GAUSSIAN BLUR TO ALL IMAGES
 for lala=1:length(fullmovie)
    filtyo = fspecial('gaussian',10,3); %create the Gaussian filter (4 x 4 pixels)
    fullmovie(lala).cdata=imfilter(fullmovie(lala).cdata,filtyo);
end
% END APPLY GAUSSIAN BLUR TO ALL IMAGES
 % Average first images before firstimage+nPBimages to divide out by
imagesum=0;
for m=1:ntiles;
    for i = 1:1:nPBimages
        imagenumber=i+(m-1)*imagedelta;
        image=fullmovie(imagenumber).cdata;
        imagesum=imagesum+double(image);
    end
    currentimage=imagesum/(nPBimages);
    currentcolormap=fullmovie(imagenumber).colormap;
    imagesum=0;
    if m==1
        image0=currentimage;
        fullimage0=currentimage;
        colormap0=currentcolormap;
    else
        fullimage0=cat(2,currentimage,fullimage0);
    end
end
 %Open initial photobleached images for display
for m=1:ntiles;
    imagenumber=1+nPBimages+(m-1)*imagedelta;
    currentimage=fullmovie(imagenumber).cdata;
    currentcolormap=fullmovie(imagenumber).colormap;
    if m==1
        imageSHOW=currentimage;
        fullimageSHOW=currentimage;
        colormapSHOW=currentcolormap;
    else
        fullimageSHOW=cat(2,currentimage,fullimageSHOW);
    end
end
 %Analyze subsequent images taken after some time period of line
%photobleaching.  Sequences of meanover images will be averaged over, and
%the minimum intensity over horizontal lines as a function of vertical
%distance will be found
 imagesc(fullimageSHOW)
colormap(colormapSHOW);
response=input('Do you want to mask out a region on the right (R) or left (L) side of
these images (R/L/N)? ','s');
if (response=='R' | response=='r')
```

```
    disp('Click on the x position of the left edge of the region to be masked. ');
    [xinput,yinput]=ginput(1);
    xinput=double(round(xinput))
    farright=horizontalthickness*floor(xinput/horizontalthickness);
    leftx=0;
elseif (response=='L' | response=='l')
    disp('Click on the x position of the right edge of the region to be masked. ');
    [leftx,lefty]=ginput(1);
    leftx=double(round(leftx));
    xinput=512*ntiles;
    farright=horizontalthickness*floor(xinput/horizontalthickness);
 else
    xinput=512*ntiles;
    farright=horizontalthickness*floor(xinput/horizontalthickness);
     leftx=0;
end
nlines=input('How many photobleached lines would you like to track? ');
disp('Click on the initial y position of each photobleached line at the rightmost edge of
the unmasked region. ');
[firstx,firsty]=ginput(nlines);
for linenum=1:1:nlines
    close all;
    clear minloc; clear pk2pkamp; clear predominantamplitude; clear midbox; clear
currentimage; clear imagenumber;
    clear mea_ranged; clear shift_deg; clear dataminloc_first; clear initialleftedge;
initialleftedge=-Inf;
    imagesum=0;
    countyo=0;
    imcount=0;
     for p=farright+horizontalthickness:-1*(horizontalthickness-
overlap):mod(farright,horizontalthickness)+horizontalthickness
        clear a0; clear a1; clear b1; clear c1;
        if p>farright
            if xinput==512*ntiles
                initialleftedge=Inf;
                continue
            end
            rightedge=xinput;   %this statement is overruled if the statement below isn't
commented out
            rightedge=horizontalthickness*floor(xinput/horizontalthickness); %get rid of
this if you don't need equally spaced depths
            leftedge=p-2*horizontalthickness+1; %change 2 to 1 and comment out the line
above you want to analyze a partial window near the edge of the masked region
            initialleftedge=leftedge;
            if leftedge>=rightedge
                continue
            end
```

```
        else
           rightedge=p;
           leftedge=p-horizontalthickness+1;
           if leftedge>=initialleftedge
              continue
           end
        end
        if (p-horizontalthickness+1)<leftx
           rightedge=p;
           leftedge=leftx;
        end
        disp(' ');
        disp(['TRACKING PHOTOBLEACHED LINE #',int2str(linenum)]);
        disp(['Right edge (pixels)=',int2str(rightedge)]);
        disp(['Left  edge (pixels)=',int2str(leftedge)]);
        disp(' ');
        countyo=countyo+1;
        if countyo==1;
           lasty=round(firsty(linenum));
        else
           lasty=dataminloc_first(countyo-1);
        end
        midbox(countyo)=(rightedge+leftedge)/2;
 %Analyze subsequent images taken after some time period of line photobleaching.
Sequences of meanover images will be averaged over, and the minimum intensity over
horizontal lines as a function of vertical distance will be found
        clear('minloc');
        for i = 1+nPBimages:nPBimages+nimages
           imcount=imcount+1;
          for m=1:ntiles;
              imagenumber=i+(m-1)*imagedelta;
              currentimage=fullmovie(imagenumber).cdata;
             if m==1
                 fullimage=currentimage;
              else
                 fullimage=cat(2,currentimage,fullimage);
              end
             end
           fullimage=double(fullimage)./fullimage0; %Divide out initial images
           if mod(i,25)==0
              disp(['Analyzing image ',int2str(i),'...'])
           end
%mean intensity over horizontal lines as a function of vertical distance
           mea=mean(fullimage(:,leftedge:rightedge)')';
           y=[1:1:size(fullimage,1)]';
            mea_nearmin=mea(max(1,lasty-maxmindisp):min(512,lasty+maxmindisp));
```

```
mea_nearmin_minloc=round(mean(find(mea_nearmin==min(mea_nearmin))));
          dataminloc=mea_nearmin_minloc+max(1,lasty-maxmindisp)-1;
          if imcount==1
             dataminloc_first(countyo)=dataminloc;
          end
         mea_ranged=mea(dataminloc-
minimathickness:1:dataminloc+minimathickness);
          y_ranged=y(dataminloc-minimathickness:1:dataminloc+minimathickness);

 %FIT A PARABOLA TO THE INTENSITY PROFILE NEAR THE MINIMUM
          [meafit,rsquare1]=fit(y_ranged,mea_ranged,'Poly2');
%location in pixels of the minimum of the curvefit
          minloc(imcount)=(-0.5)*meafit.p2/meafit.p1;
          %FIT A GAUSSIAN TO THE INTENSITY PROFILE NEAR THE
MINIMUM
meafit_ranged=meafit(y(dataminloc-
minimathickness):0.1:y(dataminloc+minimathickness));    %USE THIS!

          %PLOT INTENSITY PROFILES AND FITS TO MINIMA
         if (lastkey=='i')
             figureyo=figure;
             hold on
             box on
             plot(y,mea)
             plot(y(dataminloc-
minimathickness):0.1:y(dataminloc+minimathickness),meafit_ranged,'-k')
             plot(minloc(imcount),mea(round(minloc(imcount))),'*r','MarkerSize',20)
             xlabel('Y (Pixels)')
             ylabel('Mean Intensity')
             legend('Experimental Data','Local 2nd Order Polynomial Fit')
             legend('Experimental Data','Local Gaussian Fit')
             whattodo=input('Would you like to continue plotting intensity profiles (enter
for yes, n for no)? ','s');
             if (whattodo=='n' | whattodo=='N')
                lastkey='c';
             else
                lastkey='i';
             end
          end
          if (lastkey=='c')
             close all
          end
       lasty=mean(dataminloc);
       end
       imcount=0;
        minloc=(minloc*um_per_pix)';
        frame=[1:1:length(minloc)];
```

```
      time=frame'*sec_per_frame-sec_per_frame;

 %CALCULATE THE TIME ELAPSED SINCE IMAGING BEGAN AT THE
SURFACE (I.E., IMAGING BEGAN AT T=0)
      absolutetime=time+(nPBimages)*sec_per_frame;
   % FIT A LINE TO MINLOC
       frame=[1:1:length(minloc)]';
       time_s=frame/fps;
      [minlocfit,rsquare2]=fit(time_s,minloc,'poly1')
      % OUTPUT DATA TO SCREEN
      time_s;
      minloc;
    if lastkey2 =='m'%Plot minloc and sine fit if user types m
         figure1=figure;
         hold on
         box on
         plot(time_s,minloc)
         plot(minlocfit,'-k')
         xlabel('Time (Seconds)')
         ylabel('Y Location of Intensity Minimum (\mum)')
         legend('Experimental Data',['Linear Fit, Slope = ',num2str(minlocfit.p1)])
         whattodo2=input('Would you like to continue plotting line trajectories and fits
(enter for yes, n for no)? ','s');
         if (whattodo2=='n' | whattodo2=='N')
            lastkey2='c';
         else
            lastkey2='m';
         end
      end
      if lastkey2 =='c'
         close all
      end
%FIND THE DISPLACEMENT VS. TIME AT THE SURFACE TO COMPARE TO
THE PIEZO AND FORCE SIGNALS
      if countyo==1;
         surfminloc=minloc;
      end
   %FIND THE PHASE USING A LOCAL SIN FIT VERY CLOSE TO THE
MAXIMUM (ADDED 9/12/08)
      if (p-horizontalthickness+1)<leftx
         break
      end
  end
end
if nlines > 1
end
```

APPENDIX B

FITTING BRINKMAN-EXTENDED DARCY MODEL TO FLOW PROFILE MEASUREMENTS IN 3-D POROUS MEDIA

INTRODUCTION

The mathematical representation of flow in porous media is generally simplified by Darcy's law, which is a very good descriptor of macroscopic flow. However, this model is limited when describing flows accompanied by boundary and inertial effects [206]. Darcy's (Eq.1) is valid for isotropic and macroscopically homogenous porous media in the form

$$\langle v \rangle_i = -\frac{K}{\mu}\frac{\partial p}{\partial X_i} \tag{1}$$

where ‹v› is the average velocity, K is the permeability tensor, μ is the dynamic viscosity, p is the pressure and X is the space variable. In highly permeable porous media viscous effects due to drag at the boundary are significant and must be accounted for when describing flow profiles.

Brinkman (1947) [119] introduced a modification of the existing Navier-Stokes equation that described flow through low densities of fixed particles or fibers under specific conditions. Since the Brinkman's equation is a modification of the preexisting Navier-Stokes model of flow it was fairly easy to incorporate it into existing analytic tools. It states:

$$\frac{\partial p}{\partial X_i} = \frac{\mu}{K}\langle v \rangle_i + \mu_e \Delta_X \langle v \rangle_i \tag{2}$$

where μ_e is an effective viscosity which may be different than μ, though is often assumed equal. This model has been used to describe flow through several types of porous media [135, 136, 139, 140, 206] despite data suggesting that its application may not be valid in certain types of porous media [122, 135, 139]. One area wherein accurately describing fluid flow is of interest is cartilage. Brinkman's equation has been used to model flow through this dense tissue, but has not been experimentally verified [140].

In another approach to describing flow in boundary regions, Darcy's law was modified to more accurately predict a continuity in shear stress and fluid velocity near the scaffold-fluid interface [143] and accurately described nonlinear flow in the boundary region transitioning to Darcy flow in the bulk of the material [142]. This model, called Brinkman-extended Darcy, is based on the relationship between permeability and scaffold thickness normal to flow. The solution of Brinkman-extended Darcy used in this study is of the form

$$v(d,\sigma) = \frac{Q\cosh\frac{1}{2\sigma}}{\cosh\frac{1}{2\sigma} - 2\sigma\sinh\frac{1}{2\sigma}}\left\{1 - \frac{\cosh\left[\left(d-\frac{1}{2}\right)/\sigma\right]}{\cosh\frac{1}{2\sigma}}\right\} \qquad (3)$$

where v = velocity, d = depth, Q=flow, σ = Darcy number (k/h^2), h = chamber height (m), and k = permeability (m^2).

However, the extent to which either Brinkman-Darcy or Brinkman's formulation describe flow in porous materials typically used for cell culture is not known. Chapter 1 described the experimental technique used to measure fluid flow in alginate scaffolds. Both models of flow were fit to the data in order to calculate permeability and theoretical boundary layer thickness (Brinkman). However, the

methods used to fit these two models to the data were very different. Brinkman's equation (Eq. 2) was solved numerically using COMSOL Multiphysics (COMSOL, Burlington, MA) and fit to the data assuming apparent viscosity (μ_e) equal to fluid viscosity (μ).

Brinkman-Darcy was fit to experimental data via SigmaPlot originally. In addition to experimental data, COMSOL simulations of flow through the alginate scaffolds were also performed using hydraulic permeability calculations based on poroelastic theory [163, 165]. For comparison purposes, the flow profile from COMSOL simulations was fit to the Brinkman-Darcy model to calculate permeability and compare it to input model parameters. Due to the very low permeabilities measured the hyperbolic cosine functions approached infinity, or what analysis programs define as infinity; the curves were unable to be fit. Therefore, we found it necessary to evaluate the model fit in a more customized fashion. Therefore, an algorithm was developed to fit the model to the data and calculate permeability.

Methods

The approach used to fit this data was to separate Brinkman-Darcy into parts which could them be solved independently in Matlab [142]. The equation for Brinkman-Darcy was separated into 2 parts, f1 and f2:

$$v(d,\sigma) = \frac{Q\cosh\frac{1}{2\sigma}}{\cosh\frac{1}{2\sigma} - 2\sigma\sinh\frac{1}{2\sigma}}\left\{1 - \frac{\cosh\left[\left(d-\frac{1}{2}\right)/\sigma\right]}{\cosh\frac{1}{2\sigma}}\right\} \quad (3)$$

$$f1 = \frac{Q}{1 - 2\sigma \tan\left(\frac{1}{2\sigma}\right)} \tag{4}$$

$$f2 = 1 - \frac{\cosh\left(\frac{d}{\sigma}\right)\cosh\left(\frac{-1}{2\sigma}\right) + \sinh\left(\frac{d}{\sigma}\right)\sinh\left(\frac{-1}{2\sigma}\right)}{\cosh\left(\frac{1}{2\sigma}\right)} \tag{5}$$

Eq. 5 reduces to

$$f2 = 1 - \cosh\left(\frac{d}{\sigma}\right) + \sinh\left(\frac{d}{\sigma}\right) * \tanh\left(\frac{1}{2\sigma}\right) \tag{6}$$

for 0 < d << 1

$$\frac{d}{\sigma} << \frac{1}{\sigma} \tag{7}$$

leading to

$$f2 = 1 - \frac{e^{\frac{d}{\sigma}} + e^{\frac{-d}{\sigma}}}{2} + \frac{e^{\frac{d}{\sigma}} - e^{\frac{-d}{\sigma}}}{2} * \tanh\left(\frac{1}{2\sigma}\right) \tag{8}$$

Equation 8 can be simplified to

$$f2 = 1 - \frac{e^{\frac{d}{\sigma}}}{2}\left(1 - \tanh\left(\frac{1}{2\sigma}\right)\right) - \frac{e^{-\frac{d}{\sigma}}}{2}\left(1 + \tanh\left(\frac{1}{2\sigma}\right)\right) \tag{9}$$

Equation 9 can be evaluated as 2 different functions

$$f2a = \frac{e^{\frac{d}{\sigma}}}{2}\left(1 - \tanh\left(\frac{1}{2\sigma}\right)\right) \tag{10}$$

$$f2b = \frac{e^{-\frac{d}{\sigma}}}{2}\left(1 + \tanh\left(\frac{1}{2\sigma}\right)\right) \tag{11}$$

The components of Eq. 9, f2a and f2b are evaluated depending on the rate at which

they approach infinity. The Matlab code is composed of 3 programs. Flow profiles are input via a Microsoft Excel spreadsheet composed of 2 columns, depth from surface and fluid velocity measurements. The curve-fitting is performed using a least-squares approach wherein a range of Darcy numbers (a) and the step size for each successive guess is user defined. Output parameters are Darcy number and the model fit parameters associated with it (R^2, RMSE). The Matlab model fit was compared to SigmaPlot model fits for high permeability alginate scaffolds.

Main Program

```
clear all ; close all;

% input values from data or COMSOL sims
data= xlsread('values.xls');

x=data(:,1);
y=data(:,2);

%initial guess
a=(10^-8:10^-13:10^-7);
%a=0.001;

%chisq=10000;
for k=1:length(y);
   ysq(k)=(y(k))^2;
end

threshold=0.001*(sum(ysq));
d=x;
%d=[0:0.00001:0.001];

for i=1:length(a);

   sigma=a(i);

   f1out=f1(sigma);
   %fprintf(1,'f1out %g\n',f1out);

   f2out=f2(sigma,d);
```

```
    %plot(d,f2out);
    %title('f2out');
    %xlabel('d');

        if isfinite(f1out)~=1
         error('f1out not finite');
        end

        if isfinite(f2out)~=1
         error('f2out not finite');
        end

    f1f2=f1out.*f2out;
    %plot(d,f1f2);
    %title('f1f2');
    %xlabel('d');

    for k=1:length(d);
         chi(k)=(y(k)-f1f2(k))^2;
    end


   rmse=sqrt((sum(chi)/length(d)));
    holderc(i)=rmse;
    holders(i)=sigma;

end

holderc=holderc';
holders=holders';

[rmse,index]= min(holderc);
sigma_best= holders(index);

for p=1:length(d);

    tot = (y(p) - mean(y))^2;
    err = (y(p) - f1f2(p))^2;

end

R_SQ = 1- (sum(err)/sum(tot));
output=[sigma_best,R_SQ,rmse]
```

Evaluation of f1

```
function f=f1(sigma)
```

```
if sigma==0
 error('f1: sigma is exactly 0');
end
 twosigma=2.0 * sigma;
tmp=1.0 ./ twosigma;
f=1.0 ./ (1 - twosigma .*tanh(tmp));
```

Evaluation of f2

```
function f=f2(sigma,d)

if length(sigma)~=1
 error('f2: sigma must be a scalar');
end

doversigma=d./sigma;
expdoversigma=exp(doversigma);
isfiniteexpdoversigma=isfinite(expdoversigma);
expminusdoversigma=exp(-doversigma);
isfiniteexpminusdoversigma=isfinite(expminusdoversigma);

tanhterm=tanh(1.0 ./ (2*sigma));

f=ones(size(d));

for j=1:length(d)

 if isfiniteexpdoversigma(j)==1
   f(j)=f(j) - expdoversigma(j) .* 0.5 .* (1-tanhterm);
 end

 if isfiniteexpminusdoversigma(j)==1
   f(j)=f(j) - expminusdoversigma(j) .* 0.5 .* (1+tanhterm);
 end

 if isfiniteexpdoversigma(j)==0 & isfiniteexpminusdoversigma(j)==0
   fprintf(1,'trouble at j=%d\n',j);
 end

end
```

RESULTS AND DISCUSSION

The analysis tool developed accurately fit Brinkman-Darcy model to all flow profiles. The Matlab model fits were similar to SigmaPlot model fits for measured flow profiles in 1, 2, and 3 wt% alginate gels. These Matlab code was then applied to flow profiles from COMSOL simulation and described them well (Fig. 1; $R^2 = 1.0$; RMSE ≤ 0.06). The Brinkman-Darcy permeability calculated from the model fit was 4 orders of magnitude lower than the hydraulic permeability for all alginate mixtures (Fig. B1, inset).

While this tool is unnecessary for describing Brinkman-Darcy flow in highly permeable porous scaffolds it provides an easy way to analyze flow profiles from scaffolds with low permeability, such as cartilage. If the flow visualization technique is applied to less permeable scaffolds this tool provides a method for calculating Darcy permeability from the flow profile measurements.

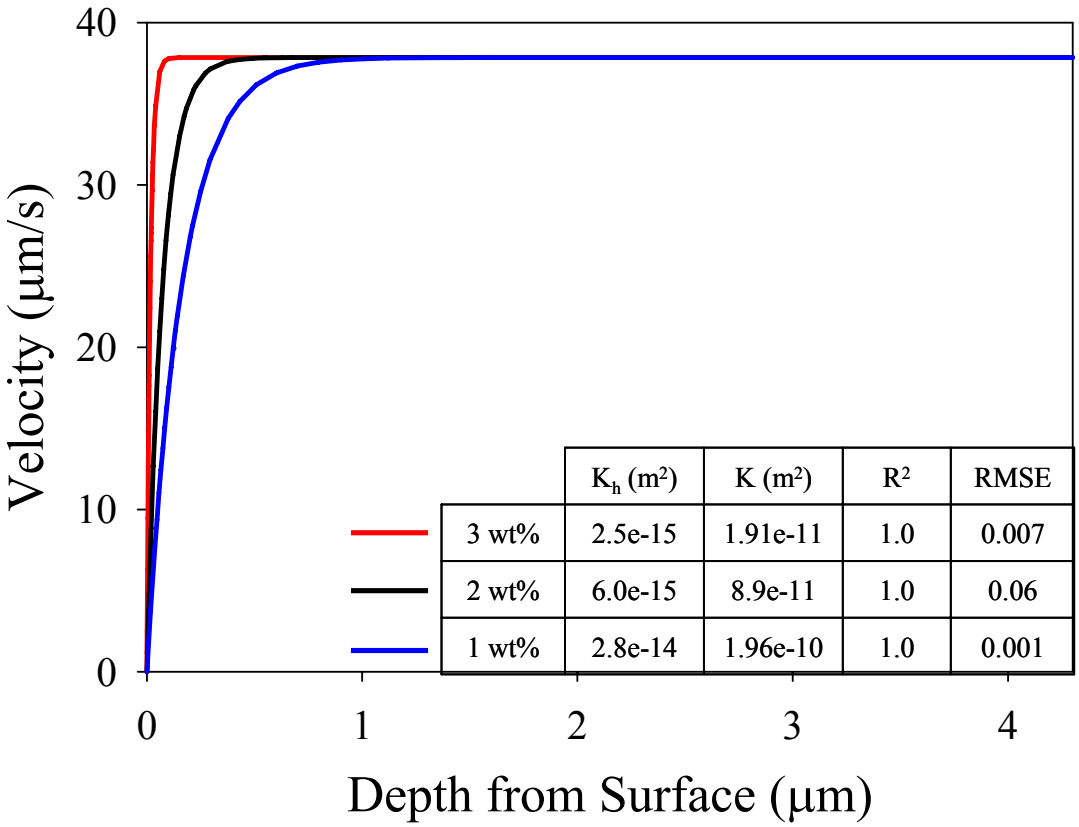

Figure B1: Brinkman-extended Darcy model fit to COMSOL simulated flow profiles for 1, 2, and 3 wt% alginate perfused at 25 μL/min. COMSOL models were based on hydraulic permeability calculations and solved with Brinkman's equation. Permeability was calculated from the Brinkman-Darcy model fits (K) and compared to hydraulic permeability measurements (K_h) (Table inset).

APPENDIX C

MEASURING CALCIUM RESPONSE IN 3-D ALGINATE SCAFFOLDS: TIME-SERIES ANALYSIS ALGORITHYM

INTRODUCTION

Calcium (Ca^{2+}) is a ubiquitous intracellular signal responsible for controlling a number of cellular processes. Changes in intracellular Ca^{2+} concentration have been shown to regulate a wide variety of processes including cell growth, secretion, and sensory perception through inositol triphosphate mediated pathways in most mammalian cell types [104]. The action of this signaling pathway occurs when Ca^{2+} concentration rises above normal levels (100 nM) to approximately 500-1000 nM [112]. The versatility of this pathway arises from variation in the speed, amplitude, and spatio-temporal patterning of the rise in Ca^{2+} concentration; these variations can be combined with interactions of Ca^{2+} dependent pathways with other signaling pathways regulate diverse cellular responses.

Ca^{2+} signaling has been shown to regulate the cellular response to mechanical loading in chondrocytes, mesenchymal stem cells, kidney epitheilial cells, osteocytes, and osteoblasts [52, 99, 110, 115, 116, 146, 207]. In chondrocytes, Ca^{2+} regulated mechanical signaling transduction is believed to be regulated by stretch activated ion channels [105, 106]. This mechanism plays a role in chondrocyte response to single cell deformation [105-107], matrix deformation [108], hydrostatic pressure [53, 106], osmotic pressure [109], small signaling molecules [110] and fluid shear stress [48, 51, 111]. The Ca^{2+} response to these mechanical stimuli is then recorded as a series of

single cell responses whereby the graduated response of the cells can be analyzed.

The ability to translate these single cell measurements of Ca^{2+} concentration as a response to a mechanical stimulus requires the analysis of time-history. Using fluorescent dyes and confocal microscopy it is possible to observe transient changes in Ca^{2+} concentration as a series of single cell measurements as stimuli are applied with the use of fluorescent dyes [105, 110]. Characterizing this data is complicated by the presence of noise and the multitude of processes controlled by changes in Ca^{2+} signaling. A number of methods have been described to analyze this data including FFT, thresholding, manual peak counting, range counting (defining a Ca^{2+} response as a specific percent increase in cell intensity), ANOVA and rainflow counting [49, 52, 53, 104, 108, 146, 208]. There are advantages and disadvantages to all of these methods.

With the exception of a single study [108], all of the methods used to describe Ca^{2+} signaling have been in monolayer culture. In monolayer, cells are contained within the same imaging plane, simplifying light collection during imaging, reducing scatter, and improving the consistency of intensity data captured across all cells. In 3-D hydrogel scaffolds, the location of the imaging plane varies by cell with random scattering and noise introduced by the scaffold itself. Therefore, applying specific parameters to the definition of the Ca^{2+} response across the entire population of cells may result in under- or over-counting cell responses to a specific stimulus.

The objective of this study is to introduce a reliable, robust method of analyzing the time-history data, taken as a series of images, of Ca^{2+} concentration of chondrocytes cultured in alginate hydrogel scaffolds.

Methods

Bovine articular chondrocytes were harvested, isolated, and encapsulated in alginate hydrogels as described in sections 2 and 3, based on established methods [74]. The cells were labeled with Fluo-4 AM, a calcium dye, to visualize relative changes in intracellular Ca^{2+} concentration. Chondrocytes were imaged with confocal microscopy (LSM 510 Meta, Carl Zeiss Inc., Jena, Germany) after compression or during perfusion in order to determine the Ca^{2+} response. Regions of interest (ROI) containing 30-100 cells were imaged every 5-6 seconds via confocal microscopy to record changes in cell intensity.

Images were converted from the *.lsm format, used to save image stacks by the microscope software, to sequential *.tiff files using ImageJ (NIH). The individual image files were saved in a folder for analysis. The time-series history of the individual cell intensities were analyzed with Matlab. For each cell, an ROI around it was selected containing the cell and some surrounding area (Fig. C1). The mean intensity of this area was calculated for the entire time-series. Thresholding for the entire image stack was performed to prevent background intensity noise from altering the mean intensity calculated from cells of interest before beginning image analysis. Background intensity was removed by defining a minimum pixel intensity recorded from the ROI such that only pixels above this minimum value were used in mean cell intensity calculations.

Intensity data from all the cells of interest were imported into a MS Excel spreadsheet for further analysis. For each cell the intensity (I) and corresponding timestamp (t) were used for further analysis (Fig. C2a). The rate of change of the intensity with time (dI/dt vs t) was calculated to remove the effects of drift present in

several time-series Fig C2b). This drift, if uncorrected, lead to artificial increases in the number of Ca^{2+} responses counted.

A Ca^{2+} signaling event was defined for each cell individually by fitting all positive dI/dt to a Gaussian distribution using a different Matlab code and defining a Ca^{2+} signaling response as a dI/dt greater than 3 standard deviations above the mean (Fig. C2c).

Results and Discussion

The method described in this study was successful in analyzing intensity data to define and count transient Ca^{2+} signaling responses of chondrocytes seeded in alginate hydrogels. The advantage of defining a Ca^{2+} response as dI/dt greater than 3 standard deviations above the mean, positive dI/dt was to differentiate background signaling and noise due to experimental conditions from significant changes indicating the activation of a signaling pathway. In combination with the normalization methods employed in sections 2 and 3, this method allowed the discrimination of background Ca^{2+} fluctuations from Ca^{2+} responses due to compression and perfusion.

Unlike other methods used, such as manual peak counting [108], ANOVA [53], or range counting [49] the threshold for counting a Ca^{2+} transient is set by the individual cell and not by a parameter set by the population as a whole. This is particularly important when imaging cells in 3-D scaffolds where a number of variables can alter the mean cell intensity. These variables include the cells themselves, taken from several animals, at different times, from different locations and cultured for varying times. In addition, the amount of AM dye absorbed by the cell and the ability of the laser to excite the fluorophores and the objective to capture the

emitted light can vary with depth. By looking at all the increases in Ca^{2+} intensity for a single cell at once these effects can be normalized across several experiments. Unlike rainfall cycle counting [208], Ca^{2+} signaling which may develop over longer times cannot be counted. However, all of the Ca^{2+} responses counted using the method described in this study appeared and disappeared during the 10-12 seconds separating 3 consecutive intensity measurements. Therefore rainfall cycle counting may be beneficial for experiments with a higher imaging rate.

These results demonstrate that the method described here identifies Ca^{2+} oscillations by changes in cell intensity and appropriately determines the presence of a significant fluctuation caused by activation of a Ca^{2+} dependent signaling response despite any distortions from background noise. Therefore, this method can be applied to accurately quantify and characterize Ca^{2+} signaling of cells encapsulated in 3-D scaffolds.

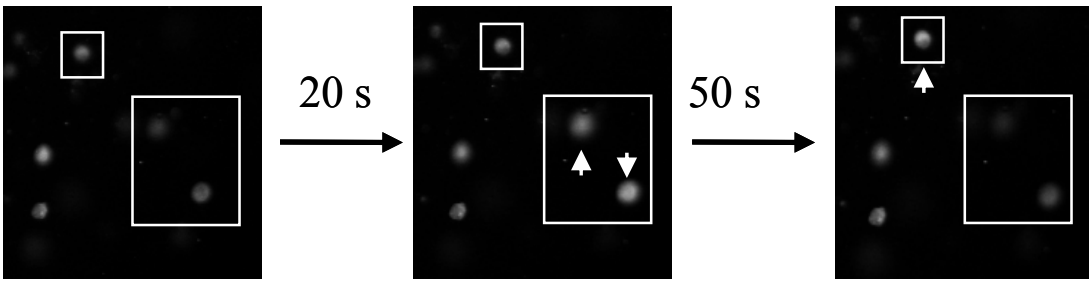

Figure C1: Images of calcium labeled cells with cells of interest marked with white boxes and cells undergoing a Ca^{2+} response marked with arrows. The intensity of each pixel is measured, but only pixels with intensities greater than the background intensity are used to calculate the mean intensity of each cell.

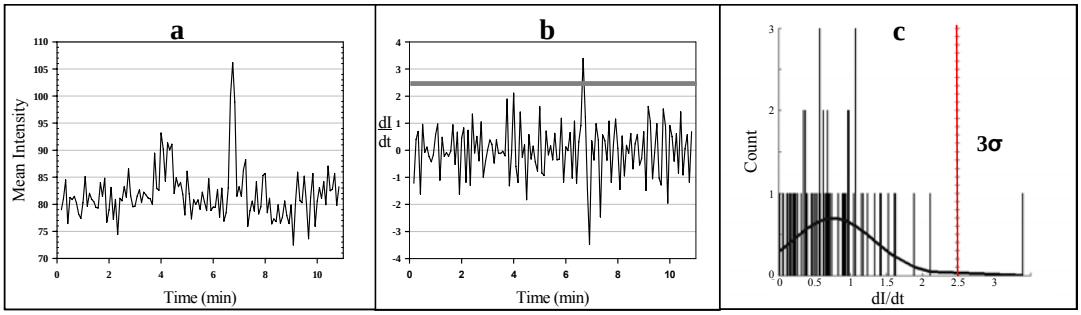

Figure C2: a) Mean intensity (I) versus time for a single cell illustrating the noise and drift present in measurements of Ca^{2+} fluctuation over time; b) dI/dt plotted with time for each cell to remove the effects of drift and to observe the amplitude of a transient Ca^{2+} fluctuation; c) All positive dI/dt for the cell were fit to a Gaussian distribution and Ca^{2+} response was defined as $dI/dt > 3\sigma$

Matlab Code for Image Analysis (all images must be in *.tif format)

```
clear all
close all
warning off MATLAB:divideByZero
cell_cnt = 5;
xarray=zeros(5,cell_cnt);
yarray=zeros(5,cell_cnt);
%%BWarray=zeros(512,512,bw_cnt);
r=[];
c=[];
%%Choose directory with images to be analyzed
delete('Thumbs.db');
dirname=uigetdir;
dirlist=dir(dirname);
mu=zeros(size(dirlist)-1,cell_cnt); %CHECK FOR EACH DIRECTORY
%%Read in all files to be analyzed
%%Read in first file for ROI
%% there are always crap files in the directory, so take that into consideration
for k = 3:size(dirlist)-1 %CHECK FOR EACH DIRECTORY
x=imread(dirlist(k).name);

if k==3
for i = 1:cell_cnt
%%Loop thru number of of ROIs
[x_temp,y_temp,BW,xi,yi]=roipoly(x);
[ROI_ind_x ROI_ind_y]=find(BW==1);
I=x(ROI_ind_x,ROI_ind_y);
I_thresh_ind=find(I>20);
mu(k-2,i)=mean(I(I_thresh_ind));
xarray(:,i)=xi;
yarray(:,i)=yi;
end
end

if k~=3
for i = 1:cell_cnt
BW = roipoly(x_temp,y_temp,x,xarray(:,i),yarray(:,i));
[ROI_ind_x ROI_ind_y]=find(BW==1);
I=x(ROI_ind_x,ROI_ind_y);
I_thresh_ind=find(I>20);
mu(k-2,i)=mean(I(I_thresh_ind));
end
end
 end
 mu; %mean intensity array for all cells chosen
 %%Loop thru other files in directory
```

Determining significant Ca^{2+} response with Gaussian distribution

```
close all
clear all
% place all dI/dt in a separate excel sheet named test.xls in the same folder as this
code
read= xlsread('test.xls');
x_raw=sort(read,1);

 for j = 1:size(x_raw,2);
    col=x_raw(:,j);
          for i = 1:size(col);
            if col(i)<0;
            index = i;
          end
    end

 %x(j) = col(index+1:size(col));
mu(j) = mean(col(index+1:size(col)));
dev(j) = std(col(index+1:size(col)));
devmid(j) = dev(j)*2 + mu(j);
devmax(j) = (3*dev(j))+mu(j);
devmin(j) = dev(j)+mu(j);
end
```

APPENDIX D

THE EFFECTS OF SOLID VOLUME FRACTION AND RGD CONJUGATION ON CALCIUM SIGNALING RESPONSE OF CHONDROCYTES IN ALGINATE UNDER STATIC COMPRESSION

Introduction

Articular cartilage is an avascular and aneural load bearing material covering the ends of diarthrodial joints. It acts to evenly distribute loads to the underlying bony surface as well as provide a low friction interface to reduce wear during joint articulation [1]. The mechanical properties of cartilage are due to the structure and function of its extracellular matrix (ECM) composed of charged proteoglycans interwoven with collagen fibers. The structure and composition of this ECM is maintained by chondrocytes which alter the synthesis and degradation of matrix components based on a number of signals. As chondrocytes only make up 5% of the volume of cartilage and have no direct connections with neighboring cells, maintenance of the ECM is dependent on cell-matrix interactions [9]. Cartilage ECM interacts with chondrocytes through a number of transmembrane receptors to regulate phenotype, metabolism and response to mechanical loading [10].

A number of studies have demonstrated the ability of chondrocytes to respond to mechanical signaling from joint loading with changes in ECM composition. *In vivo* studies have examined immobilized joints and observed an overall catabolic response in the tissue wherein ECM synthesis decreased and joint degeneration was present [14-17]. Static compression of cartilage explants, similar to *in vivo* joint

immobilization, has been shown to inhibit GAG synthesis and amino acid uptake in a dose-dependent manner [31-33]. These changes correlate with a decreased matrix stiffness and eventual erosion. Understanding the cell-matrix interactions that play a role in sensing these signaling is difficult due to the density and low permeability of cartilage ECM; it is difficult to add specific blocking antibodies or other chemical treatments to isolate specific molecular pathways of interest.

One approach to isolate signaling pathways in chondrocytes is to culture them in hydrogel culture in order to preserve the expression of cartilage-specific markers in a high-permeability scaffold [62, 76]. Unlike the cartilage ECM which provides a number of sites for cell adhesion, hydrogel scaffolds are non-adherent and prevent cells from interacting with their surrounding matrix. When hydrogel-seeded chondrocytes were statically compressed, ECM synthesis was significantly decreased compared to uncompressed controls [78, 84]. However, the full effects of mechanical loading were not apparent until the cells synthesized a pericellular matrix [77, 79].

Hydrogel scaffolds, such as alginate [81], agarose [82] and PEG [83], have been modified to incorporate the peptide sequence Arg-Gly-Asp (RGD) to facilitate cell adhesion. These scaffolds allow the assessment of cell-matrix interactions and receptor specificity in transmitting the effects of mechanical compression. Chondrocytes cultured in RGD-alginate demonstrated an immediate sensitivity to static compression at strains too low to cause any inhibition of matrix synthesis in unmodified alginate gels [84]. This study observed the synthesis of glycosaminoglycan, a matrix molecule, after two days of compression. What is not apparent is the effect of the continuous compression on chondrocyte signaling pathways.

The concentration of intracellular calcium (Ca^{2+}) has been shown to act as a real-time indicator of mechanical signaling pathway activation in chondrocytes. While the mechanisms of the signaling pathways are not well-understood, single cell deformation [105-107], matrix deformation [108], hydrostatic pressure [53, 106], osmotic pressure [109], and fluid shear stress [48, 51, 111] all cause changes in Ca^{2+} signaling response. Using fluorescent dyes and confocal microscopy it is possible to observe transient changes in Ca^{2+} concentration as a series of single cell measurements as stimuli are applied [105, 110]

In the studies discussed in chapters 2 and 3, chondrocyte-seeded alginate gels were perfused within flow chambers and the Ca^{2+} response was measured. In order to normalize for experimental conditions, which include a small applied strain, the Ca^{2+} response before perfusion was measured. However, these baseline responses from these flow studies have not been quantified and compared to determine if alginate solid volume fraction or RGD-ligand concentration altered the response of chondrocytes to static compression.

METHODS

Alginate Mixtures

Alginate hydrogels were modified with controlled densities of RGD adhesion ligands as described previously [81]. The RGD-alginate was suspended in PBS at 2 wt% with final ligand densities of 400, 100, 40, and 4 μM. Control UPLVG alginate (0 μM RGD) was also suspended in PBS at 1, 2, and 3 wt%.

Cell Isolation

Bovine articular chondrocytes were isolated and counted as described in chapters 2 and 3 with methods previously established [74]. Chondrocytes were evenly

suspended in alginate solutions at$10x10^6$ cells/mL.

Scaffold Creation and Cell Imaging

Alginate solutions containing cell suspensions were molded into custom-made devices as described in Chapters 2 and 3. The gels were made oversized such that sealing the devices resulted in ~7% compressive strain. Chondrocyte response to compression was assayed by monitoring Ca^{2+} response with confocal microscopy (LSM 510; Carl Zeiss Inc.; Jena, Germany) as previously described (Chapters 2 and 3). These measurements were done in order to establish baseline signaling activity in immediately preceding flow studies and do not include the time-series of cell equilibration after the applied strain shown in previous chapters (Figs. 2.4 and 3.3).

In order to assess the baseline signaling response of chondrocytes to static compression after 70 minutes cells were imaged for 4.5 minutes and the number of Ca^{2+} transients counted for all alginate mixtures (n = 4-27). Cells were imaged at depths greater than 100 μm from the surface in regions containing 30 or more cells.

Data Analysis (Ca^{2+} Signaling)

Images were analyzed in Matlab as previously described (Chapters 2, 3, Appendix C).

Statistics

The Ca^{2+} response induced by the 7% strain for 1, 2, and 3 wt% alginate mixtures as well as the 0, 4, 40, 100, and 400 μM RGD-alginate mixtures was compared using a paired student T-test with (SigmaStat) ($\alpha = 0.05$). Data are expressed as mean ± standard deviation unless otherwise indicated.

Results

The effects of static compression on the Ca^{2+} signaling response were not modulated by changes in the solid volume fraction of the scaffold. The fraction of cells exhibiting Ca^{2+} transients 70-80 min after the application of a static strain was similar in 1, 2, and 3 wt% alginate gels (Fig. D1). The mean fraction of cells responding was 0.14 ± 0.08 among all alginate mixtures.

The effects of static compression on the Ca^{2+} signaling response of were modulated by RGD ligand concentration. The fraction of cells exhibiting Ca^{2+} transients significantly increased, compared to controls, in the 40, 100, and 400 μM RGD-alginate gels (Fig. D2; $p < 0.05$; $n = 4\text{-}27$).

Discussion

The main finding from these results was that RGD ligand density altered the Ca^{2+} signaling response of chondrocytes to static compression in a concentration-dependent manner over an hour after the stimulus was applied. However, altering the solid volume fraction, thereby changing the modulus, pore size and permeability of the scaffold, had no effect on the signaling response.

The elevation in Ca^{2+} response after the application of a small strain in RGD-alginate gels is consistent with previous studies wherein static compression caused a reduced matrix synthesis in cartilage explants and RGD-alginate scaffolds [31-33, 84]. Cell-matrix interactions through RGD ligands increased the sensitivity to the stimulus and maintained its effect for over an hour (Fig. D2) to 2 days [84].

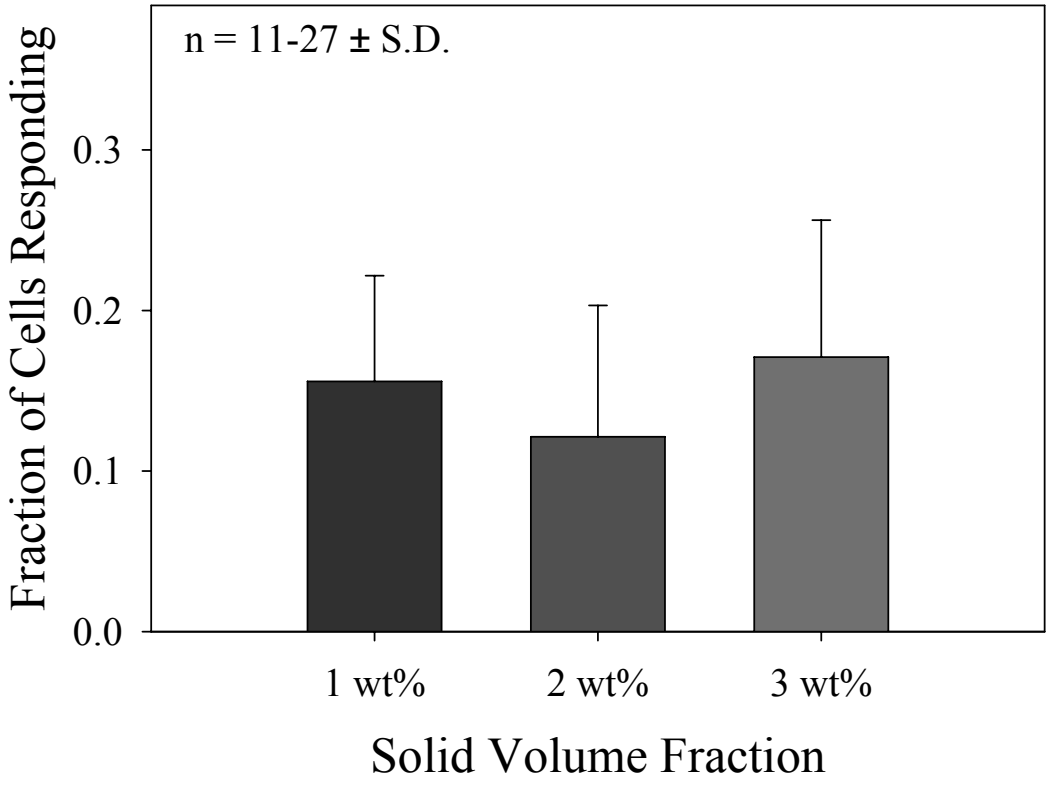

Figure D1: The fraction of cells demonstrating a significant Ca^{2+} signaling response after 70-80 minutes of static compression did not vary with solid volume fraction.

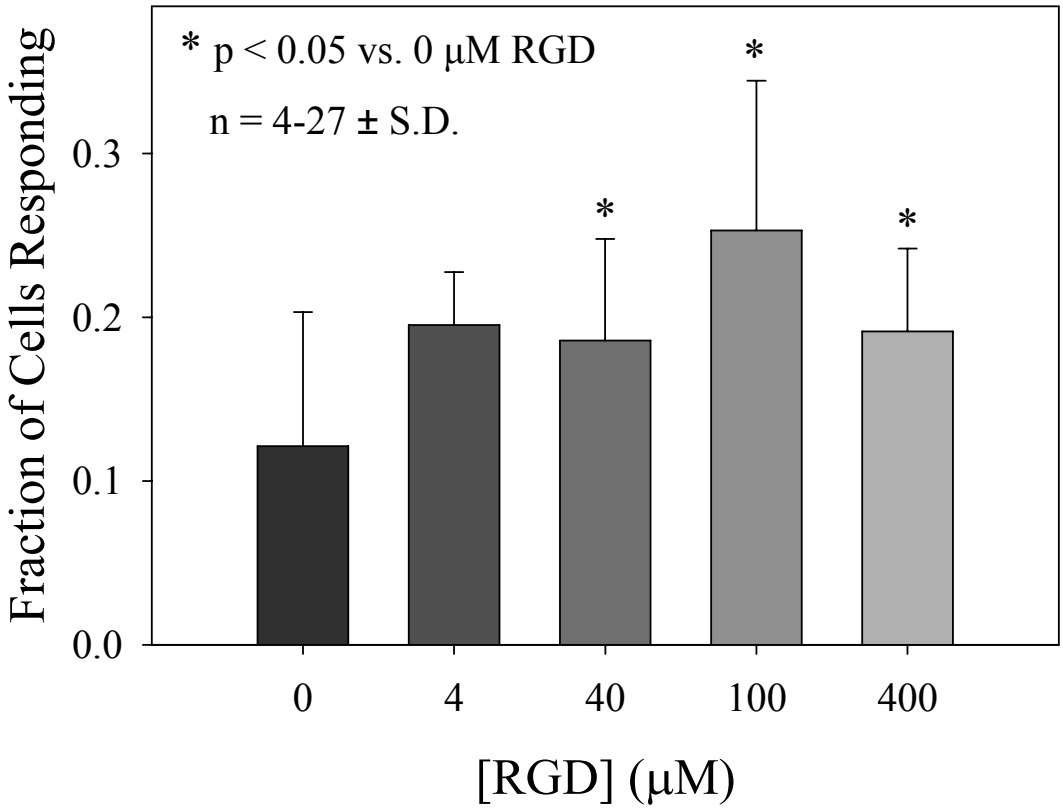

Figure D2: The fraction of cells demonstrating a significant Ca^{2+} signaling response after 70-80 minutes of static compression varied with RGD concentration. Chondrocytes in 40, 100, and 400 μM RGD-alginate (2 wt%) showed significantly more Ca^{2+} transients compared to controls (0 μM) gels ($p < 0.05$).

The degree of attachment and formation of focal adhesion complexes in cells has been shown to be dependent on RGD ligand density [191, 193, 194]. These focal adhesion complexes are associated with numerous signaling pathways and believed to mediate sensing of mechanical cues to cells [197-199]. A minimum RGD spacing of 440 nm was required for the initiation of adhesion and spreading of human foreskin fibroblasts adhesion and 140 nm for focal adhesion formation in monolayer culture [191]. The RGD formulation used in this study was shown to have a ligand spacing of 23 nm for the 400 μM RGD-alginate. Therefore, the minimum ligand density required to sense and maintain the effects of small static strains is 230 nm (40 μM); this spacing may be associated with cell adhesion and spreading, but not the formation of focal adhesion complexes. The Ca^{2+} response to the strain may have been caused by stretching of the plasma membrane during adhesion and subsequent activation of stretch-activated ion channels shown to regulate this response [105, 106].

APPENDIX E

STREAMING POTENTIALS REGULATE CHONDROCYTE CALCIUM SIGNALING RESPONSE IN 3D ALGINATE SCAFFOLDS

Introduction

Articular cartilage serves as a load-bearing connective tissue of diarthrodial joints which acts to absorb and distribute joint loads more evenly across the underlying bony surface [1]. The biomechanical function of cartilage is dependent on the structure and composition of the extracellular matrix (ECM) which makes up more than 90% of the dry weight of the tissue. The structure and composition of the ECM is maintained by chondrocytes which alter the synthesis and degradation of matrix components based on a number of signals, including mechanical signaling caused by joint loading.

The ECM is composed of a complex network of fibrillar collagen enmeshed with a high concentration of negatively charged proteoglycan aggregates and other small molecules [3]. When the tissue is hydrated at physiologic pH, the negative charges on the proteoglycan molecules become ionized and attract positive counterions from the surrounding fluid, causing osmotic swelling of the tissue. The swelling is opposed by the collagen network which enables the pressurization of the tissue and gives cartilage its load-bearing properties.

Upon joint loading and subsequent cartilage compression, a number of coupled mechanical stimuli occur that are believed to regulate chondrocyte metabolism [32, 37-41, 43]. When the ECM is deformed, hydrostatic pressure gradients cause the

tissue to exude fluid along with positive cations while also increasing the density of negative charge present. This causes a voltage drop across the tissue, creating streaming currents which may influence cell behavior either directly or indirectly through electric fields as fluid moves during both compression and subsequent relaxation of the load [39, 209].

The main electromechanical transduction phenomena in articular cartilage are compression induced streaming current and current-generated mechanical stress [210, 211]. Oscillatory compression of cartilage explants suggest that these streaming current gradients play a role in chondrocyte biosynthesis [85]. However, the direct effects of streaming current on cell metabolism during compression are difficult to isolate due to the influences of fluid flow, hydrostatic pressure, and cell matrix interactions [40, 86, 174]. This obstacle was overcome through the application of capacitive electric fields to cartilage explants [212-215] and high-density monolayer cultures of chondrocytes [216, 217]. In the presence of electric fields, chondrocyte synthesis of matrix proteins was upregulated in a frequency and amplitude dependent manner, illustrating the importance of electric forces in the regulation of chondrocyte metabolism.

Tissue engineering approaches for the generation of cartilage have employed to mimic the native environment (chemical and mechanical) of chondrocytes in a number of polymers including alginate [74, 107], collagen [218], PEG [219] and PLGA [91]. However, only recently have electromechanical properties been incorporated into polymeric scaffolds in order to quantify mechanotransduction of cells in response to chemical, mechanical, and electrical stimuli [205, 220-222].

Fluid flow is an important mediator of chondrocyte metabolism [34, 35, 77,

85] and is required to create streaming currents in cell-seeded scaffolds containing fixed charges. In Chapters 1, 2 and 3 a 3-D alginate hydrogel system was described wherein direct perfusion was applied to chondrocyte-seeded scaffolds. Using this model system, the metabolic response to fluid flow was quantified by measuring changes in intracellular calcium levels. Chondrocyte Ca^{2+} signaling was shown to increase monotonically with fluid velocity (chapter 3). Alginate hydrogels are normally ionically crosslinked [74], but the scaffold produced has a low electrokinetic coupling coefficient and a fixed charge density which cannot be altered [205]. However, an unpublished study has shown that the electrokinetic coupling coefficient of covalently crosslinked alginate can be modified by the addition of additional fixed charge in the form of silica microparticles [205].

In cartilage, neither the charge density nor the pressures generated upon tissue deformation can be altered without significantly changing either the pH or the inherent scaffold properties of the tissue. Pressure and charge density are normally coupled in cartilage and other soft connective tissues, their relationship is described by an electrokinetic coupling coefficient Ke (μV/kPa) [85, 210, 223]. By incorporating a variable charge density into perfusable alginate scaffolds values, a given flow rate and pressure can generate a range of streaming currents while maintaining cell viability [224]. Conversely, the charge density can be fixed and the permeability of the scaffold can be modified to provide an order of magnitude range in pressures for a given fixed charge (Chapters 2, 3). The ability to independently control charge density, pressure and fluid velocity are essential in understanding the role of streaming currents in regulating chondrocyte metabolism.

The hypothesis of this study was that streaming current induced by direct

perfusion of alginate scaffolds regulates chondrocyte metabolism. Specifically, our objectives were a) independently varying flow rate and particle density within the scaffolds to create a range of streaming currents b) use finite element modeling to inform our experimental approach and calculate streaming current based on measured electrokinetic coupling coefficients.

Methods

Cell Isolation

Articular cartilage was sterilely harvested from the femoral condyles and patellofemoral groove of 1-3 day old calves (Gold Medal Packing; Oriskany, NY) and digested for 12-16 hours in 0.2 mg/mL collagenase type II [74] dissolved in F-12 media, 100 U/mL penicillin and 100μg/mL streptomycin at 37°C. The cells were then washed and counted with methods previously established [74]. Chondrocytes were then suspended in an alginate solution with $10x10^6$ cells/mL.

Hydrogel Fabrication

Covalently crosslinked alginate gels were made based on established photocrosslinking techniques [225, 226] with specific modifications for alginate [205]. Anhydride chemistry was used to methacrylate alginate which was dissolved in phosphate-buffered saline (PBS) to make a 3 wt% alginate-cell mixture for photocrosslinking. The photoinitiator VA-086 was dissolved in a 70% ethanol solution to a final concentration of 10% wt/vol VA-086 solution which was then added to the alginate-cell mixture at 20 μL VA-086 per 1 mL of 3% w/v alginate [205]. In order to produce alginate gels of specific size and shape for flow/electrokinetic experiments wells were cut into 1.3 mm gasket material placed on a glass plate (Fig. E1). 120 μL

of the alginate solution was aliquotted into each well; the wells were sealed with a glass plate and placed into a large glass Petri dish. The Petri dish was placed in the center of a UV oven (Spectroline) for 5 min of exposure (365 nm longwave, 2 $\mu W/cm^2$) to covalently crosslink the alginate. The top glass plate was then removed and the hydrogels were placed in a solution of F-12 media, 100 U/mL penicillin and 100μg/mL streptomycin for at least 2 hours before testing. During this time the gels swelled within the cavities, reaching a final height of approximately 1.4 mm. Due to the swelling of the gels, the final solid-volume fraction of alginate was 1.3 wt% [205].

Particle Doping

Fixed charge density was to be controlled with the addition of negatively charged, porous silica microparticles (Polygosil, Macherey-Nagel) prior to crosslinking. However, upon mixing into alginate-cell solutions, cell viability was seen to drop to 50%. New particle incorporation techniques are currently being developed for silica particle densities of 0-10 wt%.

Flow Devices

Alginate gels were removed from the cavities and placed into the flow devices described in chapters 2, 3, and 4 (Fig. E2). Briefly, the devices were fabricated with wells of rectangular cross-sections with rounded ends containing openings for fluid movement. The wells were covered by glass coverslips seated on o-rings and sealed with metal plates attached with openings exposing the coverslips below. Because the gel was larger than the well in the device (1.2 mm), the addition of the coverslip compressed the gel approximately 15% and ensured that the construct filled the well

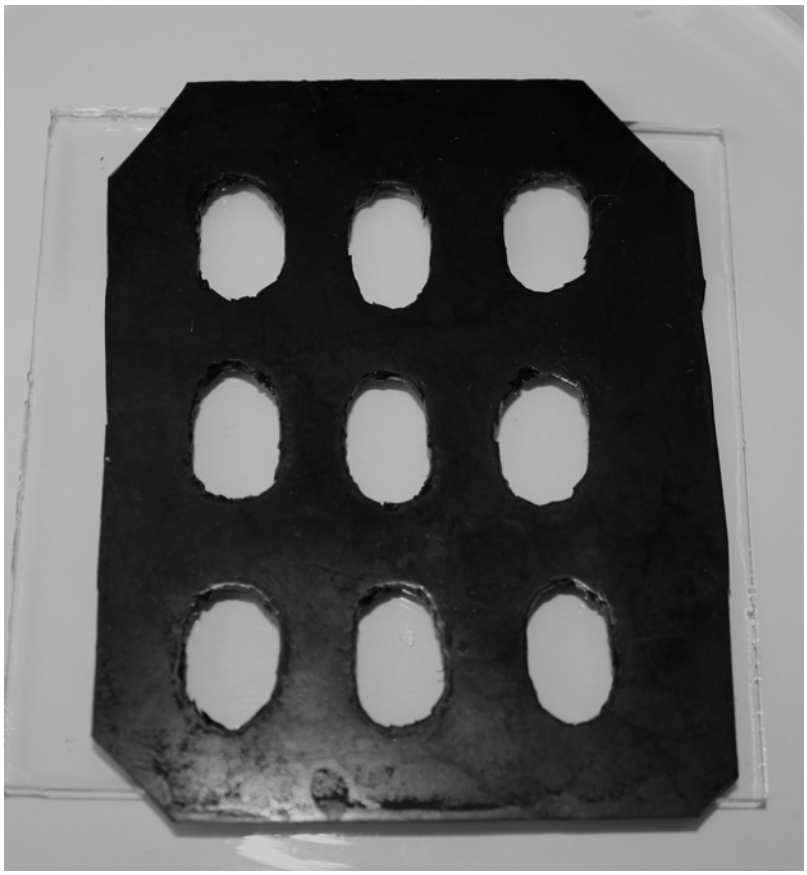

Figure E1: Gasket material with wells cut out to maintain geometry of methacrylated alginate with photoinitiator before UV crosslinking. After crosslinking the gels were maintained within the wells to minimize lateral swelling before testing.

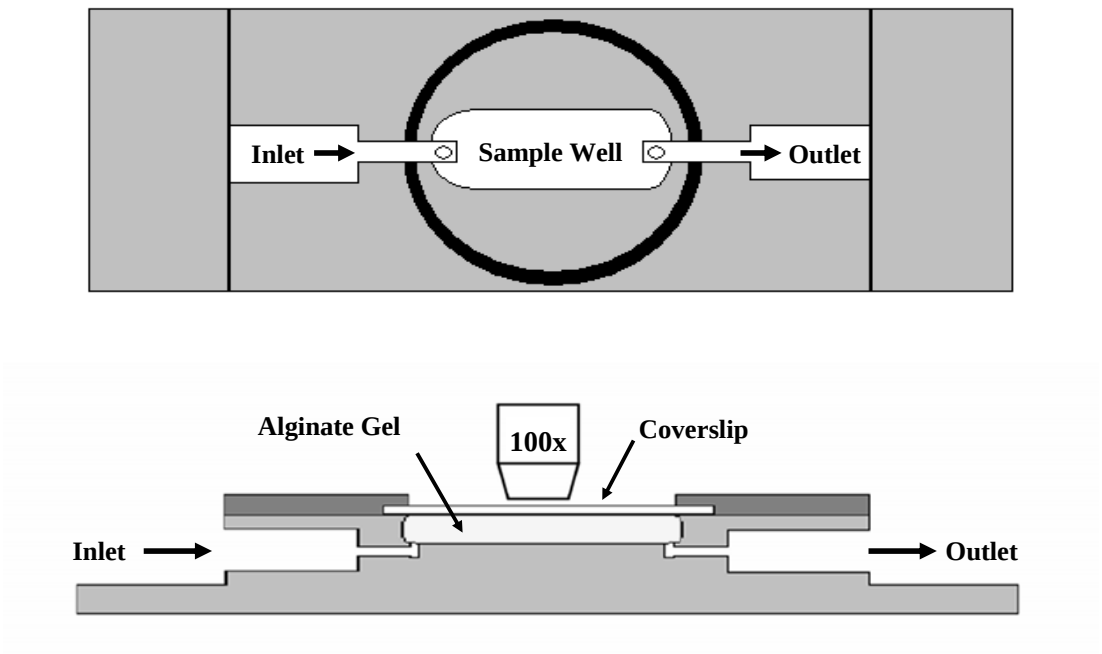

Figure E2: Top: Empty flow device illustrating the connection between flow path and sample location; Bottom: Cross-section of flow device loaded with alginate scaffold and sealed with a coverslip

completely, thereby preventing fluid from leaking around the gel. Flow was controlled via syringe pump which perfused gels from below at flow rates of 5-25 μL/min. Fluid velocities were calculated based on techniques described previously (Chapter 2).

Cell Imaging

Cells were imaged using a confocal microscope (LSM 510; Carl Zeiss Inc.; Jena, Germany) with an excitation wavelength of 488 nm and emission wavelength ranging from 500-550 nm. Images containing more than 30 well-spaced cells in the field of view were captured with a 10x objective lens at a depth of greater than 100 μm from the surface of the gel. Ca^{2+} signaling response was assessed as previously described (Chapter 3, Fig. 3.3).

Immediately after the coverslip was secured, cells were imaged every 5 s for 90 min in order to determine the effect of gel deformation on the Ca^{2+} signaling response. This was done to establish a suitable equilibration time to remove the effect of strain and determine if the response to strain varied due to changes in solid volume fraction.

Devices were incubated for 80 min after coverslip mounting before being connected to the syringe pump. Before applying flow images were taken every 5 s for 4-5 min in order to establish a baseline signaling response and account for variation between cell source and environmental variables. Flow was then applied and images taken every 5 s for 7-9 min for each flow rate. Data was normalized by subtracting the number of cells exhibiting a Ca^{2+} response without flow from the number of cells responding with flow and dividing by the total number of cells imaged for each device.

Statistics

The Ca^{2+} response induced by the 15% strain on the alginate gels fit to a 3-parameter decaying exponential function (SigmaPlot). Data are expressed as mean ± standard deviation unless otherwise indicated.

Finite Element Modeling

Finite element (FE) models were used to simulate the experimental perfusion system and calculate pressure gradients and streaming currents for different flow rates and charge densities. 2-D isotropic FE models the devices filled with covalently crosslinked alginate gels were created in COMSOL Multiphysics (Stockholm, Sweden). The governing equations for the model combined Darcy flow and plane strain to simulate fluid and mechanical forces and an interaction term linking the two. The values input into the model include solid-volume fraction, modulus and permeability and electrokinetic coupling coefficients. These values were taken from previous experimental measurements [205] and coupling coefficients were assumed to scale linearly silica particle density. No-slip conditions were imposed on all solid boundaries and quadrilateral mesh elements were constructed without optimization (Fig. E3a). Perfusion was input through the inlet with a hemi-sine loading function over 2 s and maintained as constant while the outlet was set as a pressure condition (0 Pa). Outcomes were observed at 60 s, well after steady state had been reached. Model variables calculated included fluid velocity and streaming potential gradients for a range of flow rates and coupling coefficients (Fig. E3b).

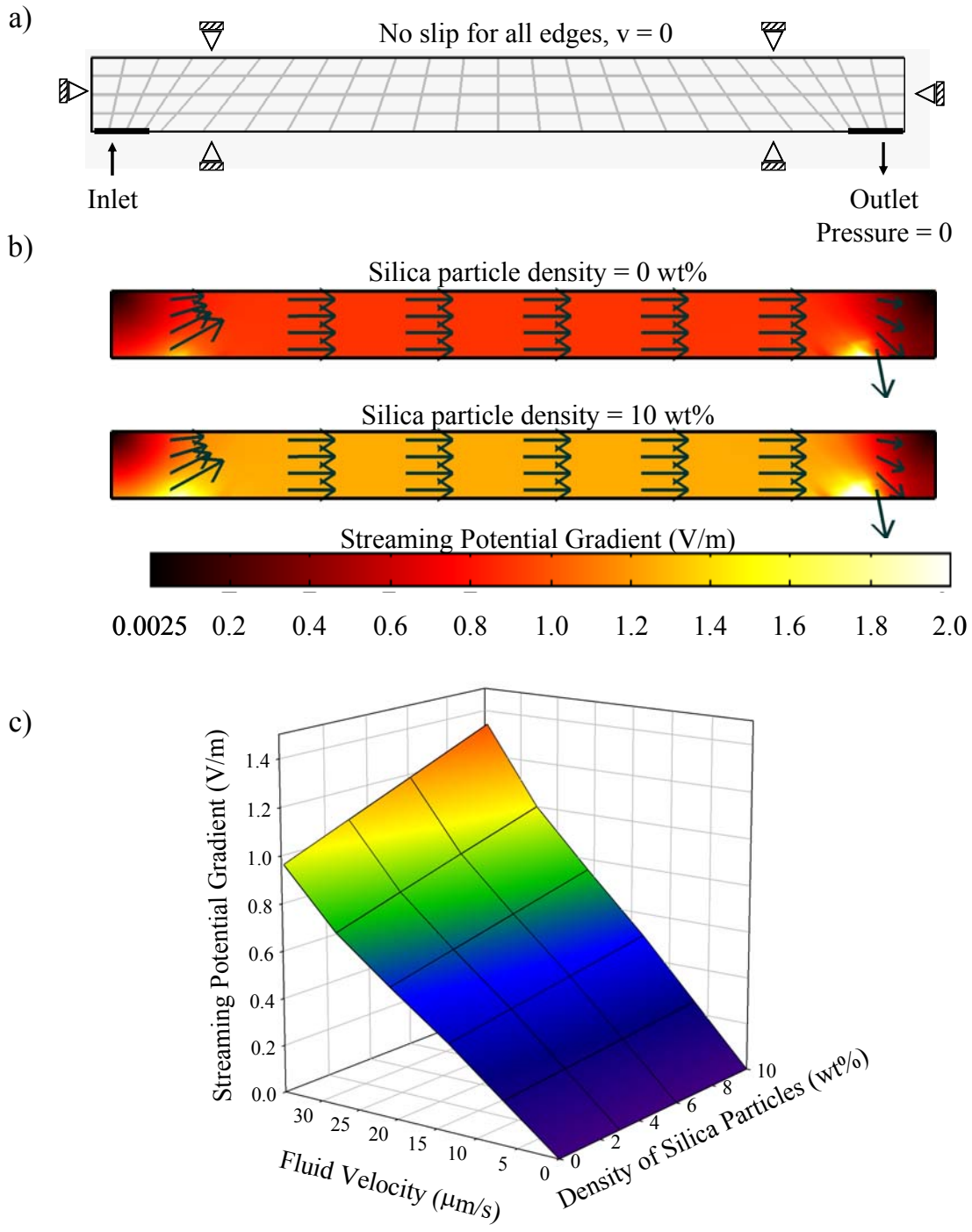

Figure E3: a) COMSOL model with mesh and boundary conditions used to simulate experimental conditions; b) COMSOL predictions of streaming current gradient (surface map) and velocity field (arrows) in a 1.3 wt% alginate scaffold with flow rate = 25 μL/min and silica fraction = 0 wt% (top) and 10 wt% (bottom); c) Streaming potential gradient as a function of silica microparticle density and fluid velocity

Results

Covalently crosslinked alginate was doped with silica microparticles to alter the fixed charge density, but viability dropped to approximately 50% upon mixing (data not shown); experiments were therefore conducted without particle doping. In response to the 15% strain induced in the alginate gels in mounting the device chondrocytes experienced an initial elevation of Ca^{2+} signaling that decayed exponentially with time (Fig. E4). The fraction of cells responding initially to the applied strain was 0.73, the equilibrium fraction of cells responding was 0.14 and the time constant of decay was 37.5 min ($R^2 = 0.95$; RMSE = 3.9% n = 4).

The Ca^{2+} signaling response of chondrocytes in alginate gels significantly increased with fluid flow for fluid velocities of 13-35 μm/s ($p < 0.001$) (Fig. E5).

Simulation of flow through porous alginate scaffolds doped with silica microparticles demonstrated the coupled effects of flow rate and charge density on streaming potential gradient. FE simulations with flow rates of 25 μL/min displayed streaming potential gradients of 0.97 and 1.34 V/m for silica particle densities of 0 and 10 wt% respectively (Fig. E3b), the full range of streaming potential gradient at the maximum flow rate. The 24 combinations of fluid velocity and charge density studied demonstrated streaming potential gradients which varied from 0-1.3 V/m (Fig. E3c). The simulation predicts an approximately 28% variation in streaming potential gradient for a given flow rate.

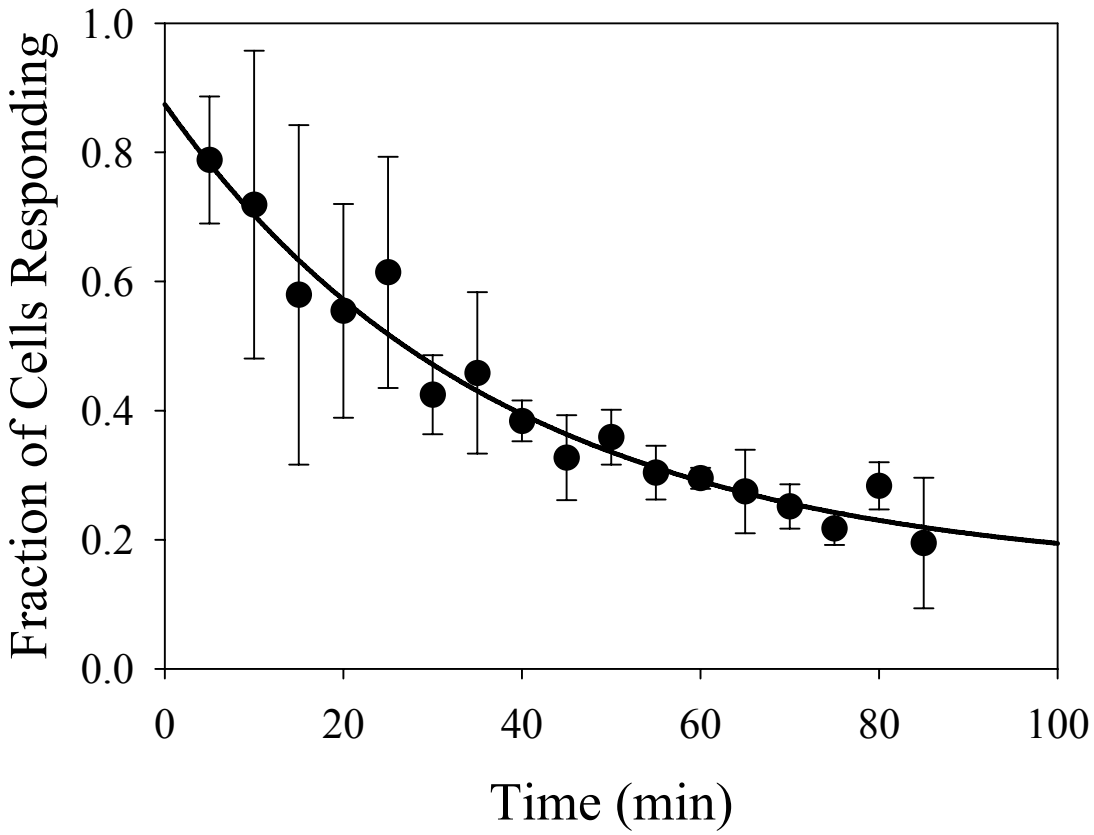

Figure E4: Time course of the Ca^{2+} signaling response of chondrocytes in covalently crosslinked alginate scaffolds (0 wt% silica particles) to the applied (15%) strain. Data corresponding to cells in each scaffold were fit to a 3-parameter exponential decay model with a time constant of 37.5 min and equilibrium value of 0.14 (n = 4; R^2 = 0.95; RMSE = 3.9%).

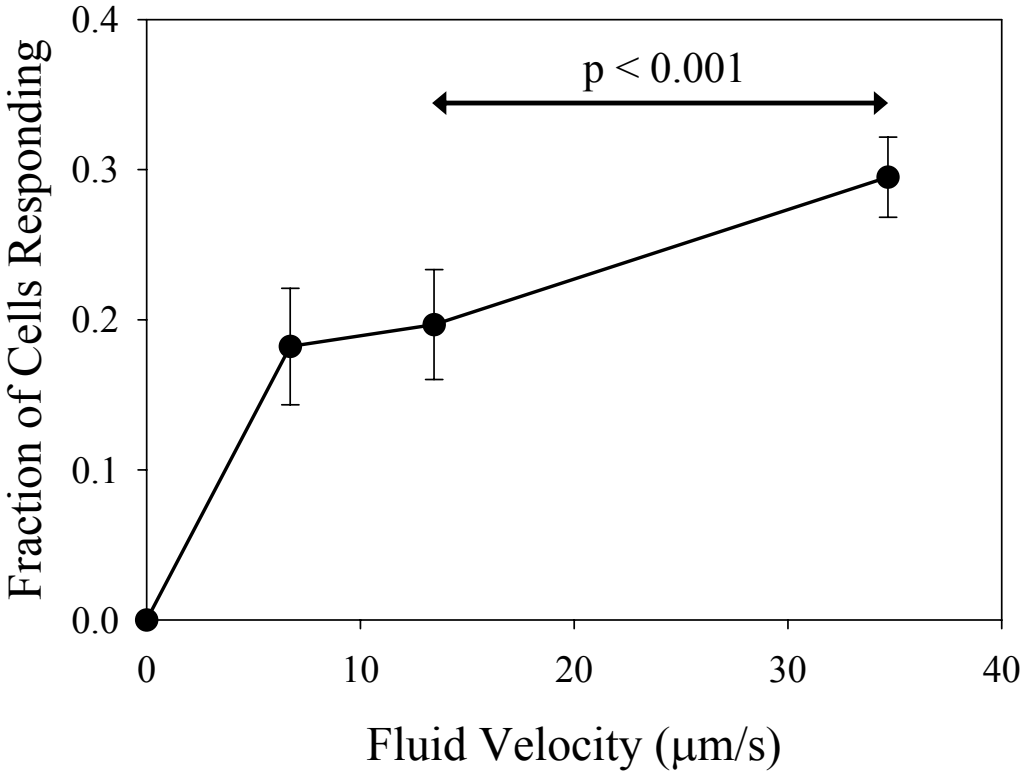

Figure E5: The fraction of cells exhibiting Ca^{2+} signaling response increased monotonically for fluid velocities of 13-35 μm/s in covalently crosslinked alginate hydrogels with 0 wt% silica particles ($p<0.05$; $n = 3$-5).

Discussion

This study was designed to utilize the properties of covalently crosslinked alginate doped with silica microparticles as a means of decoupling the effects of flow-induced electric fields and fluid flow on the metabolic response of chondrocytes in hydrogel scaffolds. While silica microparticles could not be added to alginate-cell mixtures without a drastic reduction in cell viability, the effects of fluid flow on the Ca^{2+} signaling response in covalently crosslinked alginate scaffolds were measured.

As seen in previous studies, chondrocytes in covalently crosslinked alginate gels were sensitive to the applied deformation caused during device preparation (chapters 3 and 4). We observed that chondrocytes responded to mechanical loading with an immediate increase in Ca^{2+} signaling for almost 75% of cells followed by an exponential decay in the number of cells responding over time (Fig. E4). However, almost twice as many cells in covalently crosslinked alginate scaffolds demonstrated a signaling response to gel deformation than seen in ionically crosslinked gels (Fig. 3.4). Ca^{2+} signaling response increased monotonically with fluid velocity as well (Fig. E5). The normalized fraction of cells responding was also approximately twice that seen in 1 wt% ionically crosslinked alginate gels (Fig. 3.5). This may indicate a signaling response due to variations in electrical properties between covalently crosslinked and ionically crosslinked alginate. The electrokinetic kinetic coupling coefficient of covalently crosslinked alginate was measured to be 3 times as high as that of ionically crosslinked alginate, indicating a higher fixed charge density and subsequently higher streaming current for a given flow rate [205].

Measurements of time-course intensity data demonstrated an overall reduction in amplitude changes, noise and drift in covalently crosslinked alginate. This may

have led to smaller Gaussian distributions of the data used to classify a Ca^{2+} response (chapter 3), leading to lower thresholds of intensity changes registering as signaling responses. A contributing factor to the altered response may be the lower levels of exogenous calcium present in covalently crosslinked alginate which regulate the amount of Ca^{2+} released from internal stores [52, 109]. Ionically crosslinked alginate has much higher levels of exogenous Ca^{2+} than covalently crosslinked alginate which may alter the measured metabolic response by allowing additional extracellular Ca^{2+} into the cell, interfering or altering the observed signaling response.

COMSOL finite element simulations were used to calculate the streaming potential gradients generated by a range of flow rates and silica particle densities in order to correlate these stimuli to measured Ca^{2+} responses. Simulated flow through covalently crosslinked alginate resulted in an increase in streaming potential gradients dependent on both fluid velocity and silica particle density (Fig. E3c). The variables used to calculate streaming potential were based on non-compressive flow rates (data not shown) and particle densities shown to maintain cell viability [205]. The streaming currents calculated are consistent with those shown to alter ECM synthesis in cell culture [213, 227, 228] while much lower current densities were needed to increase protein synthesis in cartilage explants [36, 215, 228]. This has been attributed to a reduced conductivity with increasing cell density and must be taken into account in future models [228].

A goal of this study was to independently vary the charge density and fluid velocity within alginate scaffolds to investigate the effects of streaming current on chondrocyte metabolism. Finite element calculations based 0 and 10 wt% silica particle fraction demonstrate a maximum variation of 28% for streaming potential

gradients at any given fluid velocity (Fig. E3c). In studies investigating the effects of fluid flow (Chapter 2) or cell adhesion (Chapter 3) on chondrocyte metabolism, fluid velocity and adhesion ligand density were varied by a factor of 10 to 100 respectively to generate significant changes in Ca^{2+} response. Therefore, a greater range of streaming potentials may be required to generate similar results. While the fraction of silica microparticles cannot be further increased, it may be possible to reduce the coupling coefficient in covalently crosslinked alginate (6 μV/kPa) to that seen in ionically crosslinked alginate (2 μV/kPa) by incorporation of positively charged silica particles. This would result in a streaming potential variation of ~80% at the highest flow rate and increase the chances of a significant cell response.

In conclusion, we have shown that the metabolic response of articular chondrocytes cultured in covalently crosslinked alginate scaffolds is sensitive to fluid flow. The Ca^{2+} response seen in covalently crosslinked alginate scaffolds was higher than that seen in ionically crosslinked alginate and that this difference may be due to the electrokinetic properties of the polymers or the variation in exogenous calcium concentration. Finite element simulations, based on measured material properties, can inform experimental methodology and further understanding of the coupled effects of fluid flow and streaming potential on chondrocyte metabolism.

APPENDIX F

CALCULATING FLUID VELOCITY BY TRACKING LOCATION OF INTENSITY MINIMA WITH TIME: AN ANALYSIS OF EXPERIMENTAL APPROACH

INTRODUCTION

In Chapter 2 I introduced a method of measuring fluid flow in porous alginate hydrogels. Briefly, the method involved perfusing alginate gels with a fluorescein solution and photobleaching a line perpendicular to the flow direction. By tracking the location of the intensity minimum of the photobleached area with time I was able to calculate the velocity of flow in a very localized area. The location of the intensity minimum was tracked by fitting a 30 pixel parabola (3.3 μm) about the minimum of the entire intensity profile (Fig. 2.2), calculating the minimum of the parabola, and tracking it with time[161].

While this approach provided reproducible results, the parabola used to fit the entire intensity profile comprised less than 10% of the photobleached region. Therefore, this appendix addresses alternate methods of fitting the intensity profile. Specifically, I quantified the accuracy of fit of 3 approaches to fitting the intensity profile to track its minimum, 1) a 30 pixel parabolic fit, 2) a 160 pixel parabolic fit, and 3) a 160 pixel Gaussian fit.

METHODS

The accuracy of the 3 different fit types in describing the intensity data was

examined for a subset of the data presented in Chapter 2. I assumed that any error caused by fitting a small, 30 pixel, parabola to the data would be magnified in the presence of noise in the intensity profile which was greater in 2 and 3 wt% alginate gels. Therefore 12 data points were reexamined from photobleaching experiments in both 2 and 3 wt% alginate gels.

Accuracy of fit was determined by fitting 4 successive intensity profiles which capture 0.04 s after the applied bleach. Each of the images was fit to a 30 pixel parabolic fit (30p), a 160 pixel parabolic fit (160p), and a 160 pixel Gaussian fit (160G) using Matlab (Fig. F1a-c). R^2 and RMSE were calculated to quantify the accuracy of the fit to each of the 4 intensity profiles used to calculate fluid velocity for a specific data point.

In order to assess the effects of fitting 160 pixels about the intensity minimum on the fluid velocities calculated, the data set describing fluid velocity at 25 μm depth for flow rates of 0-25 μL/min were reanalyzed with alternate fit parameters. An examination of the location vs. time data used to calculate the flow velocities was performed by examining the R^2 values of the slope calculations based on each of the 3 curve fitting approaches.

Statistics

R^2 and RMSE values from each curve fitting approach and alginate wt% were compared using 1-way ANOVA on ranks with a Tukey posthoc analysis. Differences between fit parameters and solid volume fraction were compared using a 2-way ANOVA with Tukey posthoc analysis. Values were reported at mean ± standard deviation.

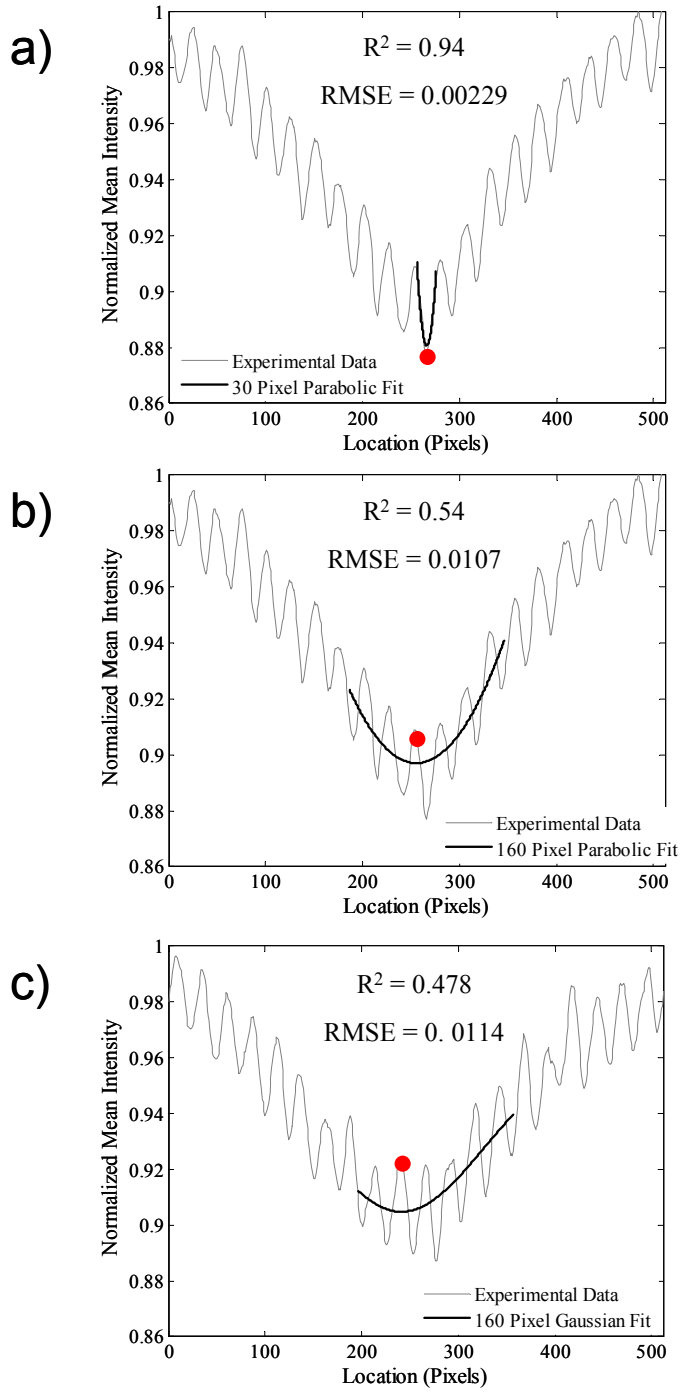

Figure F1: The location of the minimum of normalized intensity profiles from photobleached alginate samples was tracked by fitting the data to a a) 30 pixel parabola; b) 160 pixel parabola; c) 160 pixel Gaussian distribution and calculating the minimum of the curve.

RESULTS

The fit of a 30p about the intensity minimum of the photobleached area was significantly better than either a 160p or a 160G for both 2 and 3 wt%, perfused, alginate gels ($p<0.05$) as evidenced by the higher R^2 and lower RMSE values for the data analyzed (Fig. F2a,b, F3a,b). Pooled fit parameters from 2 and 3 wt% gels (Fig. F4 a,b) demonstrated a significant difference in fit parameters (both R^2 and RMSE) between 2 and 3 wt% alginate gels ($p < 0.001$) with one exception. R^2 values between 2 and 3 wt% alginate were similar for the 30p fits.

After examining accuracy of the 3 curve fits to intensity profiles I then examined the subsequent fluid velocity calculations derived from each fit and compared them to Darcy flow calculations for 2 wt% alginate gels at flow rates of 0, 5, 10, and 25 μL/min. The linearity of the calculated slopes was performed to examine the location data calculated from curve fitting to the intensity profiles. I found that the 30p curve fit resulted in a consistently higher R^2 value indicating location measurements with less noise than seen in 160p and 160G fits for data from flow rate = 25 μL/min (Fig. F5). A large deviation in fluid velocity occurred between the original 30p calculations and the 160p and 160G calculations, particularly at the highest flow rate (Fig. F6). While the 30p calculations were consistent with Darcy flow ($R^2 = 0.94$, RMSE ≤ 2.3), both 160p and 160G calculations indicated fluid velocities significantly lower.

DISCUSSION

This analysis was conducted to quantify the accuracy of a 30 pixel parabolic fit to the global minima of the series of intensity profiles used to calculate fluid velocity

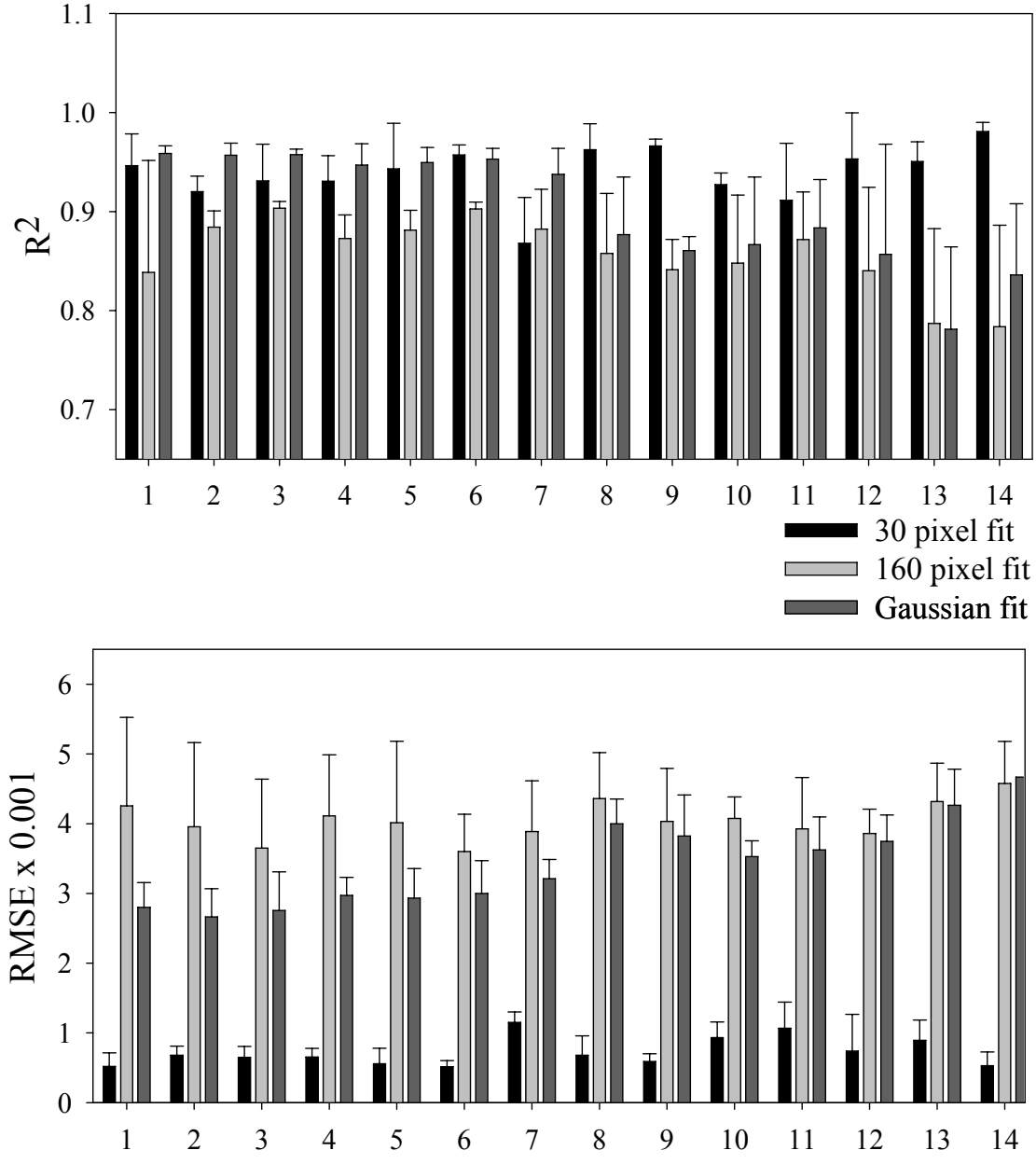

Figure F2: a) R^2 and b) RMSE values for curve fits to intensity profiles created by photobleaching in 2 wt% alginate gels. Each grouping of R^2 or RMSE values corresponds to the fit of a 30 pixel parabola, 160 pixel parabola and 160 pixel Gaussian curve fits to the same 4 consecutive intensity profiles; R^2 and RMSE values for the 3 curve fits were significantly different from each other ($p < 0.05$).

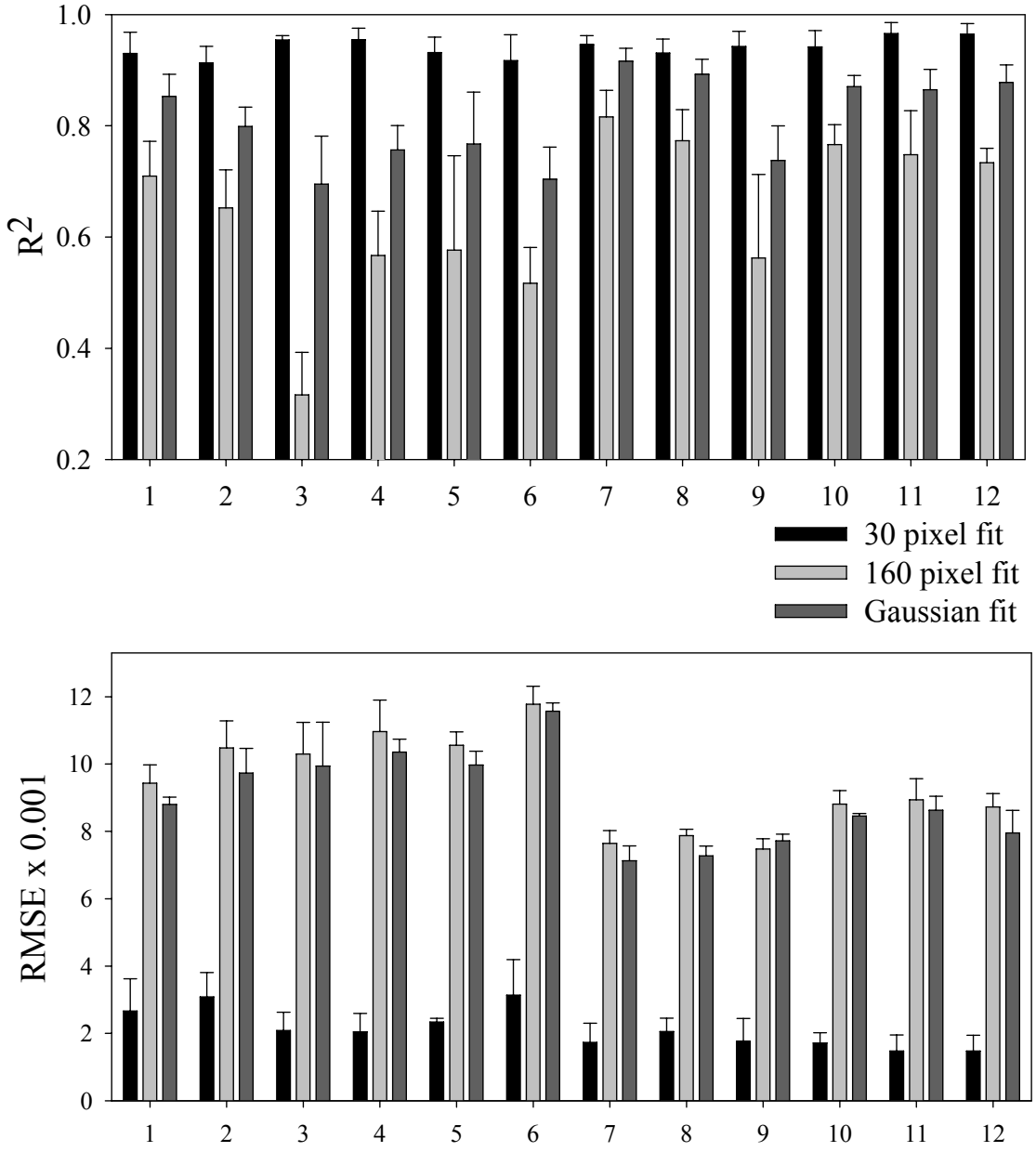

Figure F3: a) R^2 and b) RMSE values for curve fits to intensity profiles created by photobleaching in 3 wt% alginate gels. Each grouping of R^2 or RMSE values corresponds to the fit of a 30 pixel parabola, 160 pixel parabola and 160 pixel Gaussian distribution to the same 4 consecutive intensity profiles; R^2 values for the 3 curve fits were significantly different from each other ($p < 0.001$), while RMSE values for the 160 pixel parabola and 160 Gaussian distribution were significantly different from the 30 pixel parabolic fit ($p < 0.001$).

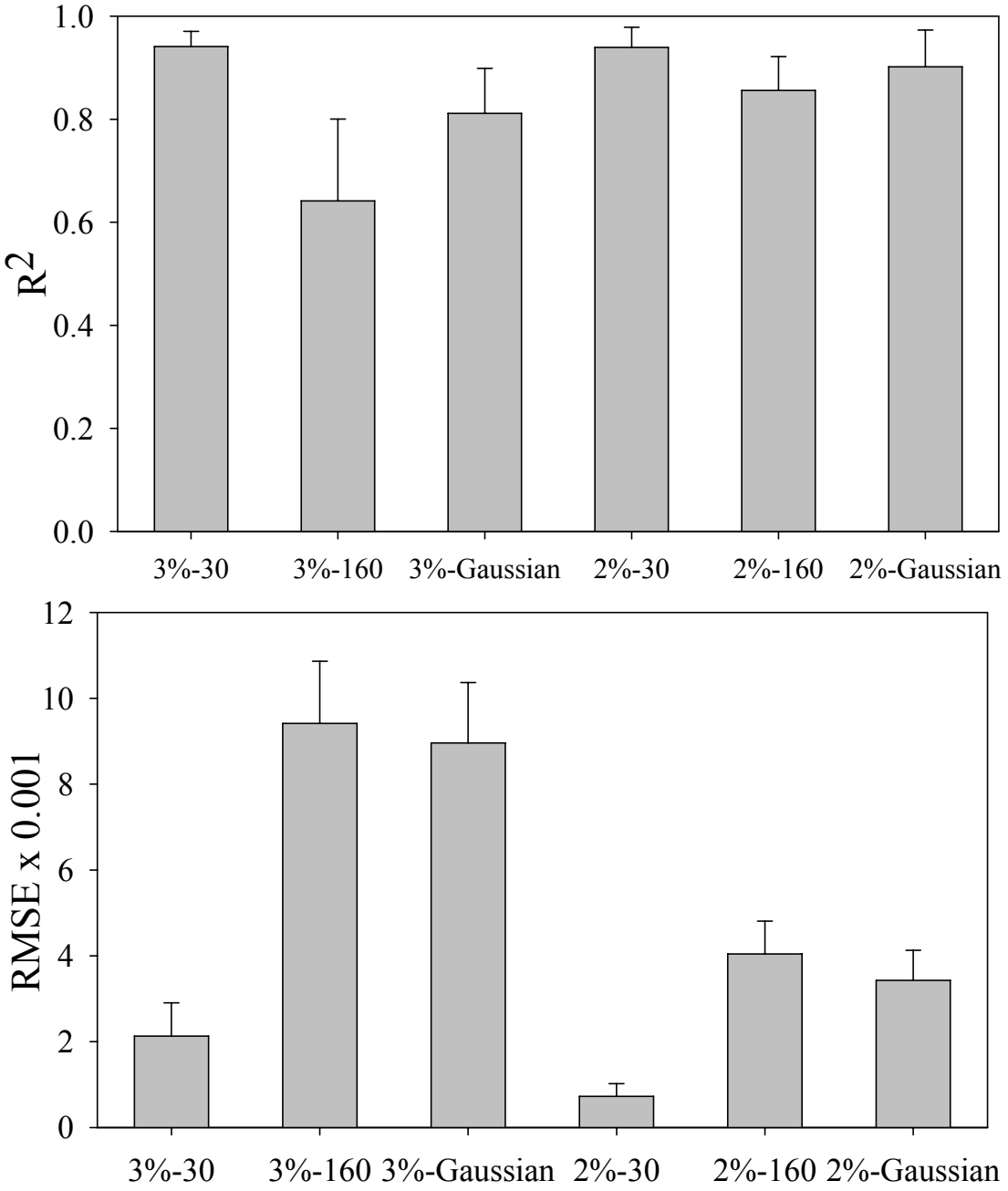

Figure F4: a) R^2 and b) RMSE values for curve fits to intensity profiles created by photobleaching in alginate gels. R^2 values for were pooled (n = 48) from individual curve fits of 30 pixel parabola, 160 pixel parabola and 160 pixel Gaussian distribution to intensity profiles.

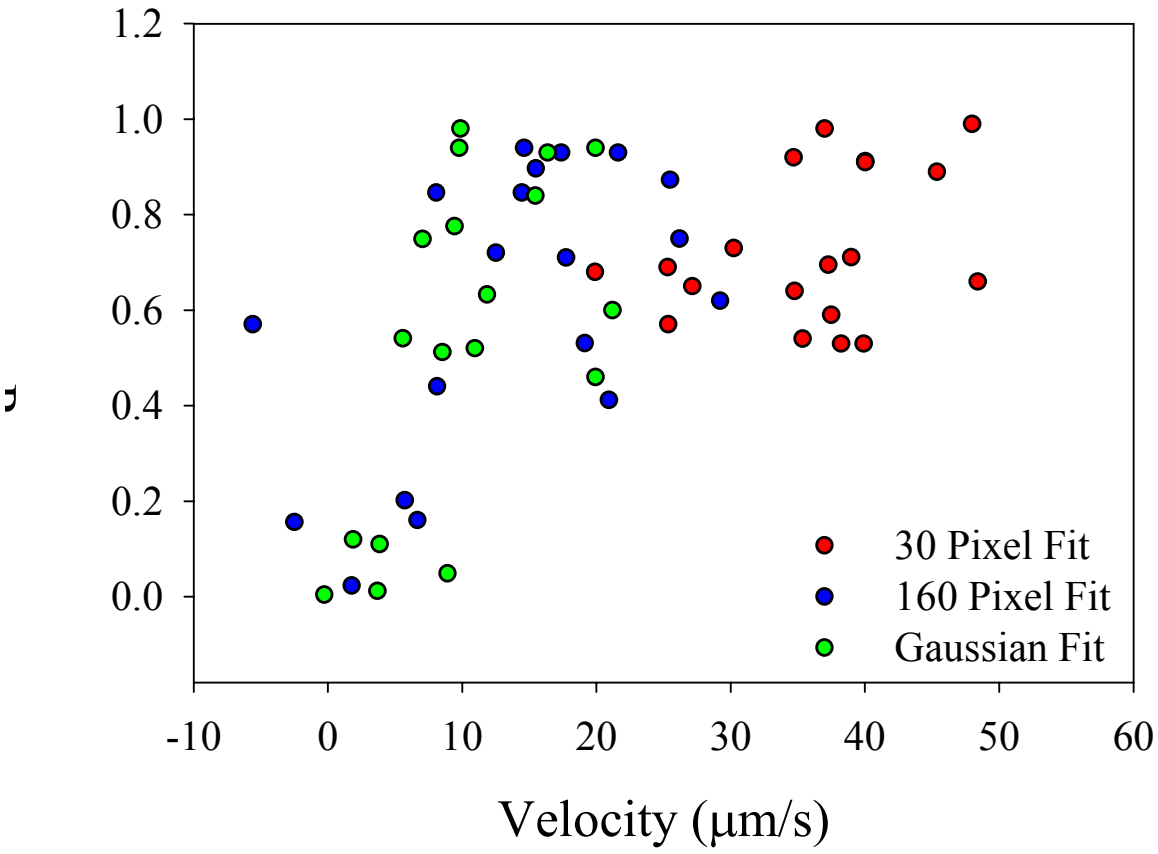

Figure F5: R^2 and fluid velocity calculalted from linear regression (slope) of intensity minima vs. time plots for 2 wt% alginate gels with flow rate = 25 μL/min.

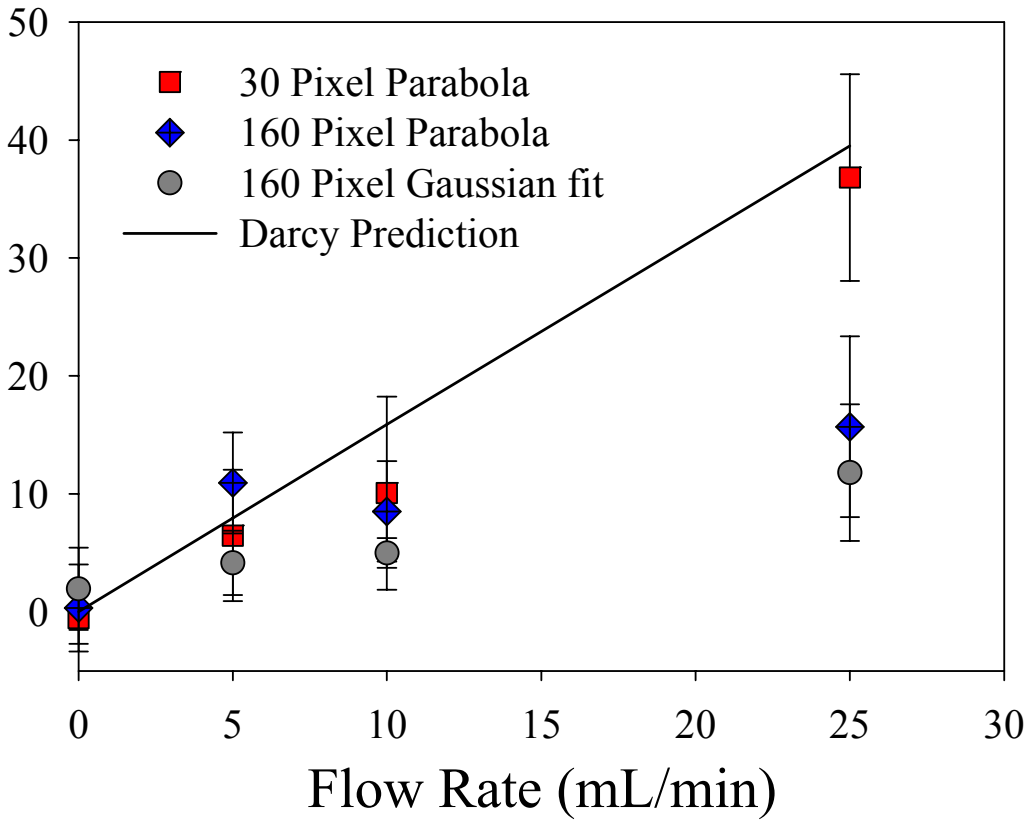

Figure F6: Fluid velocity measurements derived from fitting 30 and 160 pixel parabolas as well as 160 pixel Gaussian distributions to intensity profiles; data is plotted against Darcy flow predictions in 2 wt% alginate gels at 25 μm depth over a range of flow rates.

in Chapter 2. In order to verify the choice of a small parabolic fit to the data, a 160 pixel fit to the global minima of the intensity profiles were applied as either a parabolic or Gaussian curve fit. A comparison of the 3 methods of fitting intensity profiles indicates that fitting a smaller parabola more accurately describes the intensity profile as a whole (Figs. 2-4) and gives rise to fluid velocity measurements consistent with Darcy flow in the bulk (Fig. 6).

In fitting the 3 curves to various intensity profiles I noticed several peculiarities specific to the 160 pixel fits. When fitting the larger curves onto noisier, asymetric intensity profiles I noticed that the minima location would be shifted alternately left and right depending on the lobes created by noise from light collection after photobleaching and did not represent the shape of the curve as a whole. This was seen in the lower R2 values calculated for both 2 and 3 wt% gels. These effects are less apparent in 1 wt% alginate gels and disappear completely while tracking flow in the absence of alginate (data not shown).

Linear regression was applied to intensity minima vs. time plots in order to calculate slope, and therefore fluid velocity for 2 wt% alginate gels with flow rates of 0 – 25 μL/min. The fit of these slopes to the data was analyzed to provide a rough measure of the effect of the curve fit to the resultant velocity calculated. As seen by the consistently higher R^2 values, the 30p curve fits provided data better described by the slope taken from linear regression and resulted in a more consistent velocity calculation (Fig. F5).

Fluid velocity calculations were significantly lower using both 160 pixel fits compared to the 30 pixel fit, particularly at the highest flow rate (Fig. F6). The combination of fit parameters and the similarity of 30p velocity calculations to Darcy

flow suggest that the 30p curve fit may better describe the shape of the intensity profiles, leading to a more accurate description of flow behavior in the perfused alginate hydrogels.

REFERENCES

1. Mow, V.C., C.C. Wang, and C.T. Hung, *The extracellular matrix, interstitial fluid and ions as a mechanical signal transducer in articular cartilage.* Osteoarthritis and Cartilage, 1999. **7**(1): p. 41-58.
2. Hodge, W.A., et al., *Contact Pressures in the Human Hip-Joint Measured Invivo.* Proceedings of the National Academy of Sciences of the United States of America, 1986. **83**(9): p. 2879-2883.
3. Hardingham, T.E. and A.J. Fosang, *Proteoglycans - Many Forms and Many Functions.* Faseb Journal, 1992. **6**(3): p. 861-870.
4. Mathews, M.B. and I. Lozaityte, *Sodium Chondroitin Sulfate-Protein Complexes of Cartilage .1. Molecular Weight and Shape.* Archives of Biochemistry and Biophysics, 1958. **74**(1): p. 158-174.
5. Doege, K.J., et al., *Complete Coding Sequence and Deduced Primary Structure of the Human Cartilage Large Aggregating Proteoglycan, Aggrecan - Human-Specific Repeats, and Additional Alternatively Spliced Forms.* Journal of Biological Chemistry, 1991. **266**(2): p. 894-902.
6. Eyre, D.R., et al., *Covalent cross-linking of the NC1 domain of collagen type IX to collagen type II in cartilage.* Journal of Biological Chemistry, 2004. **279**(4): p. 2568-2574.
7. Bianco, P., et al., *Expression and Localization of the 2 Small Proteoglycans Biglycan and Decorin in Developing Human Skeletal and Nonskeletal Tissues.* Journal of Histochemistry & Cytochemistry, 1990. **38**(11): p. 1549-1563.
8. Roughley, P.J. and E.R. Lee, *Cartilage Proteoglycans - Structure and Potential Functions.* Microscopy Research and Technique, 1994. **28**(5): p. 385-397.

9. Knudson, C.B. and W. Knudson, *Cartilage proteoglycans.* Seminars in Cell & Developmental Biology, 2001. **12**(2): p. 69-78.

10. Loeser, R.F., *Integrin-mediated attachment of articular chondrocytes to extracellular matrix proteins.* Arthritis Rheum, 1993. **36**(8): p. 1103-10.

11. Hassell, J.R., J.H. Kimura, and V.C. Hascall, *Proteoglycan core protein families.* Annu Rev Biochem, 1986. **55**: p. 539-67.

12. Reid, D.L., M.B. Aydelotte, and J. Mollenhauer, *Cell attachment, collagen binding, and receptor analysis on bovine articular chondrocytes.* J Orthop Res, 2000. **18**(3): p. 364-73.

13. Cardarelli, P.M., et al., *The collagen receptor alpha 2 beta 1, from MG-63 and HT1080 cells, interacts with a cyclic RGD peptide.* J Biol Chem, 1992. **267**(32): p. 23159-64.

14. Helminen, H.J., et al., *Effects of Immobilization for 6 Weeks on Rabbit Knee Articular Surfaces as Assessed by the Semiquantitative Stereomicroscopic Method.* Acta Anatomica, 1983. **115**(4): p. 327-335.

15. Palmoski, M., E. Perricone, and K.D. Brandt, *Development and Reversal of a Proteoglycan Aggregation Defect in Normal Canine Knee Cartilage after Immobilization.* Arthritis and Rheumatism, 1979. **22**(5): p. 508-517.

16. Tammi, M., et al., *Proteoglycan Alterations in Rabbit Knee Articular-Cartilage Following Physical Exercise and Immobilization.* Connective Tissue Research, 1983. **11**(1): p. 45-55.

17. Salter, R.B. and P. Field, *The Effects of Continuous Compression on Living Articular Cartilage - an Experimental Investigation.* Journal of Bone and Joint Surgery-American Volume, 1960. **42**(1): p. 31-49.

18. Arden, N. and M.C. Nevitt, *Osteoarthritis: Epidemiology.* Best Practice & Research in Clinical Rheumatology, 2006. **20**(1): p. 3-25.

19. Caterson, B., et al., *Mechanisms involved in cartilage proteoglycan catabolism.* Matrix Biology, 2000. **19**(4): p. 333-344.

20. Grushko, G., R. Schneiderman, and A. Maroudas, *Some Biochemical and Biophysical Parameters for the Study of the Pathogenesis of Osteo-Arthritis - a Comparison between the Processes of Aging and Degeneration in Human Hip Cartilage.* Connective Tissue Research, 1989. **19**(2-4): p. 149-176.

21. Mohamedali, H., *Proteolytic-Enzymes and the Destruction of Articular-Cartilage in Rheumatoid-Arthritis and Osteoarthritis.* Wiener Medizinische Wochenschrift, 1991. **141**(4): p. 77-&.

22. Roberts, C.R., J.S. Mort, and P.J. Roughley, *Age-Related-Changes in Human Articular-Cartilage Proteoglycan Aggregate May Be Attributable to the Action of Hydroxyl Radicals.* Journal of Cell Biology, 1986. **103**(5): p. A254-A254.

23. Bauer, W. and G.A. Bennett, *Experimental and pathological studies in the degenerative type of arthritis.* Journal of Bone and Joint Surgery, 1936. **18**: p. 1-18.

24. D'Ambrosia, R.D., *Epidemiology of osteoarthritis.* Orthopedics, 2005. **28**(2): p. S201-S205.

25. Hutton, C.W., *Osteoarthritis: the cause not result of joint failure?* Ann Rheum Dis, 1989. **48**(11): p. 958-61.

26. Kreutz, A. and D. Kohn, *Joint damage by sport injuries.* Deutsche Zeitschrift Fur Sportmedizin, 2002. **53**(2): p. 45-48.

27. Sah, R.L., et al., *Physical properties of rabbit articular cartilage after transection of the anterior cruciate ligament.* Journal of Orthopaedic Research, 1997. **15**(2): p. 197-203.

28. Farkas, T., et al., *Early Vascular Changes in Rabbit Subchondral Bone after Repetitive Impulsive Loading.* Clinical Orthopaedics and Related Research,

1987(219): p. 259-267.

29. Hascall, V.C., et al., *The effect of serum on biosynthesis of proteoglycans by bovine articular cartilage in culture.* Arch Biochem Biophys, 1983. **224**(1): p. 206-23.

30. McQuillan, D.J., et al., *Stimulation of proteoglycan biosynthesis by serum and insulin-like growth factor-I in cultured bovine articular cartilage.* Biochem J, 1986. **240**(2): p. 423-30.

31. Bayliss, M.T., et al., *In vitro method for measuring synthesis rates in the intervertebral disc.* J Orthop Res, 1986. **4**(1): p. 10-7.

32. Gray, M.L., et al., *Mechanical and physiochemical determinants of the chondrocyte biosynthetic response.* J Orthop Res, 1988. **6**(6): p. 777-92.

33. Jones, I.L., A. Klamfeldt, and T. Sandstrom, *The effect of continuous mechanical pressure upon the turnover of articular cartilage proteoglycans in vitro.* Clin Orthop Relat Res, 1982(165): p. 283-9.

34. Buschmann, M.D., et al., *Stimulation of aggrecan synthesis in cartilage explants by cyclic loading is localized to regions of high interstitial fluid flow.* Arch Biochem Biophys, 1999. **366**(1): p. 1-7.

35. Kim, Y.J., et al., *Mechanical Regulation of Cartilage Biosynthetic Behavior - Physical Stimuli.* Archives of Biochemistry and Biophysics, 1994. **311**(1): p. 1-12.

36. Sah, R.L., et al., *Biosynthetic response of cartilage explants to dynamic compression.* J Orthop Res, 1989. **7**(5): p. 619-36.

37. Poole, C.A., M.H. Flint, and B.W. Beaumont, *Morphological and functional interrelationships of articular cartilage matrices.* J Anat, 1984. **138 (Pt 1)**: p. 113-38.

38. Frank, E.H. and A.J. Grodzinsky, *Cartilage Electromechanics .1.*

Electrokinetic Transduction and the Effects of Electrolyte Ph and Ionic-Strength. Journal of Biomechanics, 1987. **20**(6): p. 615-&.

39. Lee, R.C., et al., *Oscillatory Compressional Behavior of Articular-Cartilage and Its Associated Electro-Mechanical Properties.* Journal of Biomechanical Engineering-Transactions of the Asme, 1981. **103**(4): p. 280-292.
40. Mow, V.C., M.H. Holmes, and W.M. Lai, *Fluid Transport and Mechanical-Properties of Articular-Cartilage - a Review.* Journal of Biomechanics, 1984. **17**(5): p. 377-394.
41. Carver, S.E. and C.A. Heath, *Semi-continuous perfusion system for delivering intermittent physiological pressure to regenerating cartilage.* Tissue Eng, 1999. **5**(1): p. 1-11.
42. Lippiello, L., et al., *In vitro metabolic response of articular cartilage segments to low levels of hydrostatic pressure.* Connect Tissue Res, 1985. **13**(2): p. 99-107.
43. Grodzinsky, A.J., *Electromechanical and Physicochemical Properties of Connective-Tissue.* Crc Critical Reviews in Biomedical Engineering, 1983. **9**(2): p. 133-199.
44. Lee, V., et al., *The roles of matrix molecules in mediating - Chondrocyte aggregation, attachment, and spreading.* Journal of Cellular Biochemistry, 2000. **79**(2): p. 322-333.
45. Ramachandrula, A., K. Tiku, and M.L. Tiku, *Tripeptide Rgd-Dependent Adhesion of Articular Chondrocytes to Synovial Fibroblasts.* Journal of Cell Science, 1992. **101**: p. 859-871.
46. Guilak, F., et al., *Mechanically induced calcium waves in articular chondrocytes are inhibited by gadolinium and amiloride.* J Orthop Res, 1999. **17**(3): p. 421-9.

47. DAndrea, P. and F. Vittur, *Propagation of intercellular Ca2+ waves in mechanically stimulated articular chondrocytes.* Febs Letters, 1997. **400**(1): p. 58-64.

48. Edlich, M., et al., *Oscillating fluid flow regulates cytosolic calcium concentration in bovine articular chondrocytes.* J Biomech, 2001. **34**(1): p. 59-65.

49. Eifler, R.L., et al., *Oscillatory fluid flow regulates glycosaminoglycan production via an intracellular calcium pathway in meniscal cells.* J Orthop Res, 2006. **24**(3): p. 375-84.

50. Lane Smith, R., et al., *Effects of shear stress on articular chondrocyte metabolism.* Biorheology, 2000. **37**(1-2): p. 95-107.

51. Smith, R.L., et al., *Effects of fluid-induced shear on articular chondrocyte morphology and metabolism in vitro.* J Orthop Res, 1995. **13**(6): p. 824-31.

52. Yellowley, C.E., et al., *Effects of fluid flow on intracellular calcium in bovine articular chondrocytes.* Am J Physiol, 1997. **273**(1 Pt 1): p. C30-6.

53. Mizuno, S., *A novel method for assessing effects of hydrostatic fluid pressure on intracellular calcium: a study with bovine articular chondrocytes.* Am J Physiol Cell Physiol, 2005. **288**(2): p. C329-37.

54. Parkkinen, J.J., et al., *Effects of cyclic hydrostatic pressure on proteoglycan synthesis in cultured chondrocytes and articular cartilage explants.* Arch Biochem Biophys, 1993. **300**(1): p. 458-65.

55. Benya, P.D., S.R. Padilla, and M.E. Nimni, *Progeny of Rabbit Articular Chondrocytes Synthesize Collagen Type-1 and Type-3 and Type-1 Trimer, but Not Type-2 - Verifications by Cyanogen-Bromide Peptide Analysis.* Biochemistry, 1977. **16**(5): p. 865-872.

56. Mayne, R., et al., *Changes in Type of Collagen Synthesized as Clones of Chick*

Chondrocytes Grow and Eventually Lose Division Capacity. Proceedings of the National Academy of Sciences of the United States of America, 1976. **73**(5): p. 1674-1678.

57. Oegema, T.R. and R.C. Thompson, *Characterization of a Hyaluronic-Acid Dermatan Sulfate Proteoglycan Complex from Dedifferentiated Human Chondrocyte Cultures.* Journal of Biological Chemistry, 1981. **256**(2): p. 1015-1022.
58. Schiltz, J., R. Mayne, and H. Holtzer, *Synthesis of Collagen and Glycosaminoglycans by Dedifferentiated Chondrocytes in Culture.* Journal of Cell Biology, 1972. **55**(2): p. A229-A229.
59. Cukierman, E., et al., *Taking cell-matrix adhesions to the third dimension.* Science, 2001. **294**(5547): p. 1708-1712.
60. Benya, P.D. and J.D. Shaffer, *Dedifferentiated chondrocytes reexpress the differentiated collagen phenotype when cultured in agarose gels.* Cell, 1982. **30**(1): p. 215-24.
61. Aulthouse, A.L., et al., *Expression of the Human Chondrocyte Phenotype Invitro.* In Vitro Cellular & Developmental Biology, 1989. **25**(7): p. 659-668.
62. Guo, J.F., G.W. Jourdian, and D.K. Maccallum, *Culture and Growth-Characteristics of Chondrocytes Encapsulated in Alginate Beads.* Connective Tissue Research, 1989. **19**(2-4): p. 277-297.
63. Buschmann, M.D., et al., *Chondrocytes in Agarose Culture Synthesize a Mechanically Functional Extracellular-Matrix.* Journal of Orthopaedic Research, 1992. **10**(6): p. 745-758.
64. Bryant, S.J. and K.S. Anseth, *The effects of scaffold thickness on tissue engineered cartilage in photocrosslinked poly(ethylene oxide) hydrogels.* Biomaterials, 2001. **22**(6): p. 619-626.

65. Potter, K., T.A. Carpenter, and L.D. Hall, *Magnetic resonance imaging (MRI) of calcium alginate gels.* Magn Reson Imaging, 1994. **12**(2): p. 309-11.

66. Shapiro, L. and S. Cohen, *Novel alginate sponges for cell culture and transplantation.* Biomaterials, 1997. **18**(8): p. 583-90.

67. Zimmermann, H., et al., *Physical and biological properties of barium cross-linked alginate membranes.* Biomaterials, 2007. **28**(7): p. 1327-45.

68. Zmora, S., R. Glicklis, and S. Cohen, *Tailoring the pore architecture in 3-D alginate scaffolds by controlling the freezing regime during fabrication.* Biomaterials, 2002. **23**(20): p. 4087-4094.

69. Bellamkonda, R., et al., *Hydrogel-Based 3-Dimensional Matrix for Neural Cells.* Journal of Biomedical Materials Research, 1995. **29**(5): p. 663-671.

70. Chui, M.M., R.J. Phillips, and M.J. Mccarthy, *Measurement of the Porous Microstructure of Hydrogels by Nuclear-Magnetic-Resonance.* Journal of Colloid and Interface Science, 1995. **174**(2): p. 336-344.

71. Holmes, D.L. and N.C. Stellwagen, *Estimation of Polyacrylamide-Gel Pore-Size from Ferguson Plots of Linear DNA Fragments .2. Comparison of Gels with Different Cross-Linker Concentrations, Added Agarose and Added Linear Polyacrylamide.* Electrophoresis, 1991. **12**(9): p. 612-619.

72. Gutowska, A., B. Jeong, and M. Jasionowski, *Injectable gels for tissue engineering.* Anatomical Record, 2001. **263**(4): p. 342-349.

73. Martinsen, A., G. Skjakbraek, and O. Smidsrod, *Alginate as Immobilization Material .1. Correlation between Chemical and Physical-Properties of Alginate Gel Beads.* Biotechnology and Bioengineering, 1989. **33**(1): p. 79-89.

74. Chang, S.C., et al., *Injection molding of chondrocyte/alginate constructs in the shape of facial implants.* J Biomed Mater Res, 2001. **55**(4): p. 503-11.

75. Paige, K.T., et al., *Injectable Cartilage.* Plastic and Reconstructive Surgery,

1995. **96**(6): p. 1390-1398.

76. Hauselmann, H.J., et al., *Phenotypic Stability of Bovine Articular Chondrocytes after Long-Term Culture in Alginate Beads.* Journal of Cell Science, 1994. **107**: p. 17-27.

77. Buschmann, M.D., et al., *Mechanical compression modulates matrix biosynthesis in chondrocyte/agarose culture.* J Cell Sci, 1995. **108 (Pt 4)**: p. 1497-508.

78. Lee, D.A. and D.L. Bader, *Compressive strains at physiological frequencies influence the metabolism of chondrocytes seeded in agarose.* Journal of Orthopaedic Research, 1997. **15**(2): p. 181-188.

79. Giannoni, P., et al., *The mechanosensitivity of cartilage oligomeric matrix protein (COMP).* Biorheology, 2003. **40**(1-3): p. 101-9.

80. Smetana, K., *Cell Biology of Hydrogels.* Biomaterials, 1993. **14**(14): p. 1046-1050.

81. Rowley, J.A., G. Madlambayan, and D.J. Mooney, *Alginate hydrogels as synthetic extracellular matrix materials.* Biomaterials, 1999. **20**(1): p. 45-53.

82. Dodla, M.C. and R.V. Bellamkonda, *Anisotropic scaffolds facilitate enhanced neurite extension in vitro.* Journal of Biomedical Materials Research Part A, 2006. **78A**(2): p. 213-221.

83. Bryant, S.J., G.D. Nicodemus, and I. Villanueva, *Designing 3D Photopolymer Hydrogels to Regulate Biomechanical Cues and Tissue Growth for Cartilage Tissue Engineering.* Pharm Res, 2008. **25**(10): p. 2379-86.

84. Genes, N.G. and L.J. Bonassar. *The Effect of RGD Conjugation on Mechanotransduction by Chondrocytes in Alginate Under Static Compression*. in *Orthopaedic Research Society*. 2005.

85. Kim, Y.J., L.J. Bonassar, and A.J. Grodzinsky, *The role of cartilage streaming*

potential, fluid flow and pressure in the stimulation of chondrocyte biosynthesis during dynamic compression. J Biomech, 1995. **28**(9): p. 1055-66.

86. Lippiello, L., et al., *Invitro Metabolic Response of Articular-Cartilage Segments to Low-Levels of Hydrostatic-Pressure.* Connective Tissue Research, 1985. **13**(2): p. 99-107.
87. Mizuno, S., et al., *Hydrostatic fluid pressure enhances matrix synthesis and accumulation by bovine chondrocytes in three-dimensional culture.* J Cell Physiol, 2002. **193**(3): p. 319-27.
88. Toyoda, T., et al., *Hydrostatic pressure modulates proteoglycan metabolism in chondrocytes seeded in agarose.* Arthritis Rheum, 2003. **48**(10): p. 2865-72.
89. Davisson, T., R.L. Sah, and A. Ratcliffe, *Perfusion increases cell content and matrix synthesis in chondrocyte three-dimensional cultures.* Tissue Engineering, 2002. **8**(5): p. 807-816.
90. Dunkelman, N.S., et al., *Cartilage Production by Rabbit Articular Chondrocytes on Polyglycolic Acid Scaffolds in a Closed Bioreactor System.* Biotechnology and Bioengineering, 1995. **46**(4): p. 299-305.
91. Pazzano, D., et al., *Comparison of chondrogensis in static and perfused bioreactor culture.* Biotechnol Prog, 2000. **16**(5): p. 893-6.
92. Hung, C.T., et al., *Mitogen-activated protein kinase signaling in bovine articular chondrocytes in response to fluid flow does not require calcium mobilization.* J Biomech, 2000. **33**(1): p. 73-80.
93. Aikawa, R., et al., *Oxidative stress activates extracellular signal-regulated kinases through Src and ras in cultured cardiac myocytes of neonatal rats.* Journal of Clinical Investigation, 1997. **100**(7): p. 1813-1821.
94. Coppolino, M.G. and S. Dedhar, *Bi-directional signal transduction by integrin receptors.* International Journal of Biochemistry & Cell Biology, 2000. **32**(2):

p. 171-188.

95. MacKenna, D.A., et al., *Extracellular signal-regulated kinase and c-Jun NH2-terminal kinase activation by mechanical stretch is integrin-dependent and matrix-specific in rat cardiac fibroblasts.* Journal of Clinical Investigation, 1998. **101**(2): p. 301-310.

96. Wheatley, D.N., A.M. Wang, and G.E. Strugnell, *Expression of primary cilia in mammalian cells.* Cell Biology International, 1996. **20**(1): p. 73-81.

97. Donnelly, E., R. Willlams, and C. Farnum, *The primary cilium of connective tissue cells: Imaging by multiphoton microscopy.* Anatomical Record-Advances in Integrative Anatomy and Evolutionary Biology, 2008. **291**(9): p. 1062-1073.

98. Whitfield, J.F., *The solitary (primary) cilium - A mechanosensory toggle switch in bone and cartilage cells.* Cellular Signalling, 2008. **20**(6): p. 1019-1024.

99. Praetorius, H.A. and K.R. Spring, *Bending the MDCK cell primary cilium increases intracellular calcium.* Journal of Membrane Biology, 2001. **184**(1): p. 71-79.

100. Liu, W., et al., *Mechanoregulation of intracellular Ca2+ concentration is attenuated in collecting duct of monocilium-impaired orpk mice.* American Journal of Physiology-Renal Physiology, 2005. **289**(5): p. F978-F988.

101. Praetorius, H.A. and K.R. Spring, *Removal of the MDCK cell primary cilium abolishes flow sensing.* Journal of Membrane Biology, 2003. **191**(1): p. 69-76.

102. Malone, A.M.D., et al., *Primary cilia mediate mechanosensing in bone cells by a calcium-independent mechanism.* Proceedings of the National Academy of Sciences of the United States of America, 2007. **104**(33): p. 13325-13330.

103. McGlashan, S.R., C.G. Jensen, and C.A. Poole, *Localization of extracellular*

matrix receptors on the chondrocyte primary cilium. Journal of Histochemistry & Cytochemistry, 2006. **54**(9): p. 1005-1014.

104. Berridge, M.J., *Inositol trisphosphate and calcium signalling.* Nature, 1993. **361**(6410): p. 315-25.

105. Guilak, F., et al., *The deformation behavior and mechanical properties of chondrocytes in articular cartilage.* Osteoarthritis Cartilage, 1999. **7**(1): p. 59-70.

106. Wright, M., et al., *Effects of intermittent pressure-induced strain on the electrophysiology of cultured human chondrocytes: evidence for the presence of stretch-activated membrane ion channels.* Clin Sci (Lond), 1996. **90**(1): p. 61-71.

107. Grandolfo, M., A. Calabrese, and P. D'Andrea, *Mechanism of mechanically induced intercellular calcium waves in rabbit articular chondrocytes and in HIG-82 synovial cells.* Journal of Bone and Mineral Research, 1998. **13**(3): p. 443-453.

108. Pingguan-Murphy, B., et al., *Activation of chondrocytes calcium signalling by dynamic compression is independent of number of cycles.* Arch Biochem Biophys, 2005. **444**(1): p. 45-51.

109. Erickson, G.R., L.G. Alexopoulos, and F. Guilak, *Hyper-osmotic stress induces volume change and calcium transients in chondrocytes by transmembrane, phospholipid, and G-protein pathways.* J Biomech, 2001. **34**(12): p. 1527-35.

110. D'Andrea, P. and F. Vittur, *Ca2+ oscillations and intercellular Ca2+ waves in ATP-stimulated articular chondrocytes.* J Bone Miner Res, 1996. **11**(7): p. 946-54.

111. Yellowley, C.E., C.R. Jacobs, and H.J. Donahue, *Mechanisms contributing to*

fluid-flow-induced Ca2+ mobilization in articular chondrocytes. J Cell Physiol, 1999. **180**(3): p. 402-8.

112. Berridge, M.J., P. Lipp, and M.D. Bootman, *The versatility and universality of calcium signalling.* Nat Rev Mol Cell Biol, 2000. **1**(1): p. 11-21.

113. Enobakhare, B.O., D.L. Bader, and D.A. Lee, *Quantification of sulfated glycosaminoglycans in chondrocyte/alginate cultures, by use of 1,9-dimethylmethylene blue.* Analytical Biochemistry, 1996. **243**(1): p. 189-191.

114. Stegeman.H and K. Stalder, *Determination of Hydroxyproline.* Clinica Chimica Acta, 1967. **18**(2): p. 267-&.

115. Frangos, J.A., et al., *Flow effects on prostacyclin production by cultured human endothelial cells.* Science, 1985. **227**(4693): p. 1477-9.

116. Jacobs, C.R., et al., *Differential effect of steady versus oscillating flow on bone cells.* J Biomech, 1998. **31**(11): p. 969-76.

117. Mobasheri, A., et al., *Integrins and stretch activated ion channels; putative components of functional cell surface mechanoreceptors in articular chondrocytes.* Cell Biol Int, 2002. **26**(1): p. 1-18.

118. Dull, R.O. and P.F. Davies, *Flow Modulation of Agonist (Atp)-Response (Ca2+) Coupling in Vascular Endothelial-Cells.* American Journal of Physiology, 1991. **261**(1): p. H149-H154.

119. Brinkman, H.C., *A Calculation of the Viscous Force Exerted by a Flowing Fluid on a Dense Swarm of Particles.* Applied Scientific Research Section a-Mechanics Heat Chemical Engineering Mathematical Methods, 1947. **1**(1): p. 27-34.

120. Howle, L.E., R.P. Behringer, and J.G. Georgiadis, *Convection and flow in porous media .2. Visualization by shadowgraph.* Journal of Fluid Mechanics, 1997. **332**: p. 247-262.

121. Corapcioglu, M.Y., S. Chowdhury, and S.E. Roosevelt, *Micromodel visualization and quantification of solute transport in porous media.* Water Resources Research, 1997. **33**(11): p. 2547-2558.

122. Gupte, S.K. and S.G. Advani, *Flow near the permeable boundary of a porous medium: An experimental investigation using LDA.* Experiments in Fluids, 1997. **22**(5): p. 408-422.

123. Baumann, T., et al., *Flow and diffusion measurements in natural porous media using magnetic resonance imaging.* Journal of Environmental Quality, 2002. **31**(2): p. 470-476.

124. Givler, R.C. and S.A. Altobelli, *A Determination of the Effective Viscosity for the Brinkman-Forchheimer Flow Model.* Journal of Fluid Mechanics, 1994. **258**: p. 355-370.

125. Dumoulin, C.L. and H.R. Hart, *Magnetic-Resonance Angiography.* Radiology, 1986. **161**(3): p. 717-720.

126. Dvir, T., et al., *A novel perfusion bioreactor providing a homogenous milieu for tissue regeneration.* Tissue Engineering, 2006. **12**(10): p. 2843-2852.

127. Chen, A.C., et al., *Depth- and strain-dependent mechanical and electromechanical properties of full-thickness bovine articular cartilage in confined compression.* J Biomech, 2001. **34**(1): p. 1-12.

128. Laasanen, M.S., et al., *Biomechanical properties of knee articular cartilage.* Biorheology, 2003. **40**(1-3): p. 133-40.

129. Wang, C.C., C.T. Hung, and V.C. Mow, *An analysis of the effects of depth-dependent aggregate modulus on articular cartilage stress-relaxation behavior in compression.* J Biomech, 2001. **34**(1): p. 75-84.

130. Schinagl, R.M., et al., *Video microscopy to quantitate the inhomogeneous equilibrium strain within articular cartilage during confined compression.*

Ann Biomed Eng, 1996. **24**(4): p. 500-12.

131. Quinn, T.M., et al., *Mechanical compression alters proteoglycan deposition and matrix deformation around individual cells in cartilage explants.* J Cell Sci, 1998. **111 (Pt 5)**: p. 573-83.

132. Guilak, F., *The deformation behavior and viscoelastic properties of chondrocytes in articular cartilage.* Biorheology, 2000. **37**(1-2): p. 27-44.

133. Ofek, G. and K.A. Athanasiou, *Micromechanical properties of chondrocytes and chondrons: Relevance to articular cartilage tissue engineering.* Journal of Mechanics of Materials and Structures, 2007. **2**(6): p. 1059-1086.

134. Poole, C.A., M.H. Flint, and B.W. Beaumont, *Chondrons in Cartilage - Ultrastructural Analysis of the Pericellular Microenvironment in Adult Human Articular Cartilages.* Journal of Orthopaedic Research, 1987. **5**(4): p. 509-522.

135. Auriault, J.L., *On the Domain of Validity of Brinkman's Equation.* Transport in Porous Media, 2009. **79**(2): p. 215-223.

136. Durlofsky, L. and J.F. Brady, *Analysis of the brinkman equation as a model for flow in porous-media* Physics of Fluids, 1987. **30**(11): p. 3329-3341.

137. Larson, R.E. and J.J.L. Higdon, *Microscopic Flow near the Surface of Two-Dimensional Porous-Media .1. Axial-Flow.* Journal of Fluid Mechanics, 1986. **166**: p. 449-472.

138. Larson, R.E. and J.J.L. Higdon, *Microscopic Flow near the Surface of Two-Dimensional Porous-Media .2. Transverse Flow.* Journal of Fluid Mechanics, 1987. **178**: p. 119-136.

139. Martys, N., D.P. Bentz, and E.J. Garboczi, *Computer-Simulation Study of the Effective Viscosity in Brinkman Equation.* Physics of Fluids, 1994. **6**(4): p. 1434-1439.

140. Hou, J.S., et al., *Boundary conditions at the cartilage-synovial fluid interface*

for joint lubrication and theoretical verifications. Trans ASME J Biomech Eng, 1989. **111**: p. 78-87.

141. Neale, G. and W. Nader, *Practical Significance of Brinkmans Extension of Darcys Law - Coupled Parallel Flows within a Channel and a Bounding Porous-Medium.* Canadian Journal of Chemical Engineering, 1974. **52**(4): p. 475-478.

142. Huang, X.Y. and C.Y. Liu, *The developing flow in a channel filled with porous media.* International Communications in Heat and Mass Transfer, 1996. **23**(1): p. 123-132.

143. Poulikakos, D. and M. Kazmierczak, *Forced-Convection in a Duct Partially Filled with a Porous Material.* Journal of Heat Transfer-Transactions of the Asme, 1987. **109**(3): p. 653-662.

144. Auriault, J.L., C. Geindreau, and C. Boutin, *Filtration law in porous media with poor separation of scales.* Transport in Porous Media, 2005. **60**(1): p. 89-108.

145. Millward-Sadler, S.J., et al., *Integrin-regulated secretion of interleukin 4: A novel pathway of mechanotransduction in human articular chondrocytes.* Journal of Cell Biology, 1999. **145**(1): p. 183-189.

146. Hung, C.T., et al., *Real-Time Calcium Response of Cultured Bone-Cells to Fluid-Flow.* Clinical Orthopaedics and Related Research, 1995(313): p. 256-269.

147. Owan, I., et al., *Mechanotransduction in bone: Osteoblasts are more responsive to fluid forces than mechanical strain.* American Journal of Physiology-Cell Physiology, 1997. **42**(3): p. C810-C815.

148. Reich, K.M., C.V. Gay, and J.A. Frangos, *Fluid Shear-Stress as a Mediator of Osteoblast Cyclic Adenosine-Monophosphate Production.* Journal of Cellular

Physiology, 1990. **143**(1): p. 100-104.

149. Nathanson, M.H., et al., *Effects of Ca2+ Agonists on Cytosolic Ca2+ in Isolated Hepatocytes and on Bile Secretion in the Isolated Perfused-Rat-Liver.* Hepatology, 1992. **15**(1): p. 107-116.

150. Park, J., et al., *Radial flow hepatocyte bioreactor using stacked microfabricated grooved substrates.* Biotechnology and Bioengineering, 2008. **99**(2): p. 455-467.

151. Park, T.G., *Perfusion culture of hepatocytes within galactose-derivatized biodegradable poly(lactide-co-glycolide) scaffolds prepared by gas foaming of effervescent salts.* Journal of Biomedical Materials Research, 2002. **59**(1): p. 127-135.

152. Datta, N., et al., *In vitro generated extracellular matrix and fluid shear stress synergistically enhance 3D osteoblastic differentiation.* Proceedings of the National Academy of Sciences of the United States of America, 2006. **103**(8): p. 2488-2493.

153. Hosseinkhani, H., et al., *Ectopic bone formation in collagen sponge self-assembled peptide-amphiphile nanofibers hybrid scaffold in a perfusion culture bioreactor.* Biomaterials, 2006. **27**(29): p. 5089-5098.

154. Xu, S.L., et al., *Branched Channel Scaffolds Fabricated by SFF for Direct Cell Growth Observations.* Journal of Bioactive and Compatible Polymers, 2009. **24**: p. 63-74.

155. Wendt, D., et al., *Uniform tissues engineered by seeding and culturing cells in 3D scaffolds under perfusion at defined oxygen tensions.* Biorheology, 2006. **43**(3-4): p. 481-8.

156. Klein, T.J., et al., *Tissue Engineering of Articular Cartilage with Biomimetic Zones.* Tissue Engineering Part B-Reviews, 2009. **15**(2): p. 143-157.

157. Klein, T.J., et al., *Tissue engineering of stratified articular cartilage from chondrocyte subpopulations.* Osteoarthritis and Cartilage, 2003. **11**(8): p. 595-602.

158. Sharma, B., et al., *Designing zonal organization into tissue-engineered cartilage.* Tissue Engineering, 2007. **13**(2): p. 405-414.

159. Cohen, I., et al., *Slip, yield, and bands in colloidal crystals under oscillatory shear.* Physical Review Letters, 2006. **97**(21): p. -.

160. Cohen, I., T.G. Mason, and D.A. Weitz, *Shear-induced configurations of confined colloidal suspensions.* Physical Review Letters, 2004. **93**(4): p. -.

161. Buckley, M.R., et al., *Mapping the depth dependence of shear properties in articular cartilage.* Journal of Biomechanics, 2008. **41**(11): p. 2430-2437.

162. Buckley, M.R., et al., *High-resolution spatial mapping of shear properties in cartilage.* Journal of Biomechanics. **In Press, Corrected Proof**.

163. Quinn, T.M. and A.J. Grodzinsky, *Longitudinal Modulus and Hydraulic Permeability of Poly(Methacrylic Acid) Gels - Effects of Charge-Density and Solvent Content.* Macromolecules, 1993. **26**(16): p. 4332-4338.

164. Kaviany, M., *Laminar-Flow through a Porous Channel Bounded by Isothermal Parallel Plates.* International Journal of Heat and Mass Transfer, 1985. **28**(4): p. 851-858.

165. Mow, V.C., et al., *Biphasic creep and stress relaxation of articular cartilage in compression? Theory and experiments.* J Biomech Eng, 1980. **102**(1): p. 73-84.

166. Kong, H.J., E. Wong, and D.J. Mooney, *Independent Control of Rigidity and Toughness of Polymeric Hydrogels.* Macromolecules, 2003. **36**(12): p. 4582-4588.

167. Grattoni, C.A., et al., *Rheology and permeability of crosslinked*

polyacrylamide gel. Journal of Colloid and Interface Science, 2001. **240**(2): p. 601-607.

168. O'Brien, F.J., et al., *The effect of pore size on permeability and cell attachment in collagen scaffolds for tissue engineering.* Technol Health Care, 2007. **15**(1): p. 3-17.

169. Spain, T.L., C.M. Agrawal, and K.A. Athanasiou, *New technique to extend the useful life of a biodegradable cartilage implant.* Tissue Engineering, 1998. **4**(4): p. 343-352.

170. Agrawal, C.M., et al., *Effects of fluid flow on the in vitro degradation kinetics of biodegradable scaffolds for tissue engineering.* Biomaterials, 2000. **21**(23): p. 2443-2452.

171. Kemppainen, J.M. and S.J. Hollister, *Differential effects of designed scaffold permeability on chondrogenesis by chondrocytes and bone marrow stromal cells.* Biomaterials. **31**(2): p. 279-87.

172. Grayson, W.L., et al., *Effects of Initial Seeding Density and Fluid Perfusion Rate on Formation of Tissue-Engineered Bone.* Tissue Engineering Part A, 2008. **14**(11): p. 1809-1820.

173. Chen, T., M. Zuscik, and H. Awad, *Interstitial Flow Produces a Superficial Zone-Like Layer in Tissue Engineered Cartilage.* Transactions of the 55th Orthopaedic Research Society Annual Meeting, 2009. **34**: p. 1217.

174. Poole, C.A., M.H. Flint, and B.W. Beaumont, *Morphological and Functional Interrelationships of Articular-Cartilage Matrices.* Journal of Anatomy, 1984. **138**(Jan): p. 113-138.

175. Choi, N.W., et al., *Microfluidic scaffolds for tissue engineering.* Nat Mater, 2007. **6**(11): p. 908-15.

176. Gleghorn, J.P., et al., *Boundary mode frictional properties of engineered*

cartilaginous tissues. European Cells & Materials, 2007. **14**: p. 20-28.

177. Babalola, O.M. and L.J. Bonassar, *Parametric Finite Element Analysis of Physical Stimuli Resulting From Mechanical Stimulation of Tissue Engineered Cartilage.* Journal of Biomechanical Engineering-Transactions of the Asme, 2009. **131**(6): p. -.

178. Berg, H.C., *Diffusion with Drift*, in *Random Walks in Biology*. 1983, Princeton University Press.

179. Chao, P.H.G., A.C. West, and C.T. Hung, *Chondrocyte intracellular calcium, cytoskeletal organization, and gene expression responses to dynamic osmotic loading.* American Journal of Physiology-Cell Physiology, 2006. **291**(4): p. C718-C725.

180. Genes, N.G., et al., *Effect of substrate mechanics on chondrocyte adhesion to modified alginate surfaces.* Archives of Biochemistry and Biophysics, 2004. **422**(2): p. 161-167.

181. Knight, M.M., et al., *Chondrocytes express primary cilia decorated with connexin 43 hemichannels providing a pathway for purinergic mechanotransduction.* Tissue Engineering, 2007. **13**(7): p. 1655-1656.

182. Genes, N.G., et al., *Effect of substrate mechanics on chondrocyte adhesion to modified alginate surfaces.* Arch Biochem Biophys, 2004. **422**(2): p. 161-7.

183. Pierschbacher, M.D. and E. Ruoslahti, *Cell Attachment Activity of Fibronectin Can Be Duplicated by Small Synthetic Fragments of the Molecule.* Nature, 1984. **309**(5963): p. 30-33.

184. Delbuono, R., et al., *The Role of the Arginine-Glycine-Aspartic Acid-Directed Cellular-Binding to Type-I Collagen and Rat Mesenchymal Cells in Colorectal Tumor Differentiation.* Differentiation, 1991. **46**(2): p. 97-103.

185. Beekman, B., et al., *Synthesis of collagen by bovine chondrocytes cultured in*

alginate; Posttranslational modifications and cell-matrix interaction. Experimental Cell Research, 1997. **237**(1): p. 135-141.

186. Bryant, S.J., et al., *Crosslinking density influences the morphology of chondrocytes photoencapsulated in PEG hydrogels during the application of compressive strain.* J Orthop Res, 2004. **22**(5): p. 1143-9.

187. Spilker, R.L., J.K. Suh, and V.C. Mow, *Effects of Friction on the Unconfined Compressive Response of Articular-Cartilage - a Finite-Element Analysis.* Journal of Biomechanical Engineering-Transactions of the Asme, 1990. **112**(2): p. 138-146.

188. Genes, N.G., *Chondrocyte Adhesion to RGD-bonded Alginate:Effect on Mechanotransduction and Matrix Metabolism*, in *School of Biomedical Sciences*. 2003, University of Massachusetts: Worcester. p. 175.

189. Arnold, M., et al., *Activation of integrin function by nanopatterned adhesive interfaces.* Chemphyschem, 2004. **5**(3): p. 383-388.

190. Connelly, J.T., A.J. Garcia, and M.E. Levenston, *Interactions between integrin ligand density and cytoskeletal integrity regulate BMSC chondrogenesis.* Journal of Cellular Physiology, 2008. **217**(1): p. 145-154.

191. Massia, S.P. and J.A. Hubbell, *An Rgd Spacing of 440Nm Is Sufficient for Integrin Alpha-V-Beta-3-Mediated Fibroblast Spreading and 140Nm for Focal Contact and Stress Fiber Formation.* Journal of Cell Biology, 1991. **114**(5): p. 1089-1100.

192. Glass, J., et al., *Cell attachment and motility on materials modified by surface-active RGD-containing peptides.* Ann N Y Acad Sci, 1994. **745**: p. 177-86.

193. Danilov, Y.N. and R.L. Juliano, *(Arg-Gly-Asp)N-Albumin Conjugates as a Model Substratum for Integrin-Mediated Cell-Adhesion.* Experimental Cell Research, 1989. **182**(1): p. 186-196.

194. Singer, I.I., et al., *The Fibronectin Cell Attachment Sequence Arg-Gly-Asp-Ser Promotes Focal Contact Formation during Early Fibroblast Attachment and Spreading.* Journal of Cell Biology, 1987. **104**(3): p. 573-584.

195. Calderwood, D.A., et al., *The talin head domain binds to integrin beta subunit cytoplasmic tails and regulates integrin activation.* Journal of Biological Chemistry, 1999. **274**(40): p. 28071-28074.

196. Maheshwari, G., et al., *Cell adhesion and motility depend on nanoscale RGD clustering.* Journal of Cell Science, 2000. **113**(10): p. 1677-1686.

197. Critchley, D.R., *Cytoskeletal proteins talin and vinculin in integrin-mediated adhesion.* Biochemical Society Transactions, 2004. **32**: p. 831-836.

198. Giancotti, F.G. and E. Ruoslahti, *Transduction - Integrin signaling.* Science, 1999. **285**(5430): p. 1028-1032.

199. Ingber, D.E., et al., *Cell shape, cytoskeletal mechanics, and cell cycle control in angiogenesis.* Journal of Biomechanics, 1995. **28**(12): p. 1471-1484.

200. Boccaccio, A., L. Lamberti, and C. Pappalettere, *Effects of aging on the latency period in mandibular distraction osteogenesis: A computational mechanobiological analysis.* Journal of Mechanics in Medicine and Biology, 2008. **8**(2): p. 203-225.

201. Li, L.P., M.D. Buschmann, and A. Shirazi-Adl, *Strain-rate dependent stiffness of articular cartilage in unconfined compression.* Journal of Biomechanical Engineering-Transactions of the Asme, 2003. **125**(2): p. 161-168.

202. Hon, Y.C., et al., *Numerical algorithm for triphasic model of charged and hydrated soft tissues.* Computational Mechanics, 2002. **29**(1): p. 1-15.

203. Mow, V.C., N.M. Bachrach, and G.A. Ateshian, *The Effects of a Subchondral Bone Perforation on the Load Support Mechanism within Articular-Cartilage.* Wear, 1994. **175**(1-2): p. 167-175.

204. Spilker, R.L., J.K. Suh, and V.C. Mow, *A Finite-Element Analysis of the Indentation Stress-Relaxation Response of Linear Biphasic Articular-Cartilage.* Journal of Biomechanical Engineering-Transactions of the Asme, 1992. **114**(2): p. 191-201.

205. Rouillard, A.D., et al., *Control of the Electromechanical Properties of Alginate Hydrogels via Ionic and Covalent Crosslinking and Microparticle Doping*, in *In Process*.

206. Vafai, K. and C.L. Tien, *Boundary and Inertia Effects on Convective Mass-Transfer in Porous-Media.* International Journal of Heat and Mass Transfer, 1982. **25**(8): p. 1183-1190.

207. Guilak, F., A. Ratcliffe, and V.C. Mow, *Chondrocyte Deformation and Local Tissue Strain in Articular-Cartilage - a Confocal Microscopy Study.* Journal of Orthopaedic Research, 1995. **13**(3): p. 410-421.

208. Jacobs, C.R., et al., *Analysis of Time-Varying Biological Data Using Rainflow Cycle Counting*. 2000, Taylor & Francis. p. 31 - 40.

209. Grodzinsky, A.J., H. Lipshitz, and M.J. Glimcher, *Electromechanical Properties of Articular-Cartilage during Compression and Stress Relaxation.* Nature, 1978. **275**(5679): p. 448-450.

210. Frank, E.H. and A.J. Grodzinsky, *Cartilage electromechanics--II. A continuum model of cartilage electrokinetics and correlation with experiments.* J Biomech, 1987. **20**(6): p. 629-39.

211. Lotke, P.A., J. Black, and Richards.S, *Electromechanical Properties in Human Articular-Cartilage.* Journal of Bone and Joint Surgery-American Volume, 1974. **A 56**(5): p. 1040-1046.

212. Brighton, C.T., et al., *Invitro Bone Cell Response to a Capacitively Coupled Electrical-Field - the Role of Field-Strength, Pulse Pattern, and Duty Cycle.*

Clinical Orthopaedics and Related Research, 1992(285): p. 255-262.

213. Brighton, C.T., W. Wang, and C.C. Clark, *Up-regulation of matrix in bovine articular cartilage explants by electric fields.* Biochemical and Biophysical Research Communications, 2006. **342**(2): p. 556-561.

214. Brighton, C.T., W. Wang, and C.C. Clark, *The effect of electrical fields on gene and protein expression in human osteoarthritic cartilage explants.* Journal of Bone and Joint Surgery-American Volume, 2008. **90A**(4): p. 833-848.

215. Macginitie, L.A., Y.A. Gluzband, and A.J. Grodzinsky, *Electric-Field Stimulation Can Increase Protein-Synthesis in Articular-Cartilage Explants.* Journal of Orthopaedic Research, 1994. **12**(2): p. 151-160.

216. Xu, J., et al., *Signal transduction in electrically stimulated articular chondrocytes involves translocation of extracellular calcium through voltage-gated channels.* Osteoarthritis and Cartilage, 2009. **17**(3): p. 397-405.

217. Wang, W., et al., *Up-regulation of chondrocyte matrix genes and products by electric fields.* Clinical Orthopaedics and Related Research, 2004(427): p. S163-S173.

218. Lee, C.R., et al., *Effects of a cultured autologous chondrocyte-seeded type II collagen scaffold on the healing of a chondral defect in a canine model.* Journal of Orthopaedic Research, 2003. **21**(2): p. 272-281.

219. Bryant, S.J. and K.S. Anseth, *Hydrogel properties influence ECM production by chondrocytes photoencapsulated in poly(ethylene glycol) hydrogels.* Journal of Biomedical Materials Research, 2002. **59**(1): p. 63-72.

220. Vunjak-Novakovic, G., et al., *Bioreactor cultivation conditions modulate the composition and mechanical properties of tissue-engineered cartilage.* Journal of Orthopaedic Research, 1999. **17**(1): p. 130-138.

221. Malmonge, S.M. and A.C. Arruda, *Artificial articular cartilage: Mechanoelectrical transduction under dynamic compressive loading.* Artificial Organs, 2000. **24**(3): p. 174-178.

222. Schmidt-Rohlfing, B., et al., *Effects of pulsed and sinusoid electromagnetic fields on human chondrocytes cultivated in a collagen matrix.* Rheumatology International, 2008. **28**(10): p. 971-977.

223. Lai, W.M., et al., *On the electric potentials inside a charged soft hydrated biological tissue: Streaming potential versus diffusion potential.* Journal of Biomechanical Engineering-Transactions of the Asme, 2000. **122**(4): p. 336-346.

224. Rouillard, A.D., et al., *Methods for photocrosslinking alginate hydrogel scaffolds with high cell viability.*

225. Schneider, G.B., et al., *The effect of hydrogel charge density on cell attachment.* Biomaterials, 2004. **25**(15): p. 3023-8.

226. Smeds, K.A. and M.W. Grinstaff, *Photocrosslinkable polysaccharides for in situ hydrogel formation (vol 54, pg 115, 2000).* Journal of Biomedical Materials Research, 2001. **55**(2): p. 254-255.

227. Armstrong, P.F., C.T. Brighton, and A.M. Star, *Capacitively Coupled Electrical-Stimulation of Bovine Growth Plate Chondrocytes Grown in Pellet Form.* Journal of Orthopaedic Research, 1988. **6**(2): p. 265-271.

228. Lee, R.C., et al., *A Comparison of Invitro Cellular-Responses to Mechanical and Electrical-Stimulation.* American Surgeon, 1982. **48**(11): p. 567-574.